Skoltech

Skolkovo Institute of Science and Technology

HUMAN-SWARM INTERACTION FOR THE GUIDANCE AND DEPLOYMENT OF DRONES USING IMPEDANCE CONTROL AND TACTILE FEEDBACK

Doctoral Thesis

by

EVGENY TSYKUNOV

DOCTORAL PROGRAM IN ENGINEERING SYSTEMS

Supervisor
Associate Professor, Dzmitry Tsetserukou

I hereby declare that the work presented in this thesis was carried out by myself at Skolkovo Institute of Science and Technology, Moscow, except where due acknowledgement is made, and has not been submitted for any other degree.

Candidate (Evgeny Tsykunov)

Supervisor (Associate Professor Dzmitry Tsetserukou)

HUMAN-SWARM INTERACTION FOR THE GUIDANCE AND DEPLOYMENT OF DRONES USING IMPEDANCE CONTROL AND TACTILE FEEDBACK

by

EVGENY TSYKUNOV

Thursday 21st January, 2021 16:07

Abstract

Drone formations started to be actively used for addressing many real-world problems such as aerial co-manipulation, object detection, and tracking, collection of spatial data (images, depth data with LIDARs, sound, air composition, etc.). To be able to fulfill some of these tasks, robotic formations can achieve high complexity. The swarm consists of many components such as perception, goal or task assignment, feasible trajectory planning, control, etc.

One of the approaches that can simplify the swarm of aerial robots is to incorporate the human into the system. A human operator can bring additional intelligence to the swarm operation, and therefore, the complexity of the system can be reduced. When the human is integrated into the process, he or she either can extend the possibilities of the robotic group or take upon oneself some functionality that allows simplifying the swarm.

Many research laboratories actively work in the Human-Swarm Interaction (HSI) field. Such kind of interaction systems can be quite complicated. Many challenges remain open in this field. Environments, where the swarm has to operate, can be complicated, i.e., being unstructured with many obstacles and different weather conditions. Individual agents have to react to various internal (neighbor drones) and external (human and obstacles) conditions, coming from neighbor drones, human and obstacles. No strategy considers the adaptive behavior of the real fleet of micro-quadrotors, helping to get a smooth and safe response of the robots in various conditions. The human operator also needs to receive useful and clear feedback about the swarm behavior to generate proper control signals. Unstructured environments also apply safe takeoff and landing challenges, which have not been solved for micro-quadrotors. Considering mentioned challenges and technical gaps, it is essential to integrate the human into the swarm operation properly.

To achieve smooth guidance and deployment of a drone formation by a human operator, the thesis proposes a novel interaction system for human-swarm communication. The proposed Human-Swarm Interaction (HSI) system combines impedance

control and vibrotactile feedback both for the guidance and deployment of the swarm of small-scale quadrotors.

We first present an approach that takes into account the human hand velocity for the control input and changes the formation shape and dynamics accordingly using impedance interlinks simulated between quadrotors, which helps to make swarm control safe and robust. Each quadrotor relies on the local position information coming from neighbor vehicles, and, at the same time, the human operator affects all vehicles globally via impedance models. As a result, such adaptive control could lead to a natural multi robot-human interaction.

The human operator must be aware of changes in the formation (e.g., extension and contraction) while performing the control. The importance of this fact increases with the number of robots. To address this problem, we propose tactile patterns representing the swarm's static and dynamic parameters to provide feedback to the human operator. The user feels the flock state at the fingertips and receives valuable information to improve the controllability of the complex formation. A user study revealed the patterns with high recognition rates. A flight experiment demonstrated the possibility to accurately navigate the formation in a cluttered environment using only proposed tactile feedback. Subjects stated that tactile sensation allows guiding the drone formation through obstacles and makes the human-swarm communication more interactive.

If we consider the overall flight mission, takeoff and landing are the essential sub-operations of any flight. It is especially crucial in a cluttered environment with uneven surfaces. While large drones can lift high-performance vision and processing systems for autonomous navigation and landing, micro-quadrotors cannot process the visual data autonomously in most cases. We propose that human can supplement these challenging sub-operations. However, interaction strategies have not yet been appropriately considered for such cases, especially when more than one drone has to land simultaneously. Therefore, the thesis proposes a novel interaction strategy SwarmCloak to deploy (takeoff and land) multiple micro-drones from the human hands using vibrotactile wearable displays.

The thesis focuses on the interface (control and feedback) between a human operator (leader) and a robotic swarm, addressing the nascent and dynamic field of HSI. The proposed HSI system can potentially have a substantial impact on the human-swarm interaction, providing a higher level of awareness during the swarm navigation.

4

Publications

Peer-reviewed journals

1. **Evgeny Tsykunov**, Ruslan Agishev, Roman Ibrahimov, Luiza Labazanova, Akerke Tleugazy, and Dzmitry Tsetserukou. SwarmTouch: Guiding a swarm of micro-quadrotors with impedance control using a wearable tactile interface. *IEEE Transactions on Haptics*, 12(3):363–374, jul 2019b. doi:10.1109/toh.2019.2927338; Q2 ranking, IF 3.1

2. Yuri S. Sarkisov, Grigoriy A. Yashin, **Evgeny V. Tsykunov**, and Dzmitry Tsetserukou. DroneGear: A novel robotic landing gear with embedded optical torque sensors for safe multicopter landing on an uneven surface. *IEEE Robotics and Automation Letters*, 3(3):1912–1917, jul 2018. doi:10.1109/lra.2018.2806080; Q1 ranking, IF 3.6

Peer-reviewed conference proceedings

1. **Evgeny Tsykunov**, Ruslan Agishev, Roman Ibrahimov, Taha Moriyama, Luiza Labazanova, Hiroyuki Kajimoto, and Dzmitry Tsetserukou. SwarmCloak: Landing of two micro-quadrotors on human hands using wearable tactile interface driven by light intensity. In *2020 IEEE Haptics Symposium (HAPTICS)*, pages 987–992. IEEE, mar 2020. doi:10.1109/haptics45997.2020.ras.hap20.89.9286 SJR 0.562

2. **Evgeny Tsykunov**, Ruslan Agishev, Roman Ibrahimov, Luiza Labazanova, Taha Moriyama, Hiroyuki Kajimoto, and Dzmitry Tsetserukou. SwarmCloak: on human arms. In *SIGGRAPH Asia 2019 Emerging Technologies*, pages 46–47. ACM, nov 2019a. doi:10.1145/3355049.3360542; CORE rating = A

3. **Evgeny Tsykunov** and Dzmitry Tsetserukou. WiredSwarm: High resolution haptic feedback provided by a swarm of drones to the user's fingers for VR interaction. In *25th ACM Symposium on Virtual Reality Software and Technology*. ACM, nov 2019. doi:10.1145/3359996.3364789; CORE rating = A

4. **Evgeny Tsykunov**, Roman Ibrahimov, Derek Vasquez, and Dzmitry Tsetserukou. SlingDrone: Mixed reality system for pointing and interaction using a single drone. In *25th ACM Symposium on Virtual Reality Software and Technology*. ACM, nov 2019c. doi:10.1145/3359996.3364271; CORE rating = A

5. Roman Ibrahimov, **Evgeny Tsykunov**, Vladimir Shirokun, Andrey Somov, and Dzmitry Tsetserukou. DronePick: Object picking and delivery teleoperation with the drone controlled by a wearable tactile display. In *2019 28th IEEE International Conference on Robot and Human Interactive Communication (RO-MAN)*, pages 280–285. IEEE, oct 2019. doi:10.1109/ro-man46459.2019.8956344

6. Luiza Labazanova, Akerke Tleugazy, **Evgeny Tsykunov**, and Dzmitry Tsetserukou. SwarmGlove: A wearable tactile device for navigation of swarm of drones in VR environment. In *Lecture Notes in Electrical Engineering*, pages 304–309. Springer Singapore, 2019. doi:10.1007/978-981-13-3194-7$_6$7

7. A. Menshchikov, D. Lopatkin, E. Tsykunov, D. Tsetserukou, and A. Somov. Realizing body-machine interface for quadrotor control through kalman filters and recurrent neural network. In *2020 25th IEEE International Conference on Emerging Technologies and Factory Automation (ETFA)*, volume 1, pages 595–602, 2020

8. **E. Tsykunov**, L. Labazanova, A. Tleugazy, and D. Tsetserukou. SwarmTouch: Tactile interaction of human with impedance controlled swarm of nano-quadrotors. In *2018 IEEE/RSJ International Conference on Intelligent Robots and Systems (IROS)*, pages 4204–4209. IEEE, oct 2018. doi:10.1109/iros.2018.8594424; CORE rating = A, SJR 0.589

Dedicated to my family.

Acknowledgments

I would like to thank my supervisor Dzmitry Tsetserukou.

Let me thank to all my teammates who supported my research: Ruslan Agishev, Luiza Labazanova, Akerke Tleugazy, Roman Ibrahimov, Taha Moriyama, Derek Vasquez. We did a great team work with you.

Contents

List of Figures

List of Tables

Chapter 1

Introduction

This chapter aims to provide a general introduction to the swarms of aerial robots and Human-Swarm Interaction (HSI). We will discuss the main challenges of the HSI and give the scope of the work.

1.1 Swarms of Aerial Robots

Systems of aerial swarm robots can reach high complexity and consist of many components. Many challenges remain open in this area in order to achieve fully autonomous operation in various conditions.

Drone formations started to be actively used for addressing real-world issues in many scopes, such as aerial co-manipulation, mapping, surveillance monitoring, and target search and tracking. Multiple reasons accomplish this. Due to the vast spreading of mobile technologies, sensing and computational hardware components have a low price and small footprint. Members of open source and open hardware communities actively contribute to the development of the technologies. Many hardware components have become unified and are suitable for many different products, which decrease prices. Last but not least, many algorithms have been developed in research laboratories around the globe. Algorithms allow us to plan the necessary actions and cooperate while maintaining the safety of operation. As a result, we can build large groups of robots working together in diverse applications.

Chung et al. [2018] reported that many constraints have to be satisfied to fulfill
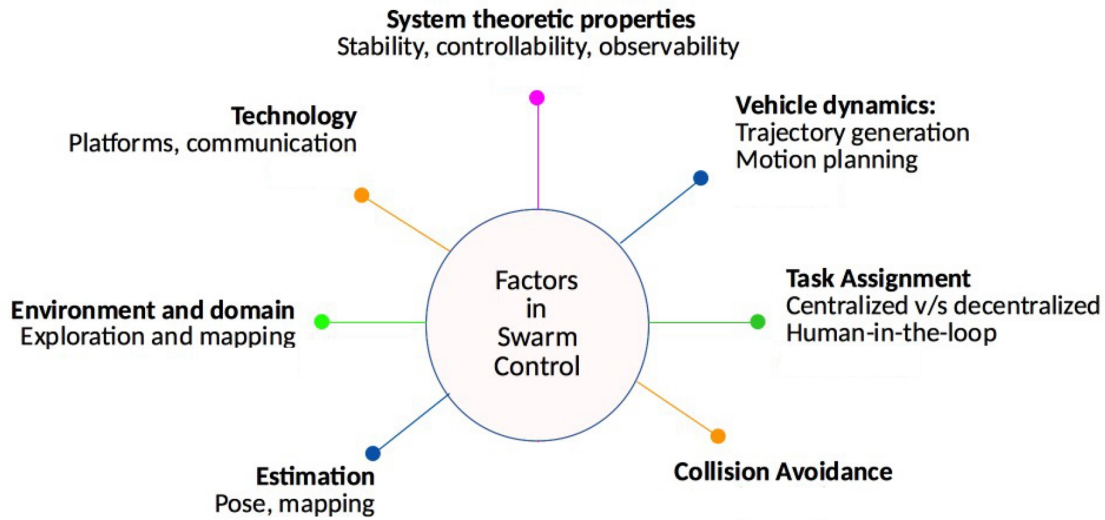
Figure 1-1: Major swarm control factors according to Chung et al. [2018].

the formation flight objective (see Fig. 1-1). Some of them include proper state estimation Montijano et al. [2016], Ledergerber et al. [2015], Teixeira et al. [2018], dynamically feasible trajectories Paranjape et al. [2013], Hönig et al. [2017], Tang et al. [2017], communication issues Mastellone et al. [2008], Zhou et al. [2014], and robust and scalable control Su et al. [2009], Bandyopadhyay et al. [2017], Turpin et al. [2015]. Being able to solve all of these challenges in an autonomous way represents a hard problem. Especially when the swarm operates in a changing environment and has to make a decision 'on the fly' in response. To be able to operate in different scenarios, swarm systems can reach high complexity.

There are two conventional paradigms in the swarm operation which are described in Tang and Kumar [2018]. The first one is the flight in a formation with the maintenance of geometric shape. The second one is when each quadrotor within a swarm individually perform a mission to the predefined goal position with preliminary goal assignment Turpin et al. [2014]. In the scope of my thesis, we consider only the first paradigm.

1.2 Human-Swarm Interaction

In this section we will discuss why it is necessary to introduce the human into the swarm operation and highlight the main problems.
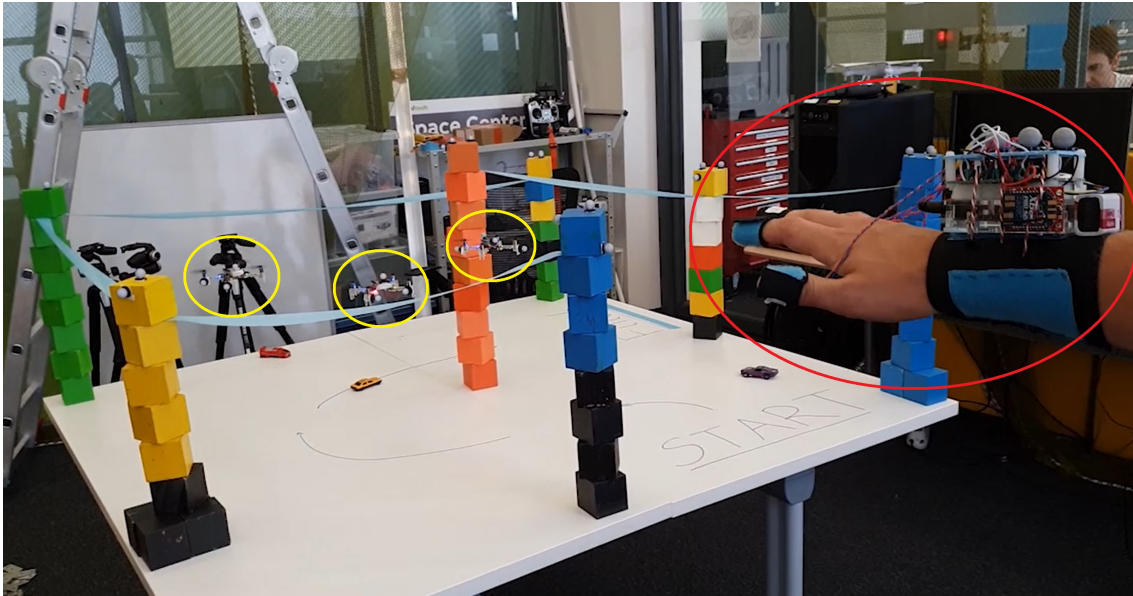
Figure 1-2: Human operator guides the group of robots through the maze.

Researchers across the globe introduce new robotic systems designed for use by or with humans. Human-Robot Interaction (HRI), especially when humans and robots are co-located, is one of the latest trends in the field of Robotics Lemaignan et al. [2017], Goodrich and Schultz [2007].

A human operator can bring additional intelligence to the swarm operation. When the human is integrated into the process, he ether can extend the possibilities of the robotic group or take upon oneself some functionality that allows simplifying the swarm.

For some specific applications in unstructured environments, fully or partially guided groups of robots are the only possible solution (see Fig. 1-2) when the attention of the robots has to be shifted by a human operator to specific points of operation Bashyal and Venayagamoorthy [2008]. Human-controlled robots are also widely used for safety, security, and rescue purposes, as reported by Birk et al. [2009], Martins and Ventura [2009]. The possible applications may include deactivating bombs, monitoring undersea oil pipelines, and cleaning radioactive and toxic waste.

Many research laboratories worldwide are working in the field, which is called Human-Swarm Interaction (HSI). Human-Swarm Interaction combines many research topics, which are well described by Kolling et al. [2016], and could vary from communication channels to a level of swarm autonomy.

The operation of a swarm is a significantly more complicated task as a human has to simultaneously supervise several agents Dhanaraj et al. [2019]. The human role can be simplified. Instead of the direct control of the robots, the human can provide the robotic group with high-level commands. Nevertheless, for the human to work with the drone formation side by side, robust and natural interaction techniques must be developed and implemented. Many research laboratories actively work in the Human-Swarm Interaction (HSI) field. Such kind of interaction systems can be quite complicated. For example, authors in Cacace et al. [2016] presented a multimodal interaction strategy between a human and a formation of drones for search and rescue operations. Gestures and speech recognition, along with a tablet, allowed the user to control the quadrotors' fleet.

1.2.1 Challenges for direct guidance and deployment during HSI

Below we cover some of the challenges that arise during the design of the HSI systems. In the thesis, we address the discussed challenges.

Complex environment

Environments, where the swarm system operates, can have different properties. The most simple case is when the operational space is empty, with no external disturbances. Unfortunately, it is not valid in most cases. In real life, we often have the opposite - when the environment is highly unstructured. In that case, we cannot predict the actual positions of different external objects or strictures, and sensing and communication capabilities can dramatically reduce during the fly. Static and dynamic obstacles can be densely distributed in space, which creates narrow passages for the robotic systems. Besides, different external disturbances, such as strong wind, can contribute to the changing state of the vehicle formation. As a result, space, where the swarm operates, can represent a complex environment. Let name all conditions described above as environmental conditions and refer them to the external factors.

To overcome the external factors related to the unstructured environments, the swarm has to be intelligent enough to withstand external disturbances and perform the obstacle avoidance with the objective of maintaining the default geometry shape.

Adaptability

While individual agents of the formation react to the environmental conditions, drone-to-drone interaction has to adapt accordingly. Each drone has to sense the neighbors to keep the velocity and therefore maintain the default drone-to-drone distances.

Apart from that, introducing a human into direct swarm control can enter disturbances into the formation flight, as shown by Goodrich et al. [2012], such as rapid acceleration and deceleration. The desirable trajectory has to be generated in a compliant manner, to make human-swarm interaction natural and safe. The formation, from the other side, has to respond to the goal positions in order to maintain the dynamic stability. When the target motion velocity of the robotic group increase, it is reasonable to increase the distance between drones. Any introduced changes into the formation flight have to be conducted in a smooth manner, avoiding rapid acceleration and deceleration. For the quadrotors, the smoothness of motions is measured by the higher derivatives of the position (for example, snap - second derivatives of the acceleration).

Let name this probity of adapting the robotic group to the external factors and human control input as adaptability.

Swarm System Feedback

As discussed above, during the HSI, the drone formation interacts with the environment, with a human operator, and each vehicle also interacts with neighboring agents.

As a result, the state of the swarm changes in time. For the human leader to be able to make the most efficient control decisions, he or she must be aware of the formation state in real-time. Profitable choices can vary, depending on the mission type. For example, when needed to cover the area with flying vehicles evenly, with

no big spacial gaps between the neighbor vehicles, it is reasonable to generate control commands that can help maintain the default geometry during flight. Although the visual channel is the most common type of feedback for HSI, it can suffer from poor quality or be overloaded. On the other side, tactile feedback is actively used in order to be aware of the robot state. Swarm state can be complicated, containing many static and dynamic parameters. It represents a hard challenge to promptly deliver the swarm state information to the human operator using the tactile feedback.

Deployment

Referring back to the complex environments, we demonstrated that it is hard to efficiently and safely guide vehicles under such conditions. After solving the guidance problem, we still face the deployment challenge - takeoff and landing. In many cases, in remote areas, we do not have a well-prepared takeoff and landing surface for Vertical Takeoff and Landing (VTOL) vehicles. It is usually the case when the landing spot is uneven and which can lead to crashes. Even if we have the landing spot, we need to set up a computationally intensive localization system to land precisely on the proper point. For the small-sized quadrotors, it is almost impossible to solve the localization problem or carry an adaptive landing gear to perform a safe deployment. We point out the deployment challenge here as the unsolved one because takeoff and landing are the essential sub-parts of any flight mission and we cannot ignore it.

1.3   Scope

Below we will discuss the scope of the developed technology along with its main components.

While completing a flight mission, the formation is guided in space, receiving the global high-level commands from the human operator, such as going towards the north or south. To ensure a safe mission, the formation of drones has to follow a set of rules during operation Mulgaonkar et al. [2015]. Different flight missions require to follow different rules. But some objectives are common and shared among the most
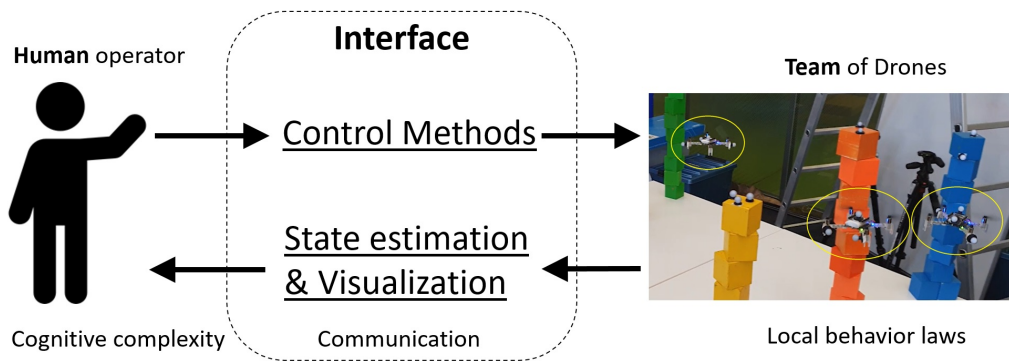
Figure 1-3: Main components of the human-swarm interface.

types of missions. Rules may include obstacle avoidance and the maintenance of the target state parameters: geometrical shape, feasible global, and relative (drone-to-drone) velocity/acceleration. Takeoff and landing are also critically important as far as the most amount of crashes happen during these sub-stages. In order to follow these objectives, the challenges described above has to be solved.

To summarize, in the doctoral thesis, we propose a new method for Human-Swarm Interaction. In particular, we focus on the interface between a human operator (leader) and a robotic swarm, as shown in Fig. 1-3, addressing the nascent and dynamic field of HSI. The interface incorporates two primary information flows: control and feedback. Control flow provides the swarm with guidance clues coming from the human. The feedback flow delivers to the human operator information about the state of the flock at the current time. Based on the received feedback, the human is supposed to generate a control input to fulfill the mission goals. Under the swarm state term, we mean geometrical shape and drone-to-drone distance. We propose to apply the developed method for the guidance and deployment of the formation in the unstructured and dynamically changing environment, such as urban areas. More generally, my thesis is framed by three-dimensional human-computer interaction (HCI) Card [2018], which is a rich field, and it is under active development in the robotics and VR/AR communities.
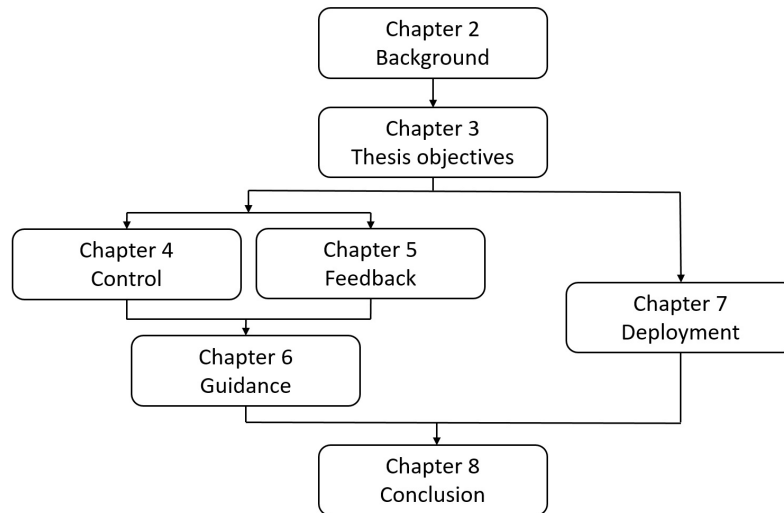
Figure 1-4: Thesis structure.

1.3.1   Global Goal of the Drone Operation

In this thesis, we target a human-guided operation of a swarm of drones in a cluttered and dynamically changing environment, such as urban area Roldan et al. [2019], Araki et al. [2017], Cooley et al. [2018]. The ultimate goal of the typical swarm mission may include: quickly collection of spatial (distributed in space) data (images/video, depth data, sounds, air composition, etc.) Aznar et al. [2014], Saska et al. [2014], transmission of a signal Shi et al. [2018], Nayyar [2018], co-manipulation Michael Jassowski [2016], Thapa et al. [2019].

1.4   Thesis Structure

The overall diagram of the thesis which present the structure is shown in Fig. 1-4. Short overview of each chapter is presented below.

Chapter 1 - Introduction Here's the general introduction. We discuss the motivation and the main challenges that are addressed by the thesis. We also nightlight the scope of the research.

Chapter 2 - Background Here's the literature review. We provide a comprehensive and critical analysis of the literature related to the interaction strategies

between the human and a swarm of drones. We highlight the research gaps that we address in the thesis.

Chapter 3 - Thesis Objectives We address the thesis objectives along with the research questions and novelty of the work.

Chapter 4 - Control Strategy for the Swarm Guidance We define the control part of the interaction system. In particular, we describe the relationship between a control input signal and a swarm motion. We also show the relationship between the agents and the environment. Besides, we describe the way we generate the control input commands.

Chapter 5 - Tactile Feedback from the Swarm of Drones We define the feedback part of the interaction system. In particular, we discuss the design of tactile patterns and their evaluation. Finally, we provide the details of the flight experiment using the tactile display.

Chapter 7 - SwarmCloak: Deployment of Drones from the Human Hands We define the deployment method. We discuss the wearable tactile interface that helps to deploy (takeoff and land) multiple drones from the human body.

Chapter 8 - Conclusion In the last chapter, we discuss the results, limitations, and future work.

1.5   Summary

In this chapter we gave the introduction to the swarms of drones and Human-Swarm Interaction (HSI) in general. We discussed the main open technical gaps of the HSI which is addressed in this thesis. Finally we provided the scope of the work and structure of the document.

Chapter 2

Background

In this chapter, we present a comprehensive and critical review of the literature related to the topic of this work. We also define the research gaps in the state-of-the-art. The structure of the information flow is presented in Fig. 2-1. We start with some of the autonomy principles behind the swarms. Then we consider the cognitive complexity of the operator and communication approaches. After that, we investigate common control strategies, control input devices, and tactile feedback. Finally, we review possible deployment methods for the UAVs and their limitations.

2.1 Autonomy in the Swarm of Drones

Below is the short review of some state-of-the-art research in the field of the autonomous aerial swarms. In the last decades, researchers archived significant results in the autonomy of the single drone systems Tang and Kumar [2018]. Based on
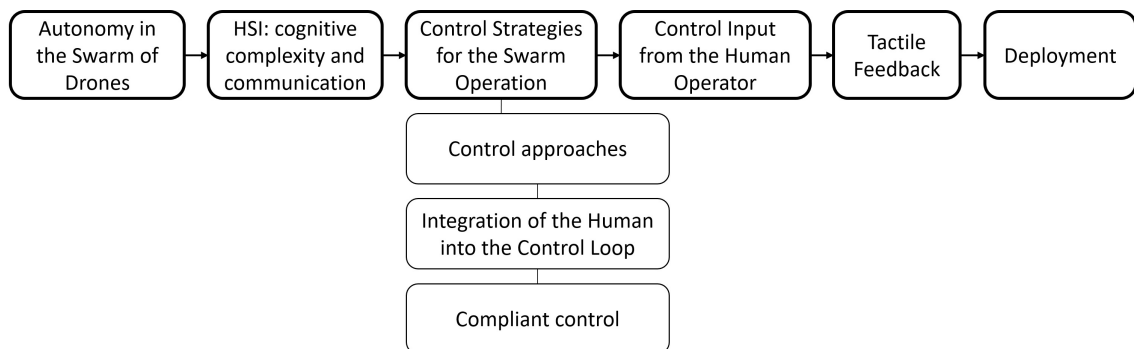
Figure 2-1: Structure of the chapter.

these improvements, many scientists started to investigate multi-agent systems. It is well known that, in many cases, a group of robots can perform much better than a single robot due to scalability and robustness Lindsey et al. [2011]. The recent advancements in robot autonomy have made it possible to reduce the number of scenarios where human intervention is necessary to support the formation flight of drones Chung et al. [2018]. Testing facilities have been constructed in many research centers around the globe to enhance the development of aerial robotics, as reported by Kushleyev et al. [2012], Lupashin et al. [2014]. The academic project with the biggest micro quadrotor swarm Preiss et al. [2017] counts 49 Crazyflie 2.0 drones performing the cooperative flight. Many of such testbeds also allow investigating the cooperation between robots and a human.

Autonomous missions of aerial robots are used in such areas as search and rescue operations Waharte et al. [2009] and precision agriculture Mogili and Deepak [2018]. Despite significant achievements in this area, many limitations are still present. Most methods are hardly scalable to a large team of quadrotors operating at high-speed Tang and Kumar [2018], especially within highly unstructured environments.

Nevertheless, many research teams pay attention to the control of multiple agent teams, and contributions vary from bio-inspired solutions to advancements of control theory. A significant portion of the algorithms for control and behavior have been inspired by biological swarm systems that can be seen in nature Webb [2002]. Sumpter [2006] described common principles of the collective behavior of biological systems. The author proposes to consider the interaction and information flow between the agents and the surrounding environment. At the same time, the author suggests not taking into account each animal as a complex individual.

2.2 HSI: Cognitive Complexity and Communication

In this section we discuss of how the operator resources vary with respect to the size the controlled system (number of robots).

It is a challenge to integrate a human into such complex multi-agent systems. A human can be a supervisor or a leader to a group of robots, or he or she can be a

teammate to other agents. The operator can supervise only one agent at a time or an unlimited number of robots simultaneously. The human role can change in time, depending on the objective being addressed.

The complexity of a multi-agent system's operation is an important parameter that has to be considered during the design of the HSI systems. The same approach, when we estimate the computational complexity, is widely used in computer science to select easily scalable algorithms. Lewis et al. [2006], Lewis [2013] classified the HSI systems in terms of human cognitive complexity. When the formation of robots operates in such a way that each individual follows independent objectives, the human operator has to guide each separate robot one by one or sequentially. Therefore the cognitive complexity is $O(n)$, where n is the number of robots (see Fig. 2-2). As a result, we have a linear relationship between human cognitive efforts and the number of robots. The only way to scale such kind of approach is to use more operators. Another paradigm is when the operator can manage an unlimited number of robots. The use case can be, for example, when the global direction of motion is delivered to the formation, and the interaction between agents and their environment performs autonomously. Mangiat et al. [2013] proposed technology for guiding a robotic swarm with the help of one-touch or one-click gestures. Therefore, the number of actions required to be completed by the operator is independent of the size of the swarm, and cognitive complexity is $O(1)$. Finally, there is also a case when the robots' interactions have to be manually handled by a human operator. In this case, the complexity is super-linear $O(> n)$, because the relationships between the individuals grow faster than the number of robots. This kind of scenario can arise when the robots have to coordinate to perform some common actions such as manipulating an object or pushing a box, as demonstrated by Wang and Lewis [2007]. All of these concepts are graphically presented in Fig. 2-2.

Most of the guided swarms operate remotely, far from the operators. The reason is that the main applications involve the collection of data in remote and dangerous areas. Therefore, along with the control signals, the transmission of the collected data to the Ground Control Station is also critically important Potdar et al. [2009]. The operator can broadcast the information to multiple agents simul-
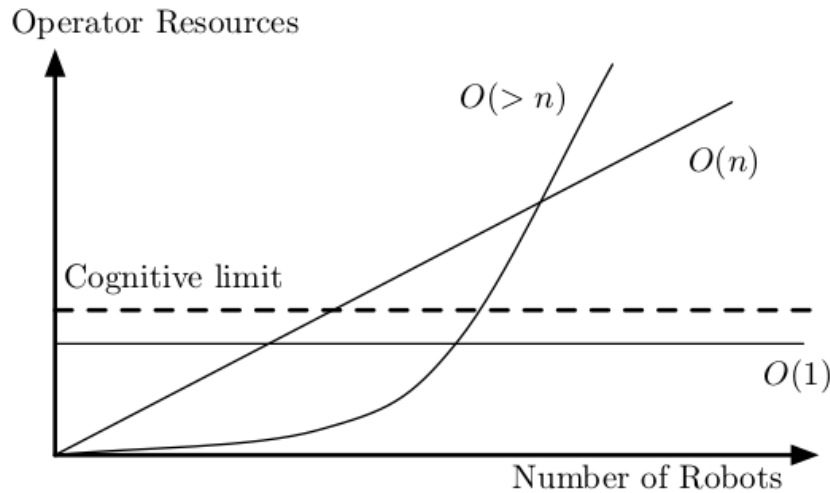
Figure 2-2: Operator cognitive complexity for different control architectures according to Kolling et al. [2016].

taneously (global one-to-many in one direction), or he or she can have direct communication with any individual vehicle (one-to-one in both directions). Mclurkin et al. [2006] proposed a distributed communication network that is managed from the ground and helps control 112 vehicles. On the other hand, it is also possible when the operator shares the same environment with the robotic group, and there is a direct line of sight between the agents and a human. Obvious approaches include gestures Giusti et al. [2012] and speech recognition Pourmehr et al. [2013] for the swarm control.

2.3 Control Strategies for the Swarm Operation

In this section we will discuss the way of how the response of the controlled drone formation is formed.

2.3.1 Control approaches

Here we will cover the methods of how the generic swarm is getting controlled.

Two possible abstractions are commonly used for swarm control in the research community, as shown in Tang and Kumar [2018]. The first one is when the group of robots is moving intending to keep a formation Mulgaonkar et al. [2015], and
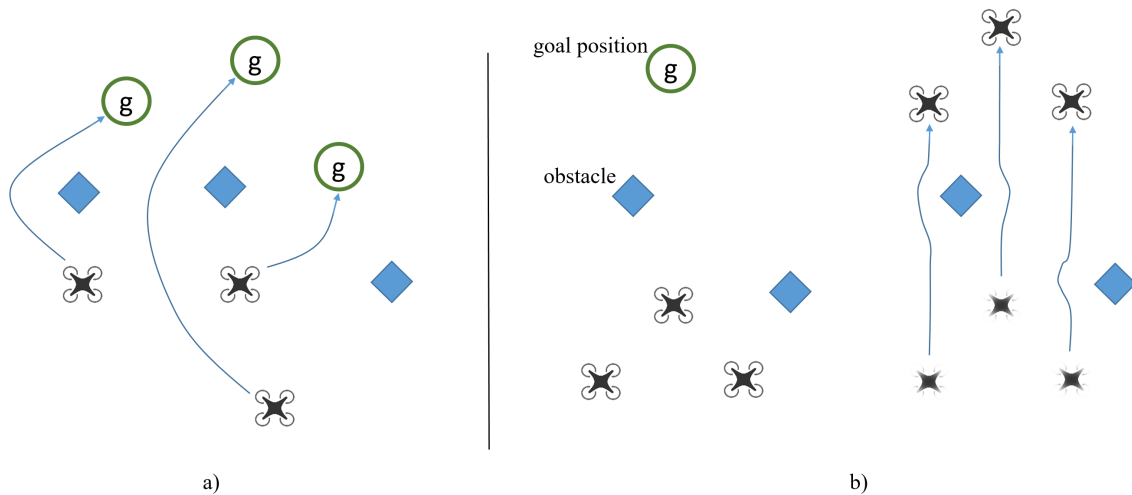
Figure 2-3: Two common paradigms of motion of a team of robots. a) Goal assignment and trajectory planning is performed for each vehicle. b) Team of robots moving with an objective of keeping the formation geometrical structure or shape.

the other is when each robot can get to the predefined goal positions independently Stephan et al. [2017] (with preliminary goal assignment). Both approaches are presented in Fig. 2-3. When the human is involved in the team guidance, it could be hard to manage multiple agents if they are acting independently (especially for large formations). In this case, the cognitive complexity grows super-linear $O(> n)$, where n is the number of robots (discussed in the previous section). Partially for this reason, in the thesis, we mainly consider the abstraction, when the drone group is supposed to maintain the geometric structure during guidance. Relative distances between the robots define the geometric structure. In Fig. 2-3(b), for example, the used geometrical shape is flat triangle located in horizontal plane.

Maintenance of geometric configuration is a useful feature that helps to address multiple needs. For example, we need to keep the drone-to-drone distance when the agents perform imaging of an area to stitch all images into a single 2-dimensional or 3-dimensional map Saeedi et al. [2015]. In the case of cooperative aerial mapping, each neighbor pair of images overlapped at a certain level (typical it is 60% of overlap) Dro [2020]. By overlap, we mean when two neighbor drones capture the same surface (see Fig. 2-4 for more details). To achieve certain overlap, drones' formation has to keep a predefined distance to each other, thus keeping the spatial geometry.
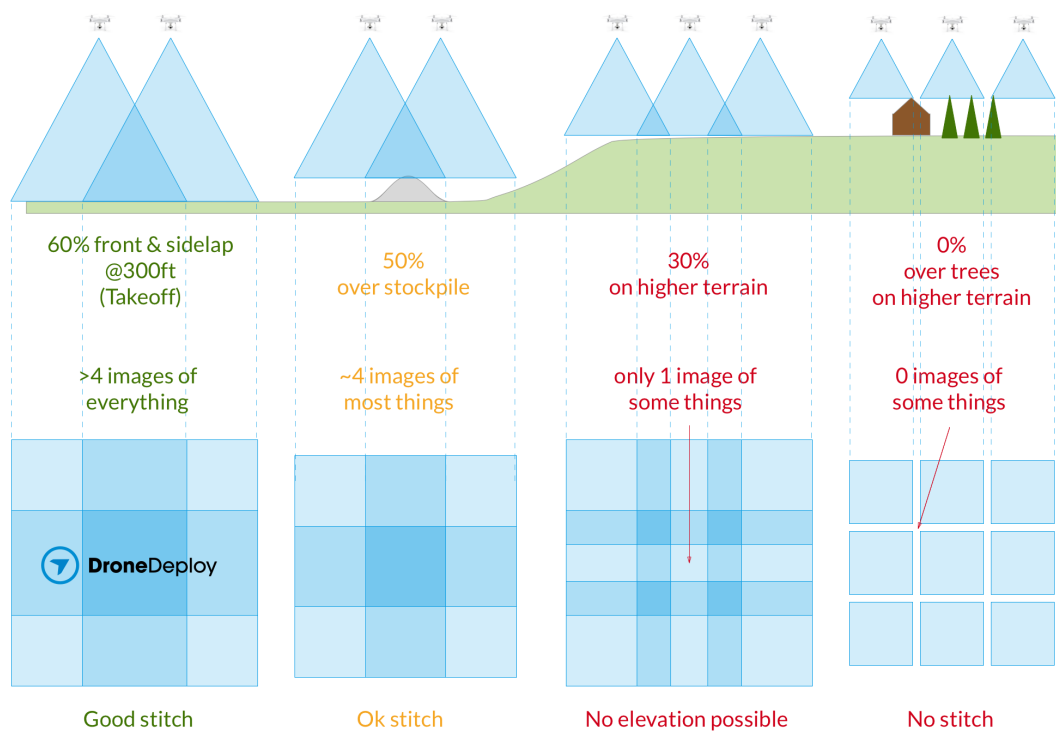
Figure 2-4: Overlap of images that is necessary for proper stitching of images into two-dimensional or three-dimensional map with elevations. According to Dro [2020] - UAV mapping platform.

On the other side, when the cooperative aerial manipulation with multiple drones is achieved (e.g., with suspended payload), we also need to tightly maintain the drone-to-drone distance to avoid flight instability Thapa et al. [2019]. The team of robots is guided by a human and manipulate a box in Wang and Lewis [2007]. In the coordination tasks, which include co-manipulation, for example, in Wang and Lewis [2007], it is critically important for the human to keep under control of the spacial relationship between the robots to ensure safe operation and follow cooperation goal.

We discussed that many swarm applications require formation maintenance. Therefore, we suggest formulating the problem with the objective of preserving the default geometry as much as possible. But along with the sub-task of default geometry keeping, every single quadrotor must avoid environmental obstacles (both moving and static) Chung et al. [2018], Mulgaonkar et al. [2015], Vásárhelyi et al. [2018]. As a result, every robot will be able to change the relative drone-to-drone distances to avoid obstacles. Therefore, quadrotors also have to avoid collisions with each other. Based on that, the control algorithms have to maintain the formation geometry and, at the same time, have to handle collision avoidance to ensure safety.

2.3.2 Integration of the Human into the Control Loop

The section will highlight the methods of integration of the human operator into the control loop. The limitations also will be covered.

For cases in which human controls a swarm directly, standard control techniques have been developed in the last few decades Kolling et al. [2016]. Applications include the interaction between a human and a single-robot or multi-robot systems. Multi-robot formations can be controlled through a central station (centralized control) Morgan et al. [2016] or, each agent can rely only on local information for making control decisions locally Gazi and Fidan, Alonso-Mora et al. [2015], Zhou et al. [2017].

The controller of a single drone usually incorporates multiple nested feedback loops, as presented by Michael et al. [2010], Tang and Kumar [2018]. The inner attitude control loop maintains the vehicle's desired Euler angles by using the information from the inertia measurement unit (IMU). The outer control loop, working
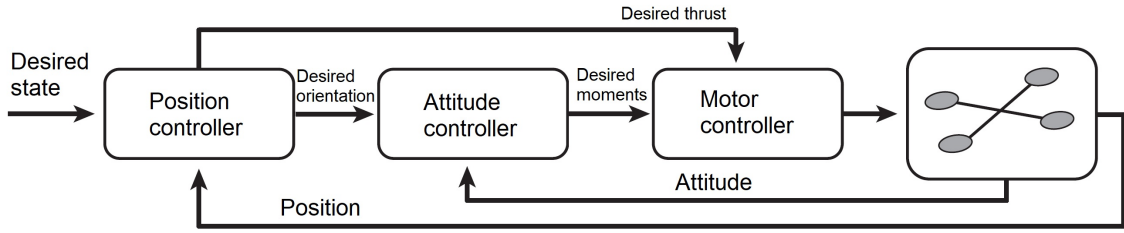
Figure 2-5: Scheme of the traditional hierarchical drone controller according to Tang and Kumar [2018].

on top of the attitude loop, maintains the trajectory by receiving the vehicle's position and velocity. Control loops are presented in Fig. 2-5. Unfortunately, the equations of motions of the quadrotor are non-linear. Therefore, the motion model is getting linearized in point where the vehicle is located (when the roll and pitch angles are close to zero).

Usually, considering the design of the control strategies for the HSI, we take into account only high-level control, i.e., position or trajectory control. This thesis also focuses on the high-level control approaches.

For the positional control a traditional proportional-integral–derivative (PID) controller is used in the majority of cases Tang and Kumar [2018]. The control input in the case of the PID controller is defined in the following way (for a single axis)

$$u_{des} = \ddot{x}_{track} + K_p(x_{track} - x) + K_d(\dot{x}_{track} - \dot{x}) + K_i \int (x_{track} - x) \tag{2.1}$$

$$e = x_{track} - x \tag{2.2}$$

where e is the error in position (used for position controller), x_{track} and x are tracked (that we want to achieve) and actual positions respectively, K_p, K_d, and K_i are proportional, derivative, and integral terms respectively. K_p, K_d, and K_i are usually estimated theoretically and then fine tuned experimentally.

PID controllers are used in most cases when a single Mellinger and Kumar [2011] or multiple robot systems Preiss et al. [2017] are controlled. Mulgaonkar et al. [2015] presented a system with scaled-down micro-quadrotors, which helps increase the agile flight and swarming abilities. The authors presented a novel Pico quadrotor
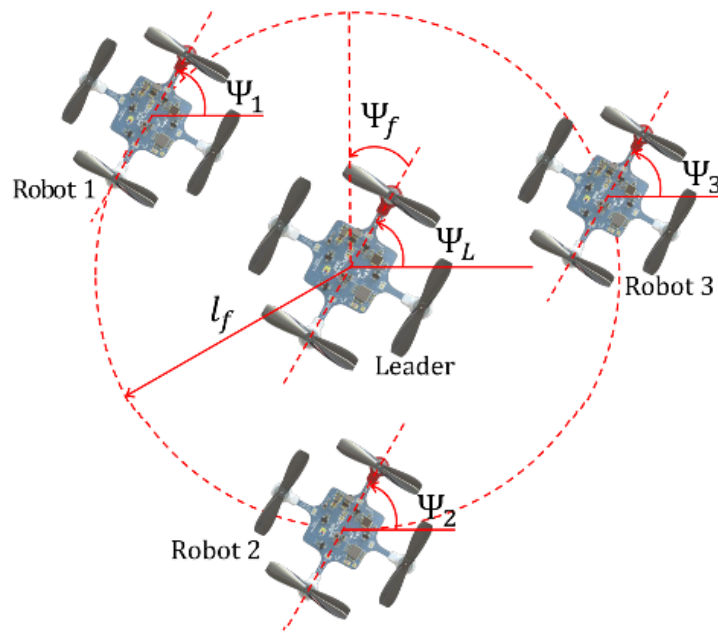
Figure 2-6: △-formation with a leader drone presented by Mulgaonkar et al. [2015]. Where Ψ_i for i in $[f, L, 1, 2, 3]$ are the formation, leader drone and following drones (1, 2,and 3) heading angles and l_f is the distance between the leader robot and the surrounding slave drones.

with the main flight controller board weight of 5 grams. Proportional-derivative (PD) controller receives the track state from the ground control station and performs the control input calculation onboard. The authors linearize the vehicle's dynamical model around the hover point and finally apply a traditional PD control. They used PD positional controller in order to perform △-formation flight, presented in Fig. 2-6.

Introducing a human into direct swarm control could enter disturbances into the formation flight, as shown by Goodrich et al. [2012]. Various types of control input devices (discussed in the next section) generate track position $x_{track}(t)$, or track velocity $\dot{x}_{track}(t)$, or track acceleration $\ddot{x}_{track}(t)$ of the agents in the fleet. The example is presented by Aggravi et al. [2018], where the displacement of the human's hand position is used to directly define the goal velocity vector of the leader drone in the simulated fleet (see Fig. 2-8). The problem is that when we have a direct relationship between the human control input and the $x_{track}(t)$, or $\dot{x}_{track}(t)$, or $\ddot{x}_{track}(t)$, rapid acceleration and deceleration can occur. This is happening because a

human is not able arbitrary to control his or here inputs commands (hand position in Aggravi et al. [2018]). The dynamics of the human control signal can be much faster than the dynamics of the current controlled system. Therefore, track trajectories are not feasible, and the controller of the robot is not able to follow them. The example of the goal trajectory generated by a human operator with the position of his hand is presented in Fig. 2-7. There is no guarantee that the guided vehicle can follow the set points. Therefore, we take this problem into account in the current work and consider it a research gap. The desirable trajectory has to be generated in a compliant manner, to make human-swarm interaction more smooth and safe, i.e., limiting rapid acceleration or deceleration. We will discuss in more detail which exact dynamical parameters we will use to evaluate the motion and how we measure them in Chapters 3 and 4. To make the current chapter more complete, we mention that for the smoothness measurement, we use acceleration (second derivative of position), snap (first derivative of acceleration), and jerk (second derivative of acceleration).

2.3.3   Compliant control

Implementation of the compliant control in the robotics field is discussed in this section.

According to Newman and Dohring [1991], Peng and Adachi [1993], Chan and Liaw [1996], the impedance control is widely used to archive a friendly and compliant interaction between the robots (such as robotic arms or manipulators) and the environment (including physical interaction with humans). The impedance of the mechanical system represents the relationship between the resistance force and applied motion. Therefore, by controlling the system's impedance, we control its resistance concerning the external motion. We discuss the general impedance control in Section 4.3 in more details.

Hogan [1984] has developed the traditional impedance control, which afterward was adopted by many researchers Albu-Schäffer et al.. Hogan [1984] declared that physical interaction requires the manipulator to be coupled with the moving object in a mechanical sense. The manipulator does not have to be considered as a standalone system during the interaction. The author demonstrated that the manipulation is
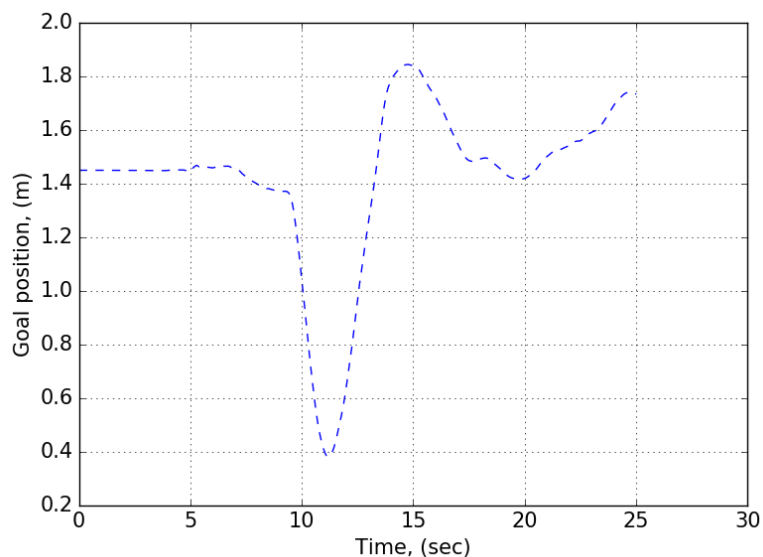
Figure 2-7: Goal trajectory generated by a human operator with position of his hand.
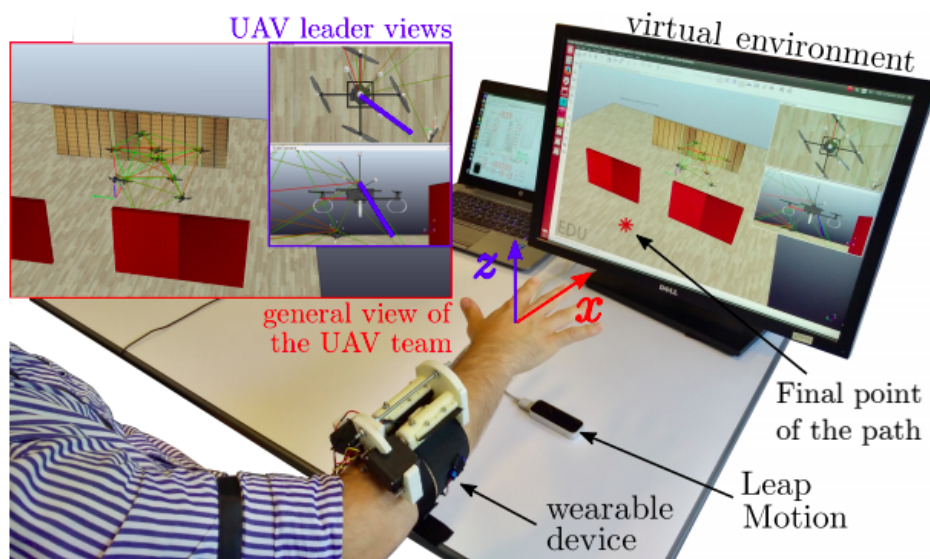
Figure 2-8: Human operator guides the simulated fleet of quadrotors with the position of a hand by Aggravi et al. [2018]

a non-linear process and that the position and force has to be controlled along with dynamic behavior. Hogan presented the feedback control that produces the desired impedance on the end effector of the robotic arm.

Tsetserukou et al. [2006] proposed to implement local impedance control at every joint of the humanoid robot (see Fig. 2-9(a)) in order to obtain stable and safe interaction. The research determined the dynamic relationship between position and force. The authors performed the impedance control with a torque sensor connected to every joint of the robotic arms of the controlled robot. The idea of the local impedance control is presented in Fig. 2-9(b).

Lippiello and Ruggiero [2012] implemented a Cartesian impedance control to successfully enhance a flight of a simulated UAV with a robotic arm onboard. The arm is supposed to interact with the environmental objects. The authors also established the dynamic relationship between the external force acting on the constriction and the robot's motion.

The problem is that traditional impedance control does not apply to facilitate the remote human operator's swarm control. In the following sections, we will implement a new position-based impedance control approach that can be used to enhance the relationship between the human operator and the guided swarm of robots.

2.4 Control Input from the Human Operator

In this section we will discuss the ways of receiving the control input commands from the human operator.

In order to deliver the control signals to the formation, a control input device is needed. A human operator could use a ground station, remote control with sticks, joystick, wearable devices, smartphones, tablets, and many other devices or even gestures to control and navigate the robots Cho et al. [2009], Micire et al. [2009], Matsuda [1998]. Listed approaches have many advantages and disadvantages.

Direct control of teleoperated devices and machines is mainly accomplished by using joysticks, which help users have straightforward guidance in remote and hazardous areas Funk [2018]. But still, the navigation of quadcopters with a joystick

a)   b)
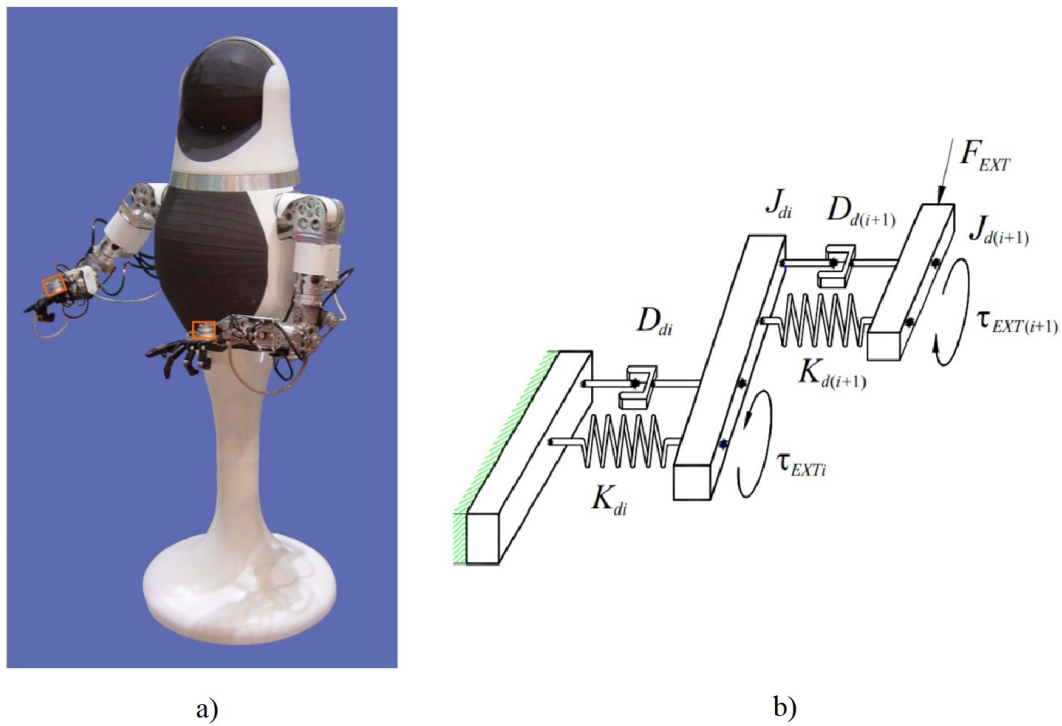
Figure 2-9: Local impedance control that was proposed by Tsetserukou et al. [2006], (a) Controlled robot with humanoid arms, (b) Impedance model. Where τ_{EXTi} is the torque that acts on joint i which is the result of external force F_{EXT}, J_{di} is the desired inertia, D_{di} is the desired damping, K_{di} is the desired stiffness

or a remote controller is a challenging task for many users. Authors in Katsumoto [2016] reproduce virtual anchoring effect in midair, replicating a regular table joystick. However, such an approach still requires holding a device all the time, limiting hands-free scenarios. Most of the control joysticks of teleoperated robots, such as quadcopters, are complicated and require additional training for non-expert users. In addition, a joystick is a handheld device that introduces further inconvenience for the user between interaction sessions. Within non-spacious environments in safety-critical scenarios, experiences and trained personnel are needed for guiding quadcopters through the predetermined flight paths Kosch et al. [2018].

In many applications, it is desirable not to carry any extra equipment by the operator. Gesture-based interactions could satisfy this requirement. In the gesture-based interface proposed by Podevijn et al. [2014], a swarm of ground robots receives commands from a human operator in the form of gestures, which are captured by an RGB-D Kinect camera. Gesture-based interfaces require a complex infrastructure setup, such as depth cameras Sanna et al. [2013], which limits the variety of possible applications and working area. The time spent on image acquisition and processing should be short to function in real-time.

Wearable devices are widely used to control remote or virtual vehicles. In Yuan et al. [2019], a human-assisted quadcopter navigation system was proposed where the user guides the robot through eye-tracker glasses. In order to intuitively operate a single drone, hand commands were proposed in [Aur, 2019]. Hand gestures were widely adopted in the research of human-robot interaction, and there is a wide variety of proposed approaches. For immersive drone control with hand gestures, Rognon et al. [2018] developed a soft upper body exoskeleton with goggles for the first-person view. In the gesture-based interface proposed by Podevijn et al. [2013], a swarm of ground robots receives commands from a human operator in the form of gestures, which are captured by a Kinect system. Gesture-based interaction requires a complex infrastructure setup, which narrows down the range of applications where it could be applied. In scenarios where the system extracts the gestures from an image, the user's background should be clear and straightforward so that the camera could quickly identify gestures. The time spent on image acquisition and processing

should be short to allow the system to function in real-time Chen et al. [2007].

Another possible option is to directly move one of the robots to control the others, as shown by Braley et al. [2018] in GridDrones. The authors highlighted how the swarm of drones could be controlled by directly holding and moving one of the quadrotors. The problem with this approach is that it is hard for the human to move the master drone smoothly. In addition, after the drone is released from the hand, it makes several quick movements to stabilize its position. These motions of the master could lead to unintended rapid accelerations of the slave robots.

In the current work, to keep the hardware simple and easy to use, we propose using the same wearable device (SwarmGlove) for both feedback and control input using a position-based approach. The wearable tactile device provides portability and, at the same time, addresses multiple purposes.

2.5 Tactile Feedback

Below we will discuss the state-of-the-art approaches of tactile feedback for robot guidance and control.

The most advanced control methods use closed-loop control. The control input or action is affected by some variable or state of the controlled process. The information from the controlled process is delivered to the controller in the way of feedback Doyle et al. [2013]. In the case of HSI, human plays the role of the high-level controller.

While guiding the robotic group, the human operator must be aware of changes in the fleet (e.g., extension and contraction) for better control. The importance of this fact increases with the number of robots. Although visual channels often suffer from poor quality (it is often overloaded), direct visual feedback or visual information presented with displays Gioioso et al. [2014] are common ways to deliver information about the formation to the operator.

On the other hand, haptics has also gained considerable attention in the research of human-swarm interaction, and various interaction methodologies have been proposed. Researchers started to investigate the sense of touch as a way of information transfer since the 1960s Geldard [1957, 1960]. Geldard [1957] proposed the first

tactile language - Vibratese. The area of the skin that can be stimulated is high. Besides, the tactile sensation can strongly grab human attention Jones and Sarter [2008]. Sense of touch can work in both directions - we can sense the environment that we touch, and at the same time, we can act on it Jones and Sarter [2008] (this is the main difference from vision sensation). One more interesting property of touch is that we can deliver information to a certain person, while the others are not aware of this communication. All of these factors contributed to the fast development of haptic devices. Our skin contains multiple types of receptors that can be activated by vibrotactile stimulation. In order to provide the proper sensation, researchers need to carefully select a necessary area of contact and vibration characteristics (frequency, amplitude, etc.).

Haptic feedback can improve the awareness of drone formation state, as reported in Il Son et al. [2011] and Stramigioli et al. [2010]. Tactile interfaces deliver information about swarm status just right to the skin. Scheggi et al. [2014] proposed a haptic bracelet with vibrotactile feedback to inform an operator about a feasible way to guide a group of ground mobile robots in terms of motion constraints. Tactile signals help the human operator to maintain the integrity of the guided team of mobile robots. An arm-worn tactile display for presentation of the collision of a single flying robot with walls was proposed in Spiss et al. [2017]. Vibrotactile signals improved users' awareness of the presence of obstacles. Aggravi et al. [2018] developed a wearable haptic display capable of providing a wide range of sensations by skin stretch, pressure, and vibrotactile stimuli. The authors evaluated the proposed device for the control of a fleet of ten simulated quadrotors. Haptic feedback delivered the information about the navigation directions and the connectivity (squeeze) of the fleet. Additional feedback improved almost all metrics of the experiment. In the robotic telepresence system developed by Tsetserukou et al. [2011], employing the laser range finders (LIDARs), the mobile robot precisely recognizes the shape, boundaries, movement direction, speed, and distance to the obstacles. The tactile belt delivers detected information to the user who regulates the movement direction and speed of the robot through the body stance (torso of the operator works as a joystick). The projects mentioned above demonstrate that kinesthetic Wang et al.
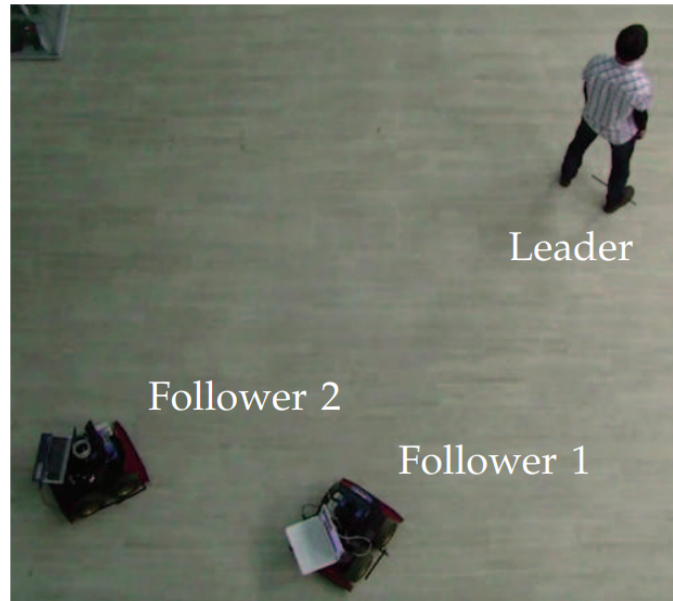
Figure 2-10: Guidance of mobile robots using tactile and visual feedback presented by Scheggi et al. [2014].

[2018] and tactile feedback Pacchierotti et al. [2017] can be effectively applied for the control and interaction with drones.

Haptic feedback also can be provided by drones and used to control other robots, as shown by **Evgeny Tsykunov** and Tsetserukou [2019]. Along with that, there are several research projects related to providing encountered-type kinesthetic and tactile feedback in VR via drones. As a result, drone technology is used to improve the human operator's immersion into different interaction scenarios. In Hoppe et al. [2018], an object or surface is connected to the drone, which is supposed to be touched by a human to deliver passive or active tactile feedback. Authors in Knierim et al. [2017] also propose to hit the user with some object connected to a small drone to provide a haptic sensation. Abdullah et al. [2018] also offered to push or pull the drone in $Z - axis$ direction to simulate force feedback for direct interaction. Abtahi et al. [2019] developed a more complicated scenario that incorporates rich interactions, including passive force feedback and texture mapping. The main limitations of the proposed solutions include low sensation resolution, instability during an interaction, low impact force, and a drone's big size. In particular, authors in Abdullah et al. [2018], Abtahi et al. [2019] selected bigger size drones. Usually, the spacial motion of human hands is fast. Although more powerful quadrotors could

provide more noticeable force feedback, they could be slow for certain applications. It is also hard to combine different types of feedback at the same time because there is not enough space for drones near the fingers.

Although there might be some advantages of haptics devices, such as getting extra information in addition to the visual channel, they have several limitations. Haptics usually requires additional equipment to set up Yang et al. [2004], which in turn makes it hard to implement in particular applications. In comparison with visual and audio feedback, low bandwidth channel for information transfer makes tactile feedback less informative Cruz-Hernandez [2011]. For example, the user might want to get altitude status and obstacle warning at the same time. In some highly demanding cases, when a person cannot focus on his/her sensory input, the stimulus might not be felt well Spirkovska [2005]. To address these issues, the design of haptics devices have to be simple and robust. The tactile stimulus has to be as clear for the user as possible. It is possible to successfully overcome the limitations by designing tailored and optimized haptic displays.

Although using the vibration motors is a common way to provide cutaneous feedback Pacchierotti et al. [2017], in contrast to state of the art, in the current work, we propose a tactile display SwarmGlove that was tailored-made for the specific application of swarm control. Vibration motors were located at each fingertip to achieve a higher recognition rate of the patterns. Positioning was provided with the integration of infrared reflective markers, which is used to generate control input. Reliable communication between the SwarmGlove and the ground control station for the distance up to 1.2 km was achieved through radio module XBee Pro s2b. Communication is needed to make a glove a wearable interface for convenient swarm control.

2.6 Deployment of Swarm of Drones

The current section will explain the challenges of takeoff and landing sub-operations along with state-of-the-art approaches to these problems.

If we consider the overall flight mission, takeoff and landing always come before

and after the actual flight. In other words, takeoff and landing are the essential sub-operations of any flight. That is true for piloted air crafts and autonomous or guided flying robots of any size. As reported by Attaccalite et al. [2012], many crashes of airplanes happen during takeoff and landing operations. Vertical takeoff and landing (VTOL) flying robots also likely to perform poorly because of their inability to land in a specific environment with unusual conditions. For example, a landing of the helicopter on the unstable ship deck in the rough sea can lead to the dynamic rollover. The strong wind blowing over rough terrain is another dangerous factor, which can result in the same consequences during landing. Also, it is almost impossible and hazardous to land on the steep slope in the mountains, even for modern helicopters. Indeed, takeoff and landing imply physical interaction with the ground, which increases the risks, especially for autonomous air crafts.

Small size quadrotors have a limited set of options to address the takeoff and landing challenge. To solve the problem, we propose a novel interaction strategy SwarmCloak to land multiple micro quadrotors on the human hands using vibrotactile feedback. Human can significantly reduce the complexity of the aerial platform, proving a cheaper way (both in terms of hardware design and computational complexity) to perform a safe landing in any environmental conditions where the human is able to get himself or herself.

While large drones Augugliaro et al. [2014], Loianno and Kumar [2018] are capable of lifting high-performance vision and processing systems for autonomous takeoff and landing, the swarm of micro-quadrotors cannot process the visual data autonomously at the same level. In many cases, the actual flight of drones often does not require a precision perception system, and, therefore, an autonomous flight can be easily accomplished with limited sensing capabilities, such as GPS or Ultra Wide Band (UWB) radios Nithya and Rashmi [2019]. However, takeoff and landing operations often require an accurate localization García-Pulido et al. [2017], Olivares-Mendez et al. [2013], and mapping, which could be a problem for micro-quadrotors due to limited payload and therefore small computational capabilities.

Special landing gears are used to ensure a safe landing for VTOLs, as reported by Mason [1974]. Fig. 2-11 shows the example of a robotic landing gear for a helicopter

Figure 2-11: Robotic landing gear by Kiefer et al. [2016].

developed by Kiefer et al. [2016]. Fig. 2-11 demonstrates how the helicopter performs landing with the usage of an adaptive landing gear. Landing gear represents a mechanical system with moving joints, which contributes to the additional weight of the system. Simulation and control strategy for robotic landing gear is described in Goh et al. [2016]. Amazon patented adjustable landing gear with telescoping legs for UAV Gentry [2017]. The main limitation of the application of landing gears for small UAVs is limited payload capabilities. The Crazyflie 2.0 quadrotor can lift just several grams of additional payload. This is a significant constrain when we want to reach the landing on the uneven unprepared surface.

Hence, the human could supplement these challenging swarm operations (takeoff and landing) for small flying robots. However, interaction strategies for such cases have not yet been appropriately considered, especially when more than one drone has to be landed at the same time. For the human operator, it is often easier and faster to catch a small size quadrotor right in the midair instead of landing it on a surface in autonomous mode. The reasons for this could be multiple. For the outdoor applications, the landing surface is usually uneven and dusty, which could lead to a crash of the swarm. Even when the landing spots (helipads) are provided, autonomous landing is not always the best solution due to position estimation errors, robustness, or high cost of a positioning system. On the other hand, the human can try to catch the drones from the formation while the fleet is descending. Nevertheless, this scenario could be dangerous both for the human and robots if the number of robots is more than one.

Although the HSI is well developed, as reported in Kolling et al. [2016], to my knowledge, up until now, there are no technologies and research on how to promptly

deploy and land the swarm of drones using the human body. Hence, a robust interaction strategy has to be developed.

Tactile feedback for interaction with robots has been widely investigated, as discussed in the above section 2.5. Based on that, we propose a SwarmCloak technology that helps deploy multiple drones from the human body using a wearable tactile display. In particular, we define the role of tactile feedback in such a way, that it helps to localize the position of the deploying drones with respect to the landing pads.

2.7 Summary

In this chapter, we presented an existing research related to the topic of this work. We also defined the research gaps.

We covered the existing control methods which is topically used for the swarm of drones operation. The literature review revealed that generation of control signals and the swarm response to the control commands are crucial parts of the control strategy. The state of the art control strategy for drones is the PID controller (when the drones strictly following the corresponding goal positions). It works well until the human is involved in the direct control of the robotic formation. Various disturbances can happen in this case because the human is not able to generate dynamically feasible control signals. Reviewing state-of-the art, no strategy considers the adaptive behavior of the guided fleet of micro-quadrotors, helping to get a smooth and safe response of the robots in various conditions. Along with that, we showed that impedance control is widely used in industrial manipulators and humanoid robotics to ensure safe interaction between the robot and the environment.

Apart from that we considered the haptic feedback that is used for the interaction of a human with robotic systems. To enhance the interaction with the robotics group, the operator has to be aware of the current state of the controlled system. For example, the operator needs to know if the fleet is split into two groups while avoiding obstacle or if the team is squeezed and drone-to-drone distances is decreasing. This is hard to achieve when the number of robots is high or when the visual feedback is poor due to the significant distance or communication problems. We hypothesize

that the tactile feedback can enhance or even sometimes fully replace the visual feedback.

Finally we discussed the deployment challenges and existing solutions along with its limitations. To complete a flight mission, the swarm of drones has to take off in the beginning and land in the end. Many crashes happening during these stages that is why we consider it as an important part of HSI. Adaptive landing gears substitute the landing and takeoff operations on the uneven surfaces. The problem is that, due to the lack of payload abilities of micro-quadrotors, it is almost impossible to carry the adaptive landing gear or significant computational power that can help to land. Up until now, no technology safely lands multiple micro-quadrotors on the uneven surface in the unprepared environment.

Chapter 3

Thesis Objectives

In the Introduction chapter, we provided the context to the modern Human-Swarm Interaction. In the previous chapter, we discussed the background and related work and the research gaps definition. In the current chapter, we define the main objectives of this work and provide the research questions.

3.1 Thesis Goal

This thesis aims to advance the field of human-swarm interaction in terms of guidance and deployment in complex environments by using impedance control and tactile feedback.

An example of such an environment can be dense and quickly changing urban areas or remote locations with a lack of infrastructure. We discussed the challenges related to the environmental conditions in the Introduction Chapter.

The thesis contributes to the HSI by ensuring safe, smooth, and scalable guidance with full awareness of the swarm state. Besides, the thesis presents a novel deployment method that fulfills the guidance and makes HSI more complete. The details are presented in the below Section 3.2.

By the deployment, we mean takeoff and landing. We intentionally outline two sub-stages of the drone operation: deployment and guidance. On one side, these sub-stages look different. But, in practice, they address the same goal and share some universal principles of operation. Besides, deployment and guidance overlap

in time. For example, while the drones take off, the transition to the guidance mode is already in progress.

3.2 Research Questions

3.2.1 Control of Drones

The literature review demonstrated in subsections 2.3 and 4.16 revealed that the generation of control signals and the swarm response to the control commands are crucial parts of the control strategy. When the human is involved in the direct, high-level control of the robotic formation, various disturbances can happen. Considering the state-of-the-art, no strategy considers the adaptive behavior of the real fleet of micro-quadrotors, helping to get a smooth and safe response of the robots in various conditions. Along with that, we showed that impedance control and potential fields are widely used in industrial manipulators and humanoid robotics to ensure safe interaction between the robot and the environment. We hypothesize that the impedance control will help to generate and follow dynamically feasible trajectories that adapt to the human control input, ensuring safe interaction. For the obstacle avoidance strategy, we consider using the potential fields.

Based on the above statements, we formulate the first research question as follows.

> **Research Question 1**: How to achieve smooth, safe, and scalable control of a group of drones by a human operator using impedance control and artificial potential fields?

As discussed by Flash and Hogan [1985], who investigated the human hand movement, the smoothest hand motion is achieved under a particular objective. The authors demonstrated that the most optimal trajectory is obtained when the jerk (first derivative of acceleration) is minimal over the entire motion. On the other hand, Mellinger and Kumar [2011] shown that in order to minimize different constraints, such as velocity, acceleration, and control input, it is necessary to use

higher-order derivatives of the position for the objective function (such as snap or the second derivative of the acceleration). Therefore, to measure the flight's smoothness, we propose to measure such dynamic parameters as acceleration, jerk, and snap. We will discuss it in details through the thesis and in section 4.1 in particular. The proposed control method does not have to introduce limitations when we scale the number of robots in the team to hundreds of agents.

By the safety, we mean the generation of dynamically feasible trajectories and the lack of collision. Smooth paths contribute to the safety of the mission since optimal trajectory limits control inputs and, therefore, increases flight stability. On the other side, safety also achieved via adaptive distances between the agents (the higher velocity, the more distance). In addition, the drone-to-drone range also has to change smoothly following the human control commands. Finally, a robust obstacle avoidance algorithm has to be implemented on the top of the smooth trajectory generation.

Contribution and Novelty

It represents a hard problem to propose a continuous control method that can address all issues described above at the same time. To enhance scalability and robustness, we do not consider applying the combination of control methods of different properties to meet all the above objectives. Instead, to answer the research question, we developed a new control paradigm where we propose a novel impedance control approach. The aim of application of the impedance control is to establish the dynamic relationship between the controlled object and the human control input. Traditional impedance control presented by Hogan [1984], used to enhance the physical interaction between the robotic arms and the environment. But when the operator guides the formation of aerial robots in space, there is no point of contact, and therefore, we cannot calculate the force that can be applied to the mass of the impedance model. To solve the problem, we introduce a new impedance control approach where force is calculated with respect to the human control input. The impedance model generates the desirable and feasible trajectory which reacts to the human hand motion in a compliant manner, avoiding rapid acceleration and de-

celeration. The comparison with the state-of-the-art PID controller demonstrated that we improved the dynamical parameters of the motion. The architecture of impedance models helps to get adaptive geometry changing, which contributes to the safe flight. The potential field helps to avoid collision with other agents and external obstacles.

3.2.2   Tactile Feedback about the State of the Swarm

As discussed above in the subsection 2.5, to enhance the interaction with the robotics group, the operator has to be aware of the current state of the controlled system. This is hard to achieve when the number of robots is high or when the visual feedback is poor due to the significant distance or communication problems. We hypothesize that the tactile feedback can enhance or even sometimes fully replace the visual feedback. In subsection 2.5, we demonstrate that haptic sensation plays a vital role in the perception of the human. Based on that, haptics is actively used for Human-Robot interaction. But haptic displays have several limitations, such as low information bandwidth. In order to overcome the barriers, haptic hardware devices have to be carefully designed. Considering state-of-the-art, there is no tactile wearable interface finely tuned for prompt swarm sensing during operation in a cluttered environment.

Hence, we formulate the second research question as follows.

Research Question 2: How to provide a human operator with static and dynamic parameters of the swarm using wearable display and tactile feedback?

The human has to be aware of the critical parameters of the swarm state, and it has to help him to make control decisions. Tactile patterns have to be intuitive, and it has to be recognizable in 80% of the cases. The tactile device has to be tailored for the swarm guidance in real-time and do not inconvenience the operator or limit his or her motions. Tactile feedback has to provide enough information to complete the guidance on a cluttered environment without visual feedback. The proposed tactile feedback does not have to introduce limitations when we scale the number of

robots in the team to hundreds of agents.

Contribution and Novelty

In contrast to state of the art, we propose to design a tailored vibrotactile wearable display SwarmGlove for the interaction of the human with a real swarm of aerial robots by providing an intuitive mapping of the formation state to the human finger pads. Human palm have flat and wide contact area with rich tactile resolution which helps to deliver relevant information Weinstein and Weinstein [1964]. It is often easier to estimate the parameters of the whole robotic group (e.g., dimensions, velocity) rather than map all the drones' environments. The main novelty is that we propose to deliver tactile feedback about the state of the swarm rather than about the distance to obstacles or the desired direction of motion. We designed tactile feedback to convey information about the formation parameters that are hard to estimate from the visual feedback, i.e., formation state (extension, contraction, and displacement) and state propagation direction (increasing or decreasing drone-to-drone distance). Therefore, tactile cues could effectively supplement the visual channel, making the swarm control more immersive. Cutaneous feedback could play a key role in enhancing the swarm navigation performance in the unstructured environment, such as cities.

3.2.3 Fusion of the Control and Feedback into the Interface

To validate the developed approaches, we fused both control and feedback in the final flight experiments to come up with the interface. We implemented a small-scale unstructured environment to test the real flight of a fleet of three drones guided by a human. The results demonstrated that the tactile feedback allows us to guide the formation of drones thought the set of obstacles maintaining the desired formation parameters.

Both control and feedback parts fulfill each other. In the control part, we propose the algorithm, which is changing the swarm static and dynamic parameters to maintain smoothness and safe formation flight. These changes have to be under control - that is another reason (in addition to the obstacles avoidance) why we need

to provide feedback to the human.

3.2.4   Deployment of Drones from the Human Hands

We discussed in section 2.6 that to complete a flight mission, the swarm of drones has to take off in the beginning and land in the end. Due to the lack of computational abilities, the problem is that it is almost impossible to land safely for the micro-quadrotors. Until now, no technology safely lands multiple micro-quadrotors in the uneven surface in the unstructured environment.

Thus, we formulate the third research question as follows.

> **Research Question 3**: How to use a human body to supplement a deployment of a fleet of micro-quadrotors in any environment by using tactile feedback?

Tactile feedback has to enhance the visual channel. As a result, the positional error during the deployment has to be decreased. The landing with pure tactile feedback has to be achieved.

Contribution and Novelty

To solve the problem, we propose that the human operator supplement the takeoff and landing operation using a novel vibrotactile wearable display SwarmCloak. The user will use his/her arms to deploy drones. Proposed technology allows us to launch drones in any remote area without any infrastructure. Human-Swarm Interaction field is well developed, but, to our knowledge, up until now, there are no technologies and research on how to promptly take off and land the swarm of micro-drones in any location using the human body.

We also consider the strengths of the SwarmCloak compared to the autonomous landing platforms, where the robust controller incorporating the accurate position information could accomplish a precision landing. Autonomous landing requires a complex infrastructure that should include a position estimation system, e.g., motion capture system with infrared (IR) markers or regular cameras with visible markers, which has to track all landing pads with centimeter accuracy. Such positioning

systems can be expensive or not reliable. Additionally, ground-based positioning systems are bulky and require additional communication channel with the drones. On the other hand, in the proposed approach, the formation only has to roughly estimate the human's position within the reachable area by the human hands to land vertically. We applied a Vicon motion capture system to provide sub-millimeter accuracy of drone and hand position detection during the experiment.

3.3   Summary

In the current chapter, we defined three research questions related to adaptive control, clear feedback and deployment in any environment. In order to do that we highlighted the technical gaps revealed in the previous chapter. Finally after every research question we explained our contribution and its novelty.

Chapter 4

Control Strategy for the Swarm Guidance

In this chapter, we overview the set of proposed control methods for the HSI. We describe the way we define the control objectives and generate the control input commands. We discuss the relationship between a control input signal and a swarm motion. We evaluated the proposed approaches both from the theoretical and experimental perspectives.

4.1 Control Objectives

First of all, we have to define the objectives that we want to achieve by developing control methods. The objectives suppose to help to generate more smooth and safe trajectories. The requirement to the objectives is that it has to be valid for any quadrotor, with any size or component selection. In this section, we will derive the equations of motion of the quadrotor. Then we discuss the typical controller design. Finally, based on the dynamic model and controller, we highlight the desired objectives.

4.1.1 Quadrotor Equations of Motion

We define two coordinate systems: world coordinate system W and body coordinate system B. The body coordinate system B is rigidly connected to the quadrotor
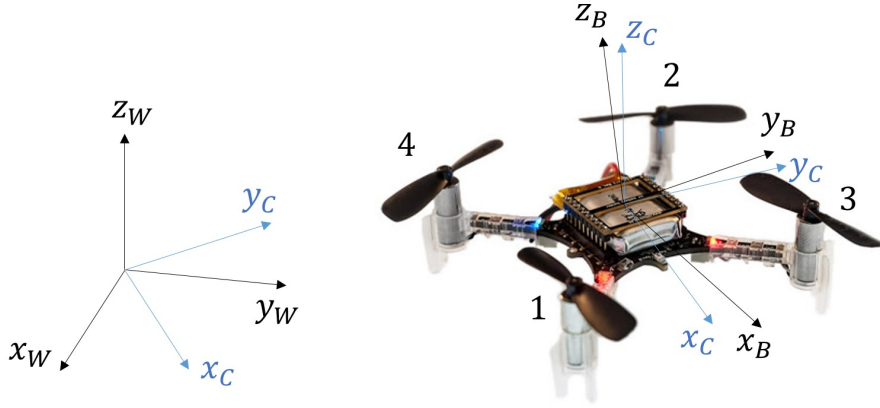
Figure 4-1: World W and body B coordinate frames.

center of mass. Euler angles (roll, pitch, and yaw) are utilized to formulate the orientation of the robot in the W coordinate frame. The coordinate frames are presented in Fig. 4-1.

The relative rotation from body to world coordinate system $^{W}R_B$ is obtained sequentially. In order to do that we introduce intermediate coordinate system C (shown in blue in Fig. 4-1). Therefore, the rotation from B to W frame can be expressed as

$$^{W}R_B = {}^{W}R_C{}^{C}R_B \tag{4.1}$$

We first rotate around $\mathbf{z}_W$ by yaw angle (ψ), then rotate around intermediate axis $\mathbf{x}_C$ by roll angle (ϕ), and finally by rotation about $\mathbf{y}_B$ axis by the pitch angle (θ). We do not provide intermediate rotation matrices. The final rotation matrix from body to world coordinate frame is expressed as

$$^{W}R_B = \begin{bmatrix} c\psi c\theta - s\phi s\psi s\theta & -c\phi s\psi & c\psi s\theta + c\theta s\phi s\psi \\ c\theta s\psi + c\psi s\phi s\theta & c\phi c\psi & s\psi s\theta - c\psi c\theta s\phi \\ -c\phi s\theta & s\phi & c\phi c\theta \end{bmatrix}, \tag{4.2}$$

where $c\psi$ and $s\psi$ is defined as $cos(\psi)$ and $sin(\psi)$ respectively. The same is true for θ and ϕ.

Angular speed of the quadrotor body with respect to the world coordinate frame W is defined as

$$\omega_{BW} = p\mathbf{x}_B + q\mathbf{y}_B + r\mathbf{z}_B, \tag{4.3}$$

where p, q, and r are the angular velocity components in B frame.

Angular velocities of the robot in the B frame have a direct relationships with the first derivatives of roll, pitch, and yaw angles

$$\begin{bmatrix} p \\ q \\ r \end{bmatrix} = \begin{bmatrix} c\theta & 0 & -c\phi s\theta \\ 0 & 1 & s\phi \\ s\theta & 0 & c\phi c\theta \end{bmatrix} \begin{bmatrix} \dot{\phi} \\ \dot{\theta} \\ \dot{\psi} \end{bmatrix} \tag{4.4}$$

Propellers of the quadrotor rotate with angular velocity ω_i. As a result, each propeller produces force F_i and moment M_i which can be described as

$$F_i = k_F \omega_i^2, M_i = k_M \omega_i^2, \tag{4.5}$$

where force F_i is pointed upwards along z_B direction and moment M_i is also applied about z_B axis.

Typical quadrotor dynamics is relatively slow comparing to the propeller dynamics. Therefore, for the simplicity, it is usually assumed that desired forces F_i and moments M_i can be reached instantly. As a result, control inputs generated by four rotors can be described as

$$\mathbf{u} = \begin{bmatrix} u_1 \\ u_2 \\ u_3 \\ u_4 \end{bmatrix} = \begin{bmatrix} k_F & k_F & k_F & k_F \\ 0 & k_F l_2 & 0 & -k_F l_4 \\ -k_F l_1 & 0 & k_F l_3 & 0 \\ k_M & -k_M & k_M & -k_M \end{bmatrix} \begin{bmatrix} \omega_1^2 \\ \omega_2^2 \\ \omega_3^2 \\ \omega_4^2 \end{bmatrix}, \tag{4.6}$$

where l_i is the distance between the center of mass of the robot and the corresponding motor, u_1 is the thrust acting along the $\mathbf{z}_B$, and u_2, u_3, u_4 are the robot moments acting along the $\mathbf{x}_B, \mathbf{y}_B$, and $\mathbf{z}_B$ axis respectively.

We also defined the u_1 as a net force acting on the body of quadrotor along the direction of z_B axis

$$F = u_1 = F_1 + F_2 + F_3 + F_4 \tag{4.7}$$

Net moment acting on the body of quadrotor also can be defined with the fol-

lowing equations

$$M = r_1 \times F_1 + r_2 \times F_2 + r_3 \times F_3 + r_4 \times F_4 + M_1 + M_2 + M_3 + M_4 \qquad (4.8)$$

Assuming that r is the vector of the position of the robot center of mass in the W frame we use (4.7) and Newton's equations to get linear accelerations

$$m\ddot{\mathbf{r}} = \begin{bmatrix} 0 \\ 0 \\ -mg \end{bmatrix} + {}^W R_B \begin{bmatrix} 0 \\ 0 \\ u_1 \end{bmatrix} \qquad (4.9)$$

We obtained the result based on the assumption that only gravity force and motor forces are acting on the body of the robot.

We use (4.8) and Euler equations to obtain the angular acceleration of the quadrotor in the following way

$$I \begin{bmatrix} \dot{p} \\ \dot{q} \\ \dot{r} \end{bmatrix} = \begin{bmatrix} u_2 \\ u_3 \\ u_4 \end{bmatrix} - \begin{bmatrix} p \\ q \\ r \end{bmatrix} \times I \begin{bmatrix} p \\ q \\ r \end{bmatrix}, \qquad (4.10)$$

where I is the matrix of the moment of the body inertia, $u_2 = r_2 \times F_2 - r_4 \times F_4$, $u_3 = r_3 \times F_3 - r_1 \times F_1$, and $u_4 = M_1 - M_2 + M_3 - M_4$. Robot body moments u_2, u_3, u_4 act along the $\mathbf{x}_B, \mathbf{y}_B$, and $\mathbf{z}_B$ axis respectively.

4.1.2 Control Loops

The dynamics of the quadrotor is non-linear. Typically, the equations of motion are linearized near the hovel point, i.e., when the roll and pitch angles are close to zero. As a result, the controllers are obtained using a linearized dynamic model. Such kind of approach is the most common one, both in academia and in the industry. We also notice that near the linearization point we get $\dot{\phi} \approx p, \dot{\theta} \approx q, \dot{\psi} \approx r$.

We already discussed in the Chapter 2 that the controllers are typically designed using the nested control loops, as shown in Fig. 4-11.

Attitude Controller

Considering (4.10) we can assume that the products of inertia are close to zero and due to symmetry we have $I_{xx} \approx I_{yy}$. Then we can derive

$$I_{xx}\dot{p} = u_2 - qr(I_{zz} - I_{yy}) \tag{4.11a}$$

$$I_{yy}\dot{q} = u_3 - qr(I_{xx} - I_{zz}) \tag{4.11b}$$

$$I_{zz}\dot{r} = u_4 \tag{4.11c}$$

The other typical assumption is that r, which is angular velocity along the z_B axis, in (4.11a) and (4.11b) is relatively small, compared to other angular speed components. This assumption is made based on the fact that, during quadrotor motion, the rate of change of yaw angle is typically much smaller compared to the roll and pitch angle changes.

Attitude controller represent an inner loop (Fig. 4-11), which accepts data from position controller and from the onboard inertia-measurement unit (IMU). As an output, attitude controller generates the desired moments $u_{2des}, u_{3des}, u_{4des}$.

Taking all being said into consideration we apply PD controller to calculate the desired moments

$$u_{2des} = K_{p,\phi}(\phi_{des} - \phi) + K_{d,\phi}(p_{des} - p) \tag{4.12a}$$

$$u_{3des} = K_{p,\theta}(\theta_{des} - \theta) + K_{d,\theta}(q_{des} - q) \tag{4.12b}$$

$$u_{4des} = K_{p,\psi}(\psi_{des} - \psi) + K_{d,\psi}(r_{des} - r) \tag{4.12c}$$

Position Controller

In order to supply the attitude controller with the desires angles we use position controller. Position controller is used to calculate the command linear accelerations $\ddot{r}^i_{des}$ in the following way

$$\ddot{r}^i_{des} = \ddot{r}^i_{track} + K^i_p(r^i_{track} - r^i) + K^i_d(\dot{r}^i_{track} - \dot{r}^i) + K^i_i\int(r^i_{track} - r^i)dt, \tag{4.13}$$

where r_{track}^i is the desired position that we want to track, r^i is the current actual position. The desired position forms a trajectory $r_{track}^i(t)$. For the slow motion $\ddot{r}_{track}^i$ can be small or even equal to zero.

In order to obtain the relationship between the desired acceleration and the Euler angles we linearize (4.9)

$$\ddot{r}_{des}^1 = g(\theta_{des}cos(\psi_{track}) + \phi_{des}sin(\psi_{track})) \tag{4.14a}$$

$$\ddot{r}_{des}^2 = g(\theta_{des}sin(\psi_{track}) - \phi_{des}cos(\psi_{track})) \tag{4.14b}$$

$$\ddot{r}_{des}^3 = \frac{u_{1des}}{m}, \tag{4.14c}$$

where ψ_{track} is the yaw angle that we want to track.

In order to obtain the desired Euler angle for the (4.12) we invert (4.14)

$$\phi_{des} = \frac{\ddot{r}_{des}^1 sin(\psi_{track}) - \ddot{r}_{des}^2 cos(\psi_{track})}{g} \tag{4.15a}$$

$$\theta_{des} = \frac{\ddot{r}_{des}^1 cos(\psi_{track}) + \ddot{r}_{des}^2 sin(\psi_{track})}{g} \tag{4.15b}$$

$$u_{1des} = m\ddot{r}_{des}^3 \tag{4.15c}$$

4.1.3 Objectives

Our ultimate goal is to achieve smooth behaviour of the controlled quadrotors. In order to have smooth motion of the quadrotor we want the control input to be minimized.

To derive the control objective, we investigate the relationships between the control inputs and the goal positions.

Considering (4.15), we can see that the u_{1des} can be calculated as a second-order derivative of the position. On the other hand, we can observe that the control inputs u_{2des} and u_{3des} are functions of the fourth derivatives of the positions. As a result, the objective is to obtain the motion trajectories that minimize the second (acceleration) and fourth (snap) derivatives of the positions.

As discussed by Flash and Hogan [1985], who investigated the human hand

movement, the smoothest hand motion is achieved under a particular objective. The authors demonstrated that the most optimal trajectory is obtained when the jerk (first derivative of acceleration) is minimal over the entire motion of a hand. Although the optimal movement is impossible to achieve in real-life experiments, we also propose considering the minimization of the jerk or third derivative of position as the objective for the proposed control method.

In conclusion, we will calculate the acceleration, jerk, and snap of the position over the entire duration of motion for the comparison of the proposed control methods with state-of-the-art control strategies. We demonstrated that the current objectives are valid for any type or quadrotor of any size or component set. Selected objectives help to generate more smooth and safe trajectories for the formation flight. In the following sections, we will present our novel impedance control approach that allows us to satisfy the proposed objectives.

4.2   Control Input

For the control input generation coming from the operator, we propose to use a human hand. We refer to Chapter 5, where the human hand will be used to deliver tactile feedback. Based on that, we intend to use it also to define a control input signal. To keep the experimental part simple (held indoors), we use the displacement of the hand with respect to its initial position for the control signal calculation. The leading drone repeats the glove trajectory with a spatial *scale* coefficient while being guided by a human operator.

$$\mathbf{X}_g = scale \cdot \mathbf{H}, \tag{4.16}$$

where $\mathbf{X}_g \in \mathbb{R}^3$ represent the position of the center of mass of the leading quadrotor that it has to track, $\mathbf{H} \in \mathbb{R}^3$ represent the human hand position. Both $\mathbf{X}_g$ and $\mathbf{H}$ are in world coordinate frame.

The details of the control signal generation will be disclosed in the current Chapter below. We will also discuss alternative methods that allow us to exclude the hand position estimation (can be applied to various applications, including outdoor).
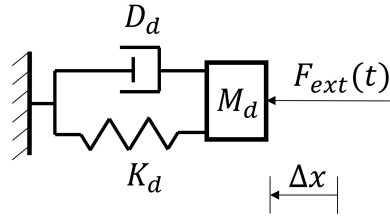
Figure 4-2: Second-order impedance model with mass-spring-damper elements.

4.3   Impedance Control for Trajectory Generation

The typical impedance control applications include the physical interaction of robotic systems, such as manipulators, with the environment. The impedance of the mechanical system represents the relationship between the resistance force and applied motion. Therefore, by controlling the system's impedance, we control its resistance with respect to the external motion. On the other hand, admittance is the inverse of impedance - it describes the motions that are the output from a force input.

The graphical presentation of the typical impedance model used for control is given in Fig. 4-2. Where M_d is the desired mass of the virtual body, D_d is the desired damping, and K_d is the desired stiffness, Δx is the difference between the current x^c_{imp} and default x^d_{imp} position, and $F_{ext}(t)$ is an external force, applied to the mass. Considering the Fig. 4-2 the impedance can be defined as a relationship between the force and velocity. When we consider the physical interaction of the robot with the environment, we usually estimate the $F_{ext}(t)$ with a force sensor.

New Impedance Control Approach

The impedance control application aims to establish the dynamic relationship between the position of the controlled object and the human control input. In the case of aerial robot guidance, we do not have a point of contact with the environment. As a result, there is no real force that can be applied to the virtual mass of the impedance model (highlighted in Fig. 4-2). Therefore, we have to change the traditional impedance control approach. We establish the virtual relationship between the human control input and the force.

To allow the human operator to change the formation shape and dynamics while
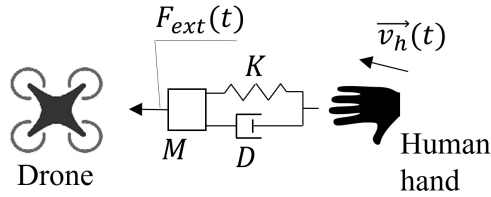
Figure 4-3: Relationship between the human hand velocity $v_h(t)$ and the virtual force $\mathbf{F}_{ext}(t)$.

navigating, we propose to calculate the external force term $\mathbf{F}_{ext}(t)$ (shown in Fig. 4-3) as a function of some human state parameter. In the thesis, for the control input, we use a human hand. Therefore, we calculate the external force as a function of the human hand's velocity $v_h(t)$. This new relationship helps to obtain a novel impedance model that we propose.

$$\mathbf{F}_{ext}(t) = K_v \frac{\mathbf{dH}}{dt} = K_v v_h(t), \tag{4.17}$$

where K_v is a scaling coefficient, which determines the effect of the human hand velocity $v_h(t)$ on the controlled system. To estimate the human hand's velocity, we assume that it is possible to track the hand motion with some positioning system. During the experimental evaluation, we used the Vicon motion capture system for localization.

To calculate the resulting setpoint, we integrate the goal position coming from the human with calculated displacement of the impedance model Δx. After that, we feed the setpoint (based on the human input with impedance correction) to the PID controller and ask it to generate the control signal for the robots, which helps us maintain the target position of the drone. The hand of the human operator controling a drone via an impedance model are shown in Fig. 4-3.

Mathematical Approach to Impedance Control

In order to calculate the impedance correction term for the robots' goal positions, we solve a second-order differential equation (4.18) that represents the impedance model. To move in three-dimensional space, we have to solve one differential equation for every axis. Here we present the solution for the X axis

$$M_d \Delta \ddot{x} + D_d \Delta \dot{x} + K_d \Delta x = F_{ext}^x(t), \tag{4.18}$$

where M_d is the desired mass of the virtual body, D_d is the desired damping, and K_d is the desired stiffness, Δx is the difference between the current x_{imp}^c and desired x_{imp}^d position, and $F_{ext}(t)$ is an external force, applied to the mass. It is well known that by selecting the desired dynamics parameters for the impedance model, we can achieve various behavior of the oscillator, described by (4.18), undamped, underdamped, critically damped, and overdamped.

We introduce two state variables: position $x(t) = \Delta x$ and velocity $v(t) = \Delta \dot{x}$. Based on that, state space representation of (4.18) has the form:

$$v(t) = 0 \cdot x(t) + 1 \cdot v(t) + 0 \cdot F_{ext}(t)$$
$$\dot{v}(t) = (-\frac{K_d}{M_d})x(t) + (-\frac{D_d}{M_d})v(t) + (\frac{1}{M_d})F_{ext}(t) \tag{4.19}$$

The matrix form of (4.19) has the form:

$$\begin{bmatrix} v(t) \\ \dot{v}(t) \end{bmatrix} = A \begin{bmatrix} x(t) \\ v(t) \end{bmatrix} + BF_{ext}(t), \tag{4.20}$$

where $A = \begin{bmatrix} 0 & 1 \\ -\frac{K_d}{M_d} & -\frac{D_d}{M_d} \end{bmatrix}$, $B = \begin{bmatrix} 0 \\ \frac{1}{M_d} \end{bmatrix}$. In discrete time-space, after integration, we write the impedance equation in the following way:

$$\begin{bmatrix} x_{k+1} \\ v_{k+1} \end{bmatrix} = A_d \begin{bmatrix} x_k \\ v_k \end{bmatrix} + B_d F_{ext}^k, \tag{4.21}$$

where $A_d = e^{AT}$, $B_d = (e^{AT} - I)A^{-1}B$, T is the sampling time, I is the identity matrix, and e^{AT} is the state transition matrix.

The impedance model, as a second order differential equation, can be classified by the shape of the step response. Assuming that the input variable $u(t)$ is a step of amplitude U, with Laplace transformation $u(s) = U/s$. Then the Laplace

transformed time-response becomes

$$x(s) = H(s)u(s) = \frac{K_d \omega_n^2}{s^2 + 2\zeta\omega_n s + \omega_n^2} \frac{U}{s} \tag{4.22}$$

$$\omega_n = \sqrt{\frac{K_d}{M_d}}, \zeta = \frac{D_d}{2\sqrt{M_d K_d}}. \tag{4.23}$$

The shape of the time-response $x(t)$, which is calculated as inverse Laplace transform of $x(s)$, depends on the poles. The poles are the roots of the characteristic equation:

$$s^2 + 2\zeta\omega_n s + \omega_n^2 = 0, \tag{4.24}$$

In order to have a critically damped response, ζ must equal 1. Then we have equal and real poles

$$p_1 = p_2 = -\zeta\omega_n = -\frac{D_d}{2M_d}, D_d^2 - 4K_d M_d = 0 \tag{4.25}$$

Poles p_1, p_2 of (4.24) and the eigenvalues λ_1, λ_2 of matrix A must be equal, real, and positive $\lambda_1 = \lambda_2 = p_1 = p_2$. The most challenging part in (4.21) is to compute the term e^{AT}. The matrix exponential is fined form Cayley-Hamilton theorem, according to which every matrix satisfies its characteristic polynomial. For the case when the poles are real and multiple (critically damped response), it is possible to find

$$A_d = e^{\lambda T} \begin{bmatrix} (1 - \lambda T) & T \\ -bT & (1 - \lambda T - aT) \end{bmatrix}, \tag{4.26}$$

$$B_d = -\frac{c}{b} \begin{bmatrix} e^{\lambda T}(1 - \lambda T) - 1 \\ -bT e^{\lambda T} \end{bmatrix}, \tag{4.27}$$

where λ is the eigenvalue variable of the matrix A, $a = -\frac{D_d}{M_d}$, $b = -\frac{K_d}{M_d}$, $c = \frac{1}{M_d}$. A_d and B_d matrices can be used to calculate the current x_{imp} position of the impedance model using equation (4.21).
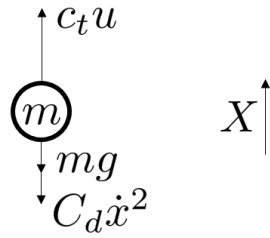
Figure 4-4: Dynamic model of the simplified system.

4.3.1 Simplified Control Problem

In this section we demonstrate the performance of the developed impedance control on the simplified system - point of mass moving in one dimension.

Dynamics

For the simplified system, we examine a point of mass that moves in a vertical direction along with the gravity force. The vertically moving point can represent a 1-dimensional quadrotor that restricted to move only upwards or downwards. We simulate the thrust with force pointed upwards, and we also add a drag force. We present the dynamic model in Fig. 4-4. Motion model can be represented as follows

$$\ddot{x} = g + \frac{c_t}{m}u - \frac{C_d}{m}\dot{x}^2, \tag{4.28}$$

where g is the gravity, c is the electro-mechanical transmission constant, m is the mass of the simulated point, u is the control input pointed upwards (actuator thrust). The drag force is proportional to the squared velocity with C_d coefficient $F_d = C_d\dot{x}^2$. The coefficient incorporates all parameters that refer to the drag force: area, shape, density, Reynolds number, etc. We set the parameters of the dynamic model to be the following, c_t=10, $m = 1.5\ kg$, $C_d = 0.15\ kgs^2/m$.

Raw trajectory provided to PID controller

We first feed the goal position of the point of mass from the human to the PID controller directly, without impedance correction. This will help us to see the performance of the controlled point of mass under the simple PID controller. We will
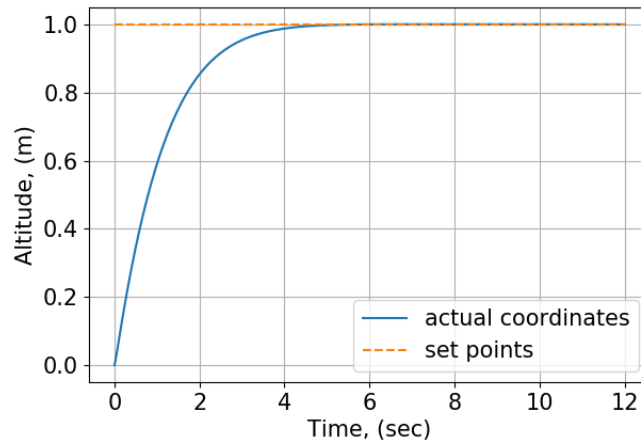
Figure 4-5: Step response.
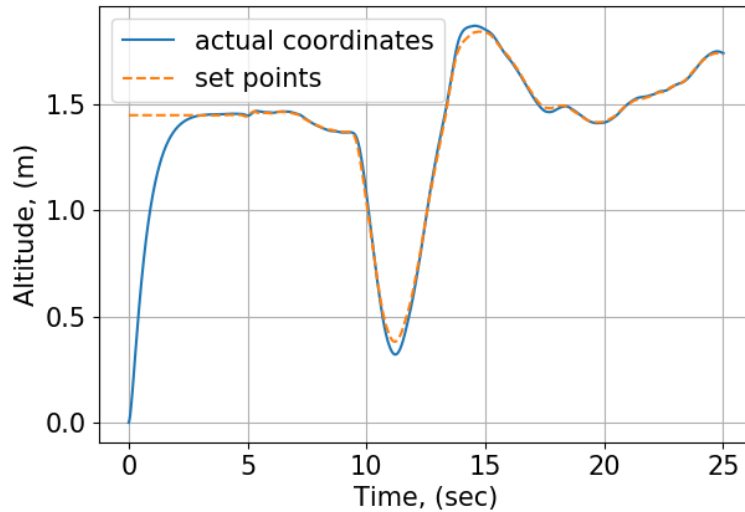
Figure 4-6: Point of mass follows a human hand with PID controller.

use it as a baseline. Our aim here is not to design the best PID controller but to use it as a tool. Therefore, we do not focus on the PID controller design itself. We set the PID coefficients in order to minimize overshoot of the system (k_p=2.6, k_d=1.4, k_i=1.4) and make the system critically damped. The step response of the described above system, governed by a traditional PID controller, is presented in Fig. 4-5.

After demonstrating the performance of the PID controller on step control input, we ask the simulated point of mass to follow a prerecorded position of the human hand. We recorded beforehand the position of the human hand with a Vicon motion capture system (shown in orange line in Fig. 4-6). For this experiment we took the motion in one dimension (the simulated point of mass can move in one dimension).

We then sequentially supplied the set positions from the human into the PID controller defined in the previous paragraph. The state of the point of mass calculated based on the (4.28). The resulting trajectory of the position of the simulated object path is presented in Fig. 4-6 in the blue line.

It is possible to see that the PID controller can perform its task, even for more complex human control input.

Impedance trajectory provided to PID control

In order to obtain the compliant behavior of the controlled system, we will update the goal position with the impedance correction or displacement term Δx calculated based on (4.18). We will discuss the stability of the impedance model later in the thesis. For now we disclose that we selected the parameters of the impedance model to be critically damped. The desired dynamic coefficients of the impedance model are the same for toy problem and for the real drone control that we will present below ($M_d = 1.9, D_d = 12.6, K_d = 21.0$). Meanwhile, the force will be obtained using (4.17). We selected the scaling coefficient K_v in (4.17) empirically ($K_v = 12$). Regarding the possible limits of K_v, the small values of K_v will leads to negligible update of the trajectory and large value of K_v will lead to the unstable trajectory. The relationship between the human velocity (as the input to the impedance model) and the impedance correction term (as the output of the impedance model, basically it is the displacement of the impedance model) are demonstrated in Fig. 4-7. It is possible to observe in Fig. 4-7 that the impedance model displacement is smoothed and slightly delayed in comparison to the human velocity.

We update the goal position (that we have to track) coming from the human with the impedance displacement term in the following way.

$$x_g = x_{hum} + x_{imp}, \tag{4.29}$$

where x_{hum} is the recorded human position.

The integrated set points are demonstrated in Fig. 4-8. In the green color there is the trajectory obtained with the impedance displacement of the model.
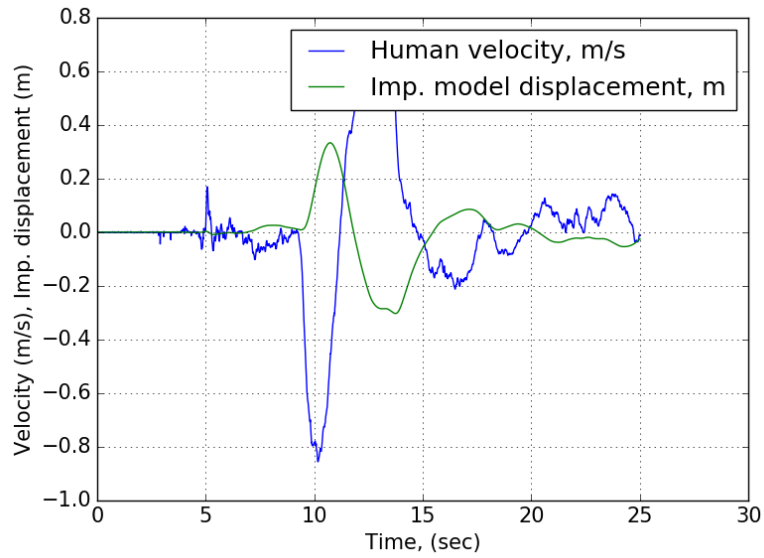
Figure 4-7: Relationship between the human hand velocity and the impedance model displacement.
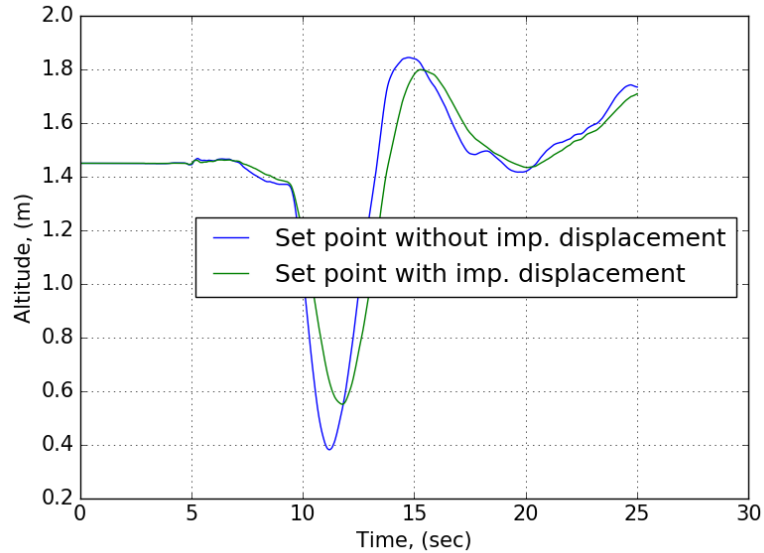
Figure 4-8: Set points coming from the human. Raw goal trajectory recorded from the position of the human hand, shown in blue. Goal trajectory obtained when the raw trajectory is updated with the impedance displacement, shown in green.

Table 4.1: Standard Deviations of the Dynamic Parameters.

	Mean standard deviation values		
	Acceleration	Jerk	Snap
Without impedance	0.82	7.89	95.1
With impedance	**0.74 ($\downarrow$10%)**	**7.75 ($\downarrow$2%)**	**86.5 ($\downarrow$9%)**

In comparison to the raw set points coming from the human hand (blue line), it is possible to observe that the trajectory with the impedance correction is more smooth and slightly delayed.

After the update of the goal position, we feed the new setpoint to the PID controller and ask it to generate the control input, which is getting applied to the model.

The goal of the proposed control method is to achieve the smooth guidance of the controlled system. Based on that, to evaluate the approach, we proposed to investigate the dynamic parameters of the model motion (as discussed in section 4.1). For the parameters, we take the second, the third, and the fourth derivatives of the position or altitude. We calculated the standard deviations (SD) for each parameter over the control session and present them in Table 4.1.

It can be seen that the proposed impedance control helped to reduce the dynamic parameters, which leads to more smooth behavior of the controlled system.

4.3.2 Proposed Impedance Control Approach for Swarm Guidance

To implement adaptive manipulation of a robotic group by a human operator, such as when the inter-robot distances and formation dynamics change following the operator state, we propose a position-based impedance control, which is described above for the single agent.

In the proposed impedance model approach, we introduce mass-spring-damper links (shown in Fig. 4-2) between each pair of agents and between the human and agent formation, as shown in Fig. 4-9(a). Basically this is the virtual impedance model which is inserted between the pairs of agents of the formation. We use this impedance model state (in particular the displacement of the mass) to update the
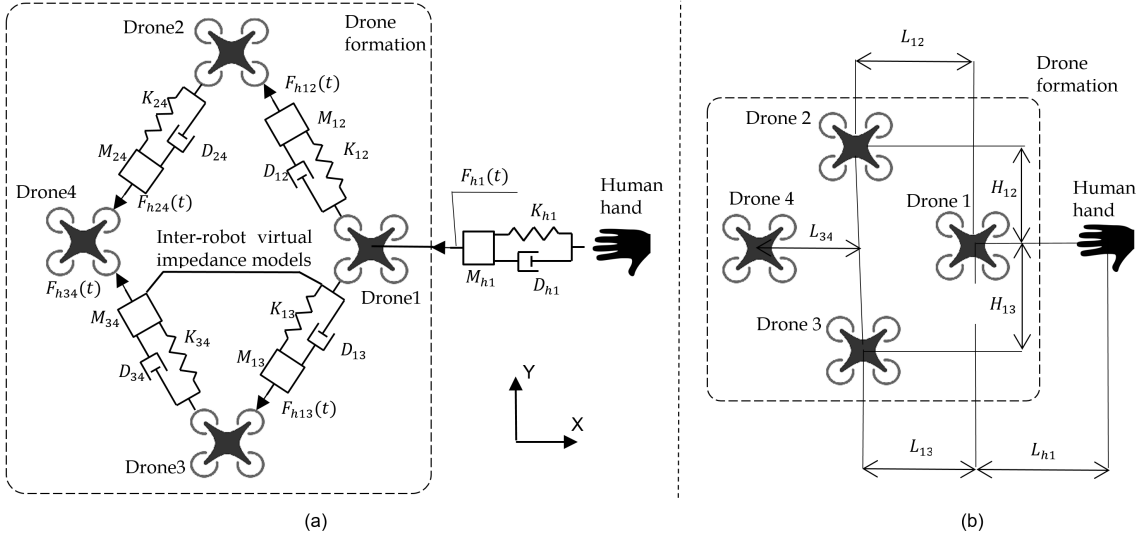
Figure 4-9: (a) Position based impedance control, (b) PID position controller with no impedance models. Subscription "h" is referred to human.

goal position of the corresponding agents. We call such impedance models impedance links or interlinks, because they simulate the link between the drones.

The target impedance trajectory is processed by PID control, which allows high precision positioning and maintains the default predefined shape (in my case, it is a rhombic shape) and orientation of the formation.

While the operator is guiding the formation in space, impedance models update the goal positions for each flying robot, which changes the default drone-to-drone distances L_{ij}, for (i,j=1,2,3,4) in our case. As a result, the operator "pushes" or "pulls" virtual masses of inter-robot impedance models, which allows the shape and dynamics of the robotic group to be changed by the human hand movement. Virtual "pushing" or "pulling" of the impedance model mass is achieved with the relationship between the human hand movements and force, which is defined in (4.17). Basically "pushing" or "pulling" is defined with the application of the force in different directions in (4.17). Each robot relies on the local position information coming from neighbor vehicles, and, at the same time, the human operator affects all vehicles globally via impedance models. Such an adaptive control could lead to a natural multi robot-human interaction, although all the impedance models' parameters remain unchanged during the flight.

The method described above is used to calculate the impedance correction vector

$\left[x_{imp}, y_{imp}, z_{imp} \right]^T$ or the current position of the virtual body of each impedance model. Impedance correction vectors are used to update the goal positions of each vehicle in the team.

The goal positions along X, Y, and Z-axis of each quadrotor (that we have to track) are determined as follows (see the structure presented in Fig. 4-9(a)):

$$
\begin{bmatrix} x_{1\_g} \\ x_{2\_g} \\ x_{3\_g} \\ x_{4\_g} \end{bmatrix} = scale \begin{bmatrix} x_h \\ 0 \\ 0 \\ 0 \end{bmatrix} + \begin{bmatrix} -L_{h1} \\ x_1 - L_{12} \\ x_1 - L_{13} \\ \frac{x_2 + x_3}{2} - L_{34} \end{bmatrix} - \begin{bmatrix} |x_{imp\_h1}| \\ |x_{imp\_12}| \\ |x_{imp\_13}| \\ |x_{imp\_24} + x_{imp\_34}| \end{bmatrix}, \qquad (4.30)
$$

$$
\begin{bmatrix} y_{1\_g} \\ y_{2\_g} \\ y_{3\_g} \\ y_{4\_g} \end{bmatrix} = scale \begin{bmatrix} y_h \\ 0 \\ 0 \\ 0 \end{bmatrix} + \begin{bmatrix} 0 \\ y_1 + H_{12} \\ y_1 - H_{13} \\ \frac{y_2 + y_3}{2} \end{bmatrix} + \begin{bmatrix} y_{imp\_h1} \\ y_{imp\_12} \\ y_{imp\_13} \\ y_{imp\_24} + y_{imp\_34} \end{bmatrix}, \qquad (4.31)
$$

$$
\begin{bmatrix} z_{1\_g} \\ z_{2\_g} \\ z_{3\_g} \\ z_{4\_g} \end{bmatrix} = scale \begin{bmatrix} z_h \\ 0 \\ 0 \\ 0 \end{bmatrix} + \begin{bmatrix} 0 \\ z_1 \\ z_1 \\ \frac{z_2 + z_3}{2} \end{bmatrix} + \begin{bmatrix} z_{imp\_h1} \\ z_{imp\_12} \\ z_{imp\_13} \\ z_{imp\_24} + z_{imp\_34} \end{bmatrix}, \qquad (4.32)
$$

where x_{imp_ij}, y_{imp_ij}, and z_{imp_ij} for $i, j = h, 1, 2, 3, 4$ are corresponding impedance correction terms, L_{ij} and H_{ij} for $i, j = h, 1, 2, 3, 4$ are displacements for the quadrotors, as could be seen in Fig. 4-9(b), x_i, y_i, z_i for $i = 1, 2, 3, 4$ are the actual positions of UAVs, x_h, y_h, z_h are the position coordinates of the human hand, and $scale$ is a mapping coefficient.

4.3.3 Boundedness of External Conditions

The impedance model is supposed to be critically damped (as we will show further), which prevent from unexpected inputs. On the other side, the human hand velocity is also limited with human capabilities of moving hand in space. Nevertheless,

to exclude any risks and to demonstrate the performance under assumption on the boundedness of the external inputs, the impedance terms are limited with the maximum values:

$$
\begin{bmatrix} x_{imp} \\ y_{imp} \\ z_{imp} \end{bmatrix} \leq \begin{bmatrix} x_{imp\_limit} \\ y_{imp\_limit} \\ z_{imp\_limit} \end{bmatrix},
\tag{4.33}
$$

where the right side represents the safety thresholds that prevent an overrun of the impedance model.

4.3.4 Graph Representation

One of the ideas behind the proposed impedance control is safer operation when the agents' distances are increasing with increasing velocity. In particular, when the formation is moving fast, we want the drones to always split apart in the negative direction of the X axis (from the human), that is why we subtract the absolute values of impedance terms in (4.30). On the other hand, considering motion in the Y and Z axes, the formation has to be shifted in different directions, with respect to the human motion. If the human starts to move in the left direction, the robotic swarm, following the human, has to shift to the right, demonstrating a "tail" behavior, as shown in Fig. 4-17. Based on the presented discussion, we conclude that the developed impedance control introduces a directional behavior - from the human to the last quadrotor. Thus, the set of impedance links represents a connected directional graph.

4.3.5 Generalization of the Proposed Approach

To make the above equations more general, we introduce several terms. Let $\mathbf{X}_i \in \mathbb{R}^3$ represent the actual position of the center of mass of i_{th} quadrotor, $\mathbf{X}_{gi} \in \mathbb{R}^3$ represent the goal position (that we have to track) of the center of mass of i_{th} quadrotor, $\mathbf{H} \in \mathbb{R}^3$ represent the human hand position, $\mathbf{G} \in \mathbb{R}^{n^2}$ is a two-dimensional array and represent the default geometry configuration for the vehicles (where n is the number of agents), and $\mathbf{Imp} \in \mathbb{R}^{n^2}$ is a two-dimensional array and represent the impedance
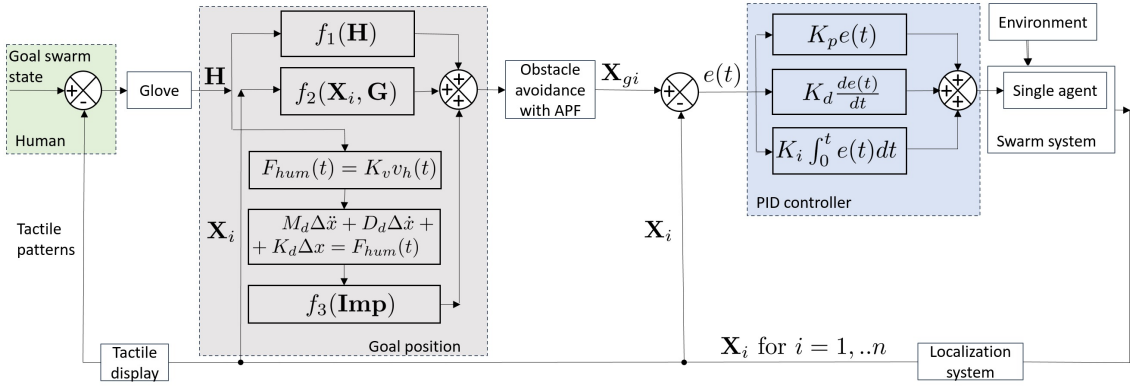
Figure 4-10: Control diagram of the proposed HSI with impedance control.

correction terms (which is the displacements of the impedance models). Geometry configuration $\mathbf{G}$ and impedance corrections $\mathbf{Imp}$ express the relationships between the agents within the group. In the most general case we can have some unique relationship between every pair of drones. That is why we propose to represent $\mathbf{G}$ and $\mathbf{Imp}$ as square matrices with n-by-n size where n is the number of agents. In the less general cases $\mathbf{G}$ and $\mathbf{Imp}$ can be not full rank matrices with some level of sparsity. Finally, we can define the agent goal positions in the following generalized way

$$\mathbf{X}_g = f_1(\mathbf{H}) + f_2(\mathbf{X}, \mathbf{G}) + f_3(\mathbf{Imp}). \tag{4.34}$$

The overall control diagram is presented in Fig. 4-10. Feedback line with tactile display and tactile patterns will be discussed in the Chapter 5. To ensure safe operation, obstacle avoidance module corrects the goal positions and works on top of the block described by (4.34). We will disclose more detailed about the obstacle avoidance in the following sections.

Equations (4.30) to (4.34) consist of three parts. The first part $f_1(\mathbf{H})$ is the spacial mapping function with the coefficient *scale* between the human position and the formation leader (drone 1) motion, where the vector $\mathbf{H}$ denote, how far the human moved his/her hand from an initial position along each Cartesian axis. The hand's initial position is determined when the current control session started (at that moment, we initialized the frame with respect to which we estimate the $\mathbf{H}$). Units of $f_1(\mathbf{H})$ is meters. The second part $f_2(\mathbf{X}, \mathbf{G})$ determines the default geometrical

shape of the formation (rhombus, which is located in the XY plane in our case). Basically this can be distances between the agents. The units of $f_2(\mathbf{X}, \mathbf{G})$ is meters. The third part $f_3(\mathbf{Imp})$ describes the displacement of impedance models which we inserted (virtually) between the agents. The units of the displacements are meters. All three parts of the equations are independent and could be designed separately, following the specific application needs. Although in this work, we consider the rhombic shape, the formation could have an arbitrary geometry, which is defined in the second part of (4.30) to (4.34). The number of UAVs also could be arbitrary. Given some shape, the impedance connections could be designed in such a way that they do not have to replicate the geometry. We select the impedance links based on the behavior we want to achieve. For example, if we want the distance between Drone 2 and Drone 3 to increase when the formation is moving in the Y direction (to make it wider for safety or any other concerns), then we could introduce an additional impedance interlink between Drone 2 and 3, see Fig. 4-9.

4.3.6   Communication

Computational complexity coming from (4.18) increases linearly with the number of impedance links. As can be seen in (4.30) to (4.32), each agent relies on local information about the distances to neighbor vehicles (geometric part of the equations), and at the same time on the state of local impedance models. The human affects all impedance interlinks globally. Based on that, it is possible to implement computation on board or on the ground station with corresponding advantages and disadvantages of both approaches.

Centralized Approach

For the experiment, we utilized a centralized approach by using a Ground Control Station (GCS). On one side, this approach simplifies the implementation of the HSI system. Each drone does not need to measure the distances to the neighbors and communicate with them. But on the other hand, we introduce a single point of failure - GCS, which reduces the system's reliability. We used the ground-based Linux-based computer to accumulate all current positions (from the localization

system) and compute desired drone trajectories in real-time. We used a Vicon motion capture system for human positioning. Alternative approaches to tracking the human hand position, which allows for more varied applications, are discussed in future work. For the communication between the GCS and drones, we used a duplex radio channel. Each drone received its current position and next waypoint through the radio link (communication bandwidth increases linearly with the number of robots). The details of implementation are discussed in Section 4.3.8.

Decentralized Approach

Decentralized onboard computation is also an option, which can reduce the load of the single point of failure - GCS. On the other side, this approach requires additional setup, which is a weak point. Similar to the centralized approach, we also need a communication channel. It can be a simplex radio channel for this case. Human control input has to be delivered to the leader drone via the radio channel. The human hand velocity also has to be measured and broadcasted to each drone. Therefore, calculation regarding impedance models (4.18) can be done on board of each quadrotor. In addition to the position of the human hand, each agent has to know the distances to the neighbors, according to (4.30-4.31). The experimental setup in this thesis does not support measuring relative distances with onboard sensors. However, it is possible to achieve this with vision-based methods, for example, as shown by Petráček and Saska [2018]. Another option is to set up the communication channels between the closest neighbors.

4.3.7 Generalization to Other Types of Robotic Systems

The initial intention was to developed methods for quadrotor vehicles. It is well known that the control scheme of the typical quadrotor (or mostly any VTOL vehicle) consists of multiple control loops. Generalized and simplified control loops are presented in Fig. 4-11.

In section 4.1, we demonstrated that the proposed objectives are valid for any quadrotor and do not limit the specific implementation of our hardware validation that we will present in the following sections.
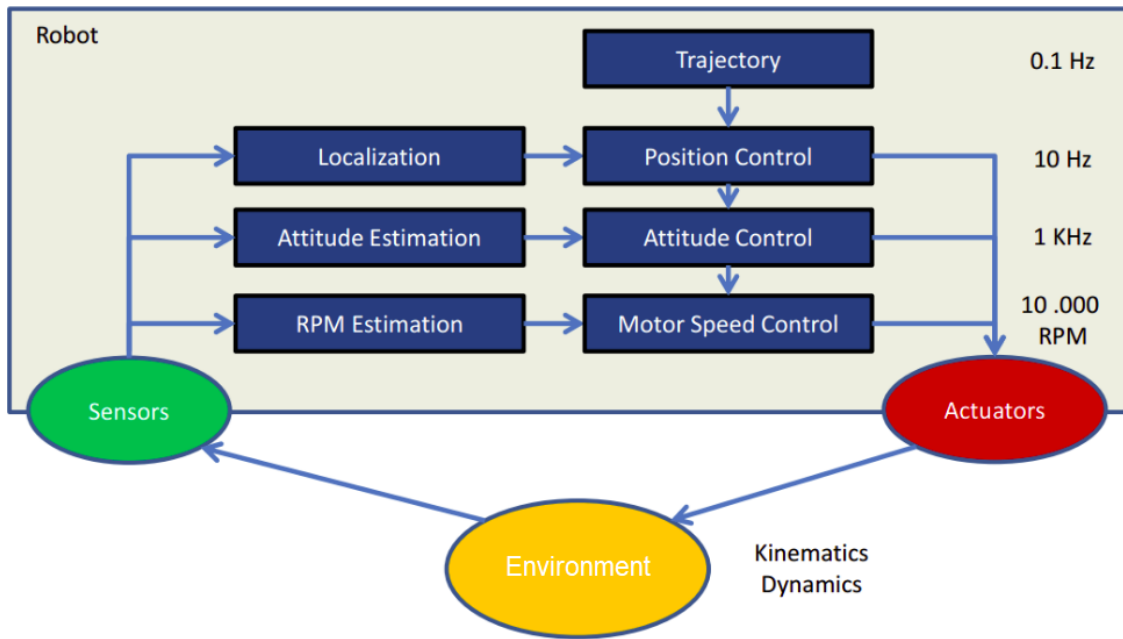
Figure 4-11: Control loops of the typical quadrotor controller, according to Sturm and Cremers [2015].

But we also want to discuss the generalization to other types of hardware platforms. Considering the control diagram in Fig. 4-10 and the way we propose to calculate the goal positions (4.34), we can make the following conclusions. The operator directly influences the desired trajectory of the flight with the help of the impedance control. Also, the human received feedback about the velocity and positions of the swarm. Therefore, it is possible to conclude that developed methods focus on the vehicle's high-level control. High-level control does not consider plant dynamics directly. Plant dynamics is addressed by the attitude controllers, which is unique for different types of aerial robots. The human is not able to control the attitude of the vehicles in the swarm, and he is not able to control the rotational speed of every motor of every drone.

High-level control approaches do not strongly depend on the dynamics of the vehicle. In a more general sense, we can consider the vehicles that can hover in space (maintain the same position $\mathbf{X} \in \mathbb{R}^3$) and at the same time can translate along any direction. The vehicles can be ether under-actuated, such as quadrotors, or fully actuated. We can limit the proposed approach from three-dimensional to two-dimensional case and apply it to the control of the swarm of ground mobile

robots with omnidirectional motion ability.

Therefore we can conclude that the proposed control diagram, presented in Fig. 4-10, can be scaled to most types of VTOL vehicles without modification. Regarding the correction term $f_3(\mathbf{Imp})$ coming from impedance control and the objectives that it helps to follow, we have to provide the analysis similar to the one presented in Section 4.1 in order to prove the applicability to the particular vehicle type.

4.3.8　Experimental Validation

Hardware Setup

We used a formation of four Crazyflie 2.0 quadrotors to perform the validation flight tests. The Crazyflie 2.0 quadrotor is one of the smallest commercially available drones that can fit in the palm of a hand. Small size (9 cm^2) and weight (27 grams) provide safety, which is required for applications that involve human participation. The small size also leads to small inertia parameters that help to react to control inputs fast enough. The low weight contributes to withstand crashes between quadrotors and collisions with walls. The maximum takeoff weight is just 42 grams, but it allows us to carry expansion boards and infrared (IR) markers. Four IR reflective markers lead to a total weight of 31 grams, which reduces the flight time to 5 minutes. Honig et al. [2015] has well-described dynamics of the Crazyflie 2.0. The Crazyflie 2.0 is supplied with two controllers. The first one is 32 bits ARM Cortex-M4 (STM32F405) for the main applications; the second one is ARM CortexM0 (nRF51822) for power and communication purposes.

To get the high-quality tracking of the quadrotors and human glove during the experiments, we used a Vicon motion capture system with 12 cameras (Vantage V5) covering a 5 m × 5 m × 5 m space. Vicon software package Vicon Tracker 3.6 is running on a separate server with Windows OS. All other computations are performed on a separate Linux-based machine with Ubuntu 16.04 LTS. We used the Robot Operating System (ROS) Kinetic framework to run the development software and ROS stack Honig et al. [2015] for Crazyflie 2.0. The position and attitude update rate was 100 Hz for all drones. To extract the coordinates from the Vicon Tracker
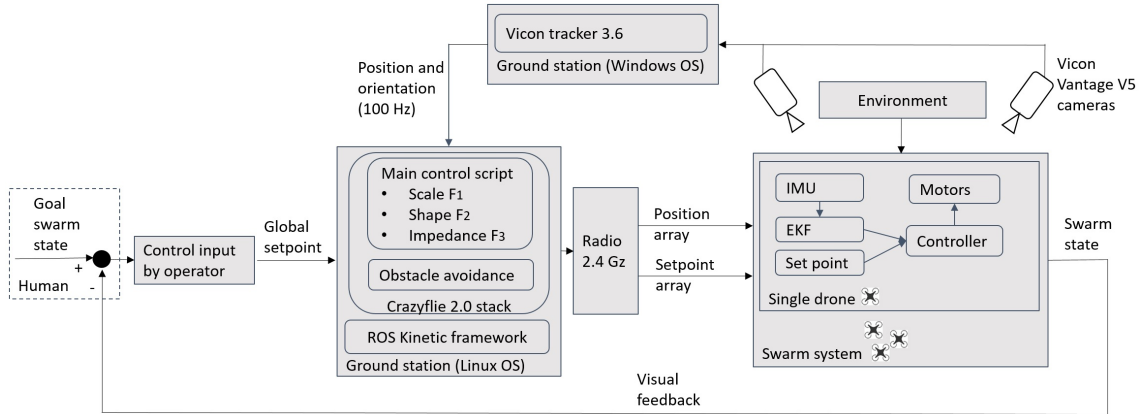
Figure 4-12: Overall control system architecture.

3.6, we used a ROS package Vicon Bridge. Both Windows and Linux computers were connected to the same network via a wired connection to ensure reliable data transfer from Vicon Tracker to ROS.

Communication between a Linux computer and drones has been established via 2.4 GHz Crazyflie PA radio module (with controller nRF24LU1+ by Nordic Semiconductor and 20dBm power amplifier). The range of Crazyradio reaches 1 km (between the drone and the radio module) with the direct line of sight. Typically we used one radio module to maintain a link with up to 5 drones.

The overall system architecture is shown in Fig. 4-12. We added an obstacle avoidance module that corrects the goal positions. We will describe more details about obstacle avoidance in the following sections.

During the validation of the control approaches, we provide only direct visual feedback to the operator.

Default Flight

Before conducting any type of experiment, we ensured that we could perform a stable and smooth flight, following the desired trajectory. In order to do so, all PID coefficients for position controller were set to default values for Crazyflie 2.0, according to Honig et al. [2015] (for x,y-axis k_p=40, k_d=20, k_i=2; for z-axis k_p=5000, k_d=6000, k_i=3500). For testing purposes, we first completed an autonomous flight: takeoff and horizontal flight in line. After that, we also make sure that the drone can smoothly follow the setpoints coming as a control input from the human op-

80

erator (without impedance correction). If both tests accomplished, we started the experiment.

Dynamical Stability of the Impedance Models

In this section we consider the selection of the impedance model dynamic parameters M_d, D_d, and K_d to obtain a critically damped response of the system, which we assume to be the most comfortable for the human.

As a preliminary setup, the selection of the impedance parameters was carried out. Second-order systems (such as our impedance model) are classified by the shape of the step response. The type of step response is determined by a value of ζ in (4.24), as shown in Fig. 4-13. M_d, D_d, and K_d coefficients of the impedance model were set in order to get a critically damped response, which would be smooth and most comfortable for a human operator. To archive this, ζ must equal 1 in (4.24), which produce real and equal poles (Fig. 4-13). Therefore, based on (4.23), the following condition has to be satisfied $D_d^2 - 4K_dM_d = 0$ or $D_d^2 = 4K_dM_d$. Making sure that it is true, we selected the desired dynamic coefficients ($M_d = 1.9, D_d = 12.6, K_d = 21.0$).

To maintain the stability of the systems, we also carefully selected the human velocity coefficient K_v, used for force calculation in (4.17). We assume that the impedance correction of the goal position has to be no more than 30-50% of the distances to the neighbors L_ij and H_ij (which is 0.5 meters in this case). We also estimated that the average human hand velocity, which was estimated from a set of consecutively measured positions provided by a motion capture system, does not go over $1.5m/sec$ while manipulating the formation. Based on this, we selected K_v to be $-7Nsec/m$. A negative K_v value is used because when the human is moving in one direction, drones retreat towards the opposite direction (see Section 4.3). Finally, we set the threshold limit of impedance correction term x_{imp_limit} to be 0.25 meters for the experiments for safety reasons. For simplification purposes, we used the same dynamic parameters for all impedance models in the experiment.
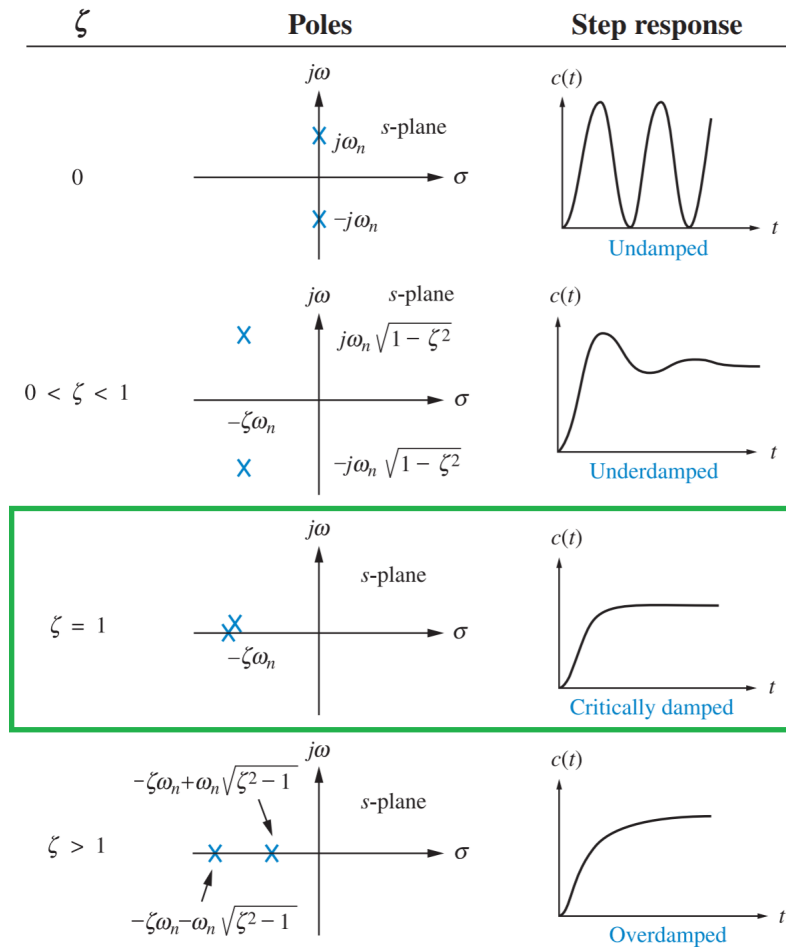
Figure 4-13: Classification of second order systems by the value of damping ratio ζ, according to Nise [1995].

Single Drone Behaviour

After the selection of all impedance parameters, we checked the single drone behavior, while being guided by the human operator with the proposed impedance controller. To do so, we took Drone 1 and the human wearing a glove, as seen in Fig. 4-9. For simplicity, we present the values along Y-axis. Human hand velocity $v_h(t)$ used in (4.17) and the impedance correction term y_{imp_h1} used in 4.31 are shown in Fig. 4-14. From Fig. 4-14 it can be seen that the impedance model changes its state smoothly following the human hand movement. Due to the negative velocity coefficient, K_v, human velocity, and impedance term are moving in opposite directions. It is also possible to notice (for the time range 8.5-9 seconds in Fig. 4-14) that the safety threshold y_{imp_limit} helps to prevent dangerous behavior
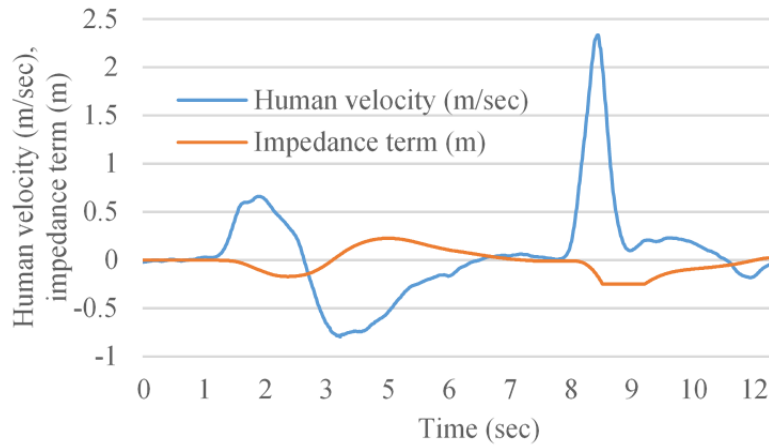
Figure 4-14: Human hand velocity (blue) and impedance correction term (orange) versus time. Movement is along Y-axis.
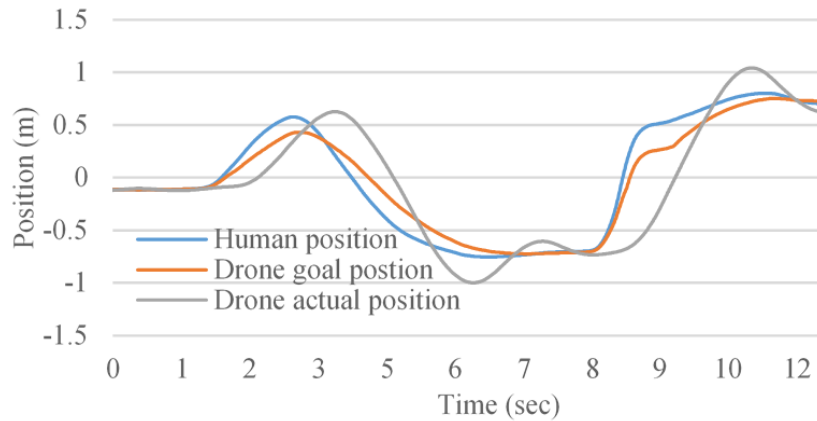
Figure 4-15: Human hand position while guiding the drone (blue), drone goal position while following the human (orange), drone actual position (gray) versus time. Along Y-axis.

due to high values of the input parameter (human velocity $v_h(t)$).

Fig. 4-15 shows the actual position of the human hand along with the goal and actual positions of Drone 1 (along Y-axis). According to Fig. 4-9(b), Y-coordinates of the human and Drone 1 goal position have to be equal, in the case of a simple PID controller. However, due to the impedance correction of the goal position in (4.31), in Fig. 4-15 it can be seen that the Drone 1 goal position is slightly behind the human position (this difference is equal to the impedance term y_{imp_h1}). The result could be represented as a sort of filtering of the robot goal position, which leads to smoother drone guidance, especially in the case of extreme external inputs. Afterward, the Drone 1 goal position is provided to the positional PID controller.
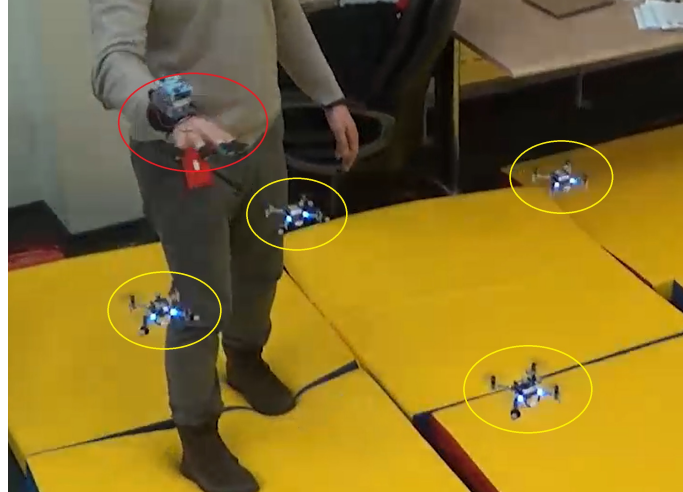
Figure 4-16: Guidance of four drones.

t = 0 sec   t = 0.29 sec   t = 0.67 sec
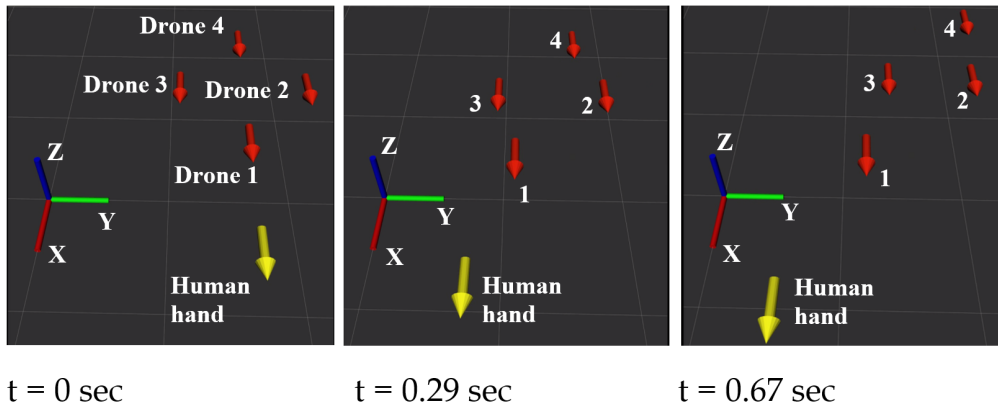
Figure 4-17: Formation of four drones (red arrows) following a human hand (yellow arrow). The beginning of the yellow arrow represents the human's actual position, and the beginning of red arrows represents the quadrotor goal positions. The orientation of the arrows represents the orientation of drones and the human hand. The magnitude of the arrows has no significance.

A delay occurs between a human command and a drone reaction, which is expected due to the impedance controller's nature as the second-order system.

Behaviour of the Formation of Drones

The next step is to demonstrate the performance of the proposed algorithm for the guidance of the formation of four drones.

We firstly refer to Fig. 4-17, where a human guides four quadrotors with the control structure presented in Fig. 4-9(a). An operator moves their hand towards the negative Y and the positive X direction. This figure presents an interesting

feature of the impedance control, which was mentioned before in Section 4.3. When the human starts to move fast enough, the formation immediately spreads along the direction, which is opposite to the human motion. When the human hand velocity starts to decrease, the formation contracts back to its initial shape. The axis, along which the formation changes its shape, coincides with the human velocity vector.

Fig. 4-18 shows the distance along the Y-axis between Drone 1 and Drone 4, which are placed in accordance with Fig. 4-9(a). The formation is guided along the Y-axis in this case. Zero human hand velocity generates no control input and the default distance between drones is zero. It is possible to see that the distance between Drone 1 and Drone 4 changes in accordance with the human hand velocity, when the human guides the formation in one or another direction along Y-axis. The bigger gap between drones corresponds to the higher velocity of the control signal, which produces more safe guidance. Fig. 4-18 also present the area of the formation in projection to the horizontal plane. It is possible to see that the whole area adapts to the control input signals in a compliant manner. It is possible to change the dynamic behaviour of the controlled swarm system by changing the default dynamic parameters of the impedance models and by changing the structure of the impedance links.

The actual drone positions are presented in Fig. 4-19. It is possible to notice that the more the velocity of the human control input the more distance between neighbor drones in the controlled formation. The plots also demonstrate that, despite agile human movements, the drones are able to adjust accordingly in a compliant manner, and the area is changing in response.

4.4   Collision Avoidance with Potential Fields

Apart from internal factors that affect the swarm state, such as mass-spring-damper links between the drones, there could also be external factors that could cause the formation to change, e.g., obstacles. We assume that, within the swarm, every agent decides where to go next using both the local information about surroundings and the global goal (direction and velocity of motion). In this scenario, each quadrotor

can plan its obstacle avoidance while considering the position of the nearest obstacles and neighbor agents. The planning algorithm is described below.

The location of drones and obstacles is defined by a Vicon motion capture system, as described in Section 4.3.8. Each quadrotor is aware of the position of local obstacles. Additionally, each obstacle has a safety zone around its center, which is defined as a cylinder (a circle for planar motion) with a predefined radius.

Every controlled robot in the swarm should not only be aware of static obstacles on the map but also take into account moving obstacles, such as humans and other agents in the formation. The collision avoidance method based on the artificial potential field method, Khatib [1986], was applied in this work to ensure safe real-time robots swarm navigation in a dynamic environment. Many other related works have been carried out on inter-robot collision avoidance, such as using fast marching square and virtual potential fields to influence the location of each robot during movement in prescribed formations Gomez et al. [2013] or in very populated groups Leonard and Fiorelli [2001]. Other techniques are based on the inclusion of springs and dampers Kokubo et al. [2017] to create virtual forces that are transformed into velocity commands. For each agent in formation, other robots are treated as moving obstacles that affect each robot's motion. We first consider the collision avoidance problem of a single robot in a plane and assume further, that obstacles map is known. Fig. 4-20 shows 2-dimensional Cartesian space with obstacles. The environment is represented as a grid, each cell of which could be free or occupied (it is assigned with 0 or 1 values respectively).

The obstacle avoidance algorithm's basic idea is to construct a smooth function over the extent of the robot's configuration space with high values when the robot is near an obstacle and lower values when it is further away. This function should have the lowest value at the desired location of the robot. If such a function is constructed, its gradient can be used to guide the drone to the goal configuration. Typically this function consists of two components, attractive and repelling.

In our case, the artificial potential affects a robot's motion in X- and Y- directions. An attractive potential function, $U_a(x, y)$, can be constructed by considering the distance between the current position of the robot, $\boldsymbol{p} = [x, y]^T$, and the desired
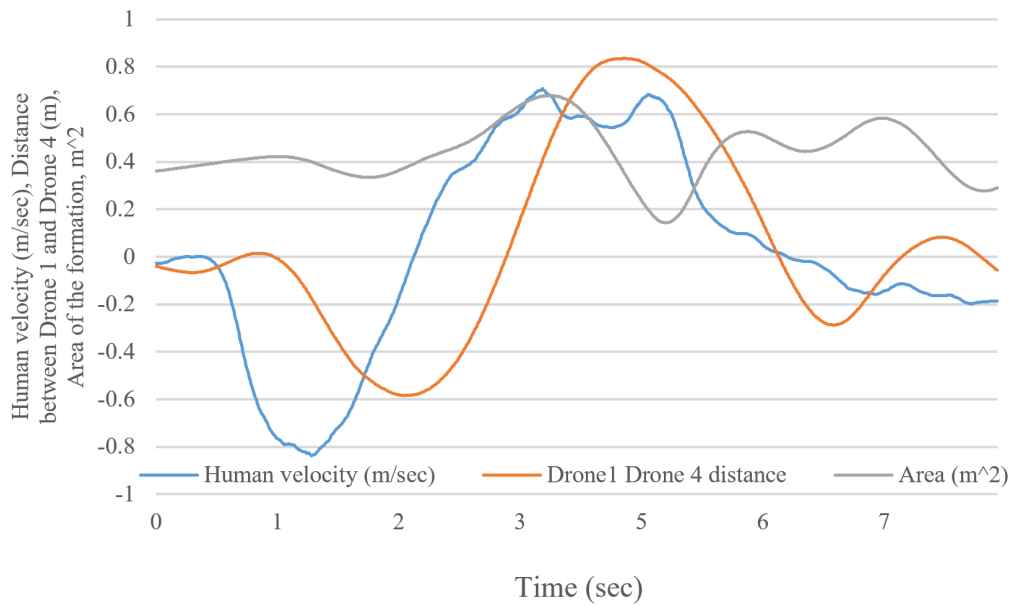
Figure 4-18: The blue line represents human hand velocity versus time, the orange line represents distance between Drone 1 and Drone 4. Along Y-axis. The gray line represent the area of the formation on the Horizontal plane.
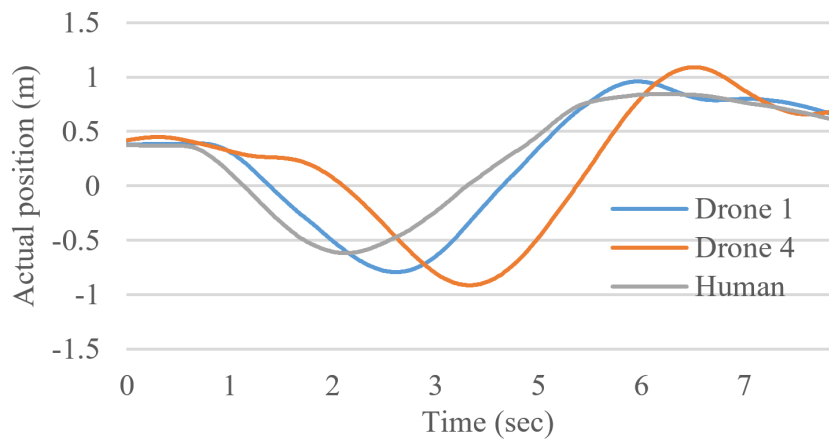
Figure 4-19: Actual positions of Drone 1 (blue), Drone 4 (orange), human hand (gray) versus time. Along Y-axis.
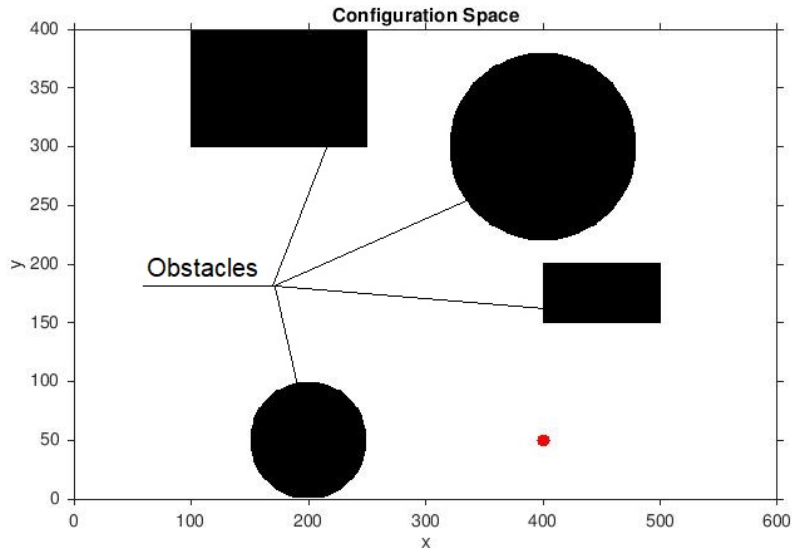
Figure 4-20: Operational environment 400×600 grid representation. Obstacles are depicted in black, collision free area is drawn in white. Robot's desired destination is a red dot on the grid.

goal location, $\boldsymbol{p}_g = [x_g, y_g]^T$, as follows:

$$U_a(x, y) = \xi ||\boldsymbol{p} - \boldsymbol{p}_g||^2. \tag{4.35}$$

Here ξ is the constant scaling parameter. For a 2-dimensional map, potential functions could be visualized as a surface.

A repulsive potential function in the plane, $U_r(x, y)$, can be constructed based on the distance, $\rho(x, y)$, to the closest obstacle from a given point, $[x, y]$, in configuration space.

$$U_r(x, y) = \begin{cases} \eta(\frac{1}{\rho(x,y)} - \frac{1}{d0})^2 & \text{if} \quad \rho(x, y) < d0, \\ 0 & \text{if} \quad \rho(x, y) \geq d0. \end{cases} \tag{4.36}$$

Here η is simply the constant scaling parameter, and $d0$ is a parameter that defines the influence radius of the repulsive potential.

Once the combined potential, $U(x, y) = U_a(x, y) + U_r(x, y)$ is constructed as shown in Fig. 4-21(c), a robot's desired velocity can be estimated as $\boldsymbol{v} \propto -\nabla U(x, y)$.
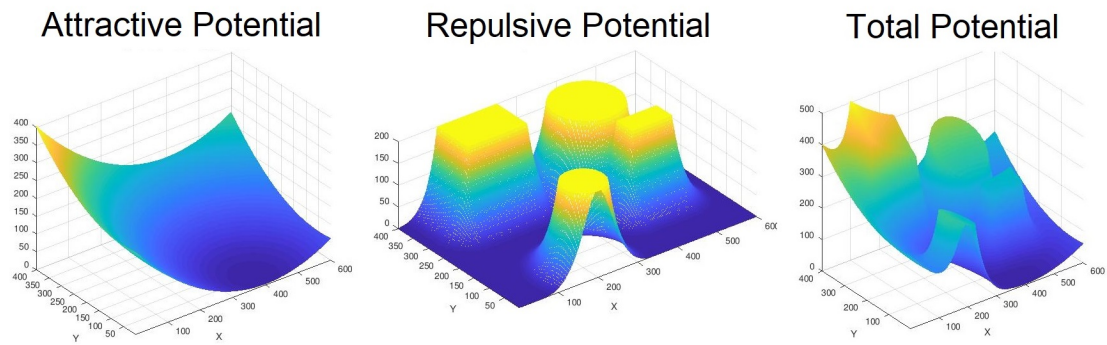
Figure 4-21: Artificial potential functions (400 × 600 grid).
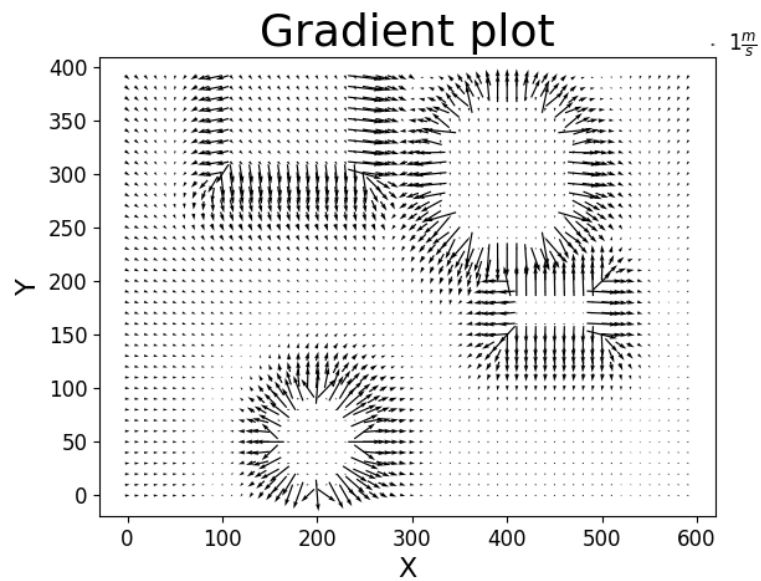
Figure 4-22: Gradient of the combined potential function (400 × 600 grid).
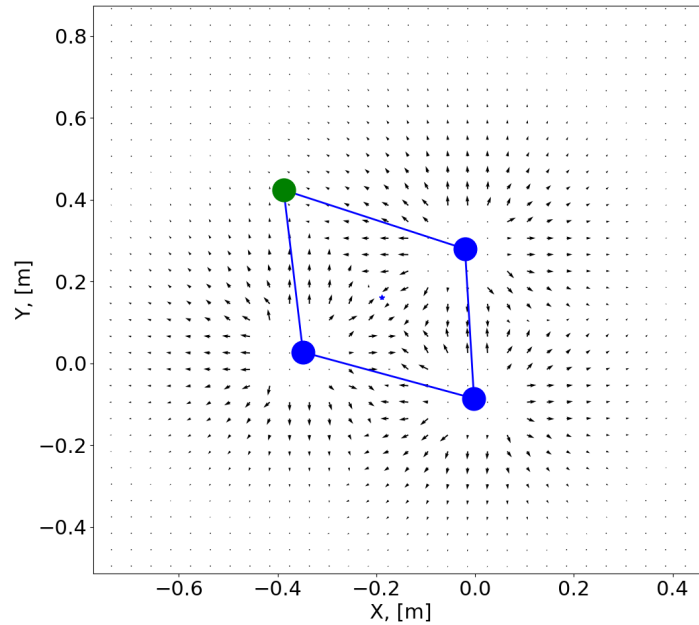
Figure 4-23: Inter-agent collision avoidance strategy, based on potential-field method. Quiver plot represents, how the green robot sees the other 3 drones (depicted in blue color) in the gradient map.

Fig. 4-22 represents the gradients plot, where each arrow defines local movement direction and velocity magnitude.

Swarm of drones is much more challenging to control than one drone for a single operator. However, local motion planner based on artificial potential fields allows formation agents positions correction, preventing collisions. The algorithm tracks static as well as dynamic obstacles. In our case of the human-guided swarm, a point of attraction, $\boldsymbol{p}_g^d$, (goal location) is assigned to every drone, d, relative to the leader-drone position with a prescribed geometrical shape. Each robot possesses its local potential, which contributes to the global field. These artificial potentials define interaction forces between neighboring robots.

Fig. 4-23 represents these forces inside the formation of four drones, depicted as connected circles. This gradient plot is visualized for the robot depicted with the green circle. It recognizes other drones in the swarm as obstacles, while its desired position (one of the vertices of the rhomboid formation) is an attractive point for itself.

In such a way, a drone swarm can adapt its shape according to local obstacle positions. Fig. 4-24 represents the simulation of four drone formation (blue connected circles) guided by a human near the static obstacles (red circles), closely located to each other. Obstacles map is depicted in red, while small black arrows represent here the gradient map for the left-most robot. The algorithm tracks static as well as dynamic obstacles (other drones in the formation). The prescribed diamond-shaped formation is getting deformed as drones come closer to obstacles (Fig. 4-24(b-c)), due to the repulsive forces affecting the robots. After passing the narrow gate, the formation stretches back to its default shape.

The guidance of Four drones swarm through a passage between two static obstacles is depicted in Fig. 4-25. It can be noticed that formation adopts its shape to avoid collisions, and drones do not fly too close to the obstacles.

4.5   Summary

We developed a new control paradigm, where we propose a novel impedance control approach. We aimed to make a controlled multi-agent system to adapt to the human operator's control input dynamically. The main novelty of the control method is that we calculate the virtual external force applied to the impedance model to be proportional to the operator's hand velocity. We combine the impedance trajectory with the goal trajectory coming from the human control input. As a result, we decreased the dynamic parameters of the controlled system (snap standard deviation is decreased by 9% compared with the traditional PID control). We demonstrated the generalized way of how to apply the proposed method to the teams of robots. Stability and communication issues have been discussed. Using the real experimental validation, we showed that the formation dynamics and geometrical shape adapts to the human control signals, helping to achieve smooth and safe guidance. Finally, we proposed to use artificial potential fields approach to prevent any collisions between agents and with any external objects. We presented how the swarm adapts when passing through the narrow gap.

The nature of the formation's geometry changes can be different: impedance

91

(a) before entering the obstacle gate

(b) entering the obstacle gate

(c) exiting the obstacle gate

(d) after passing the obstacle gate
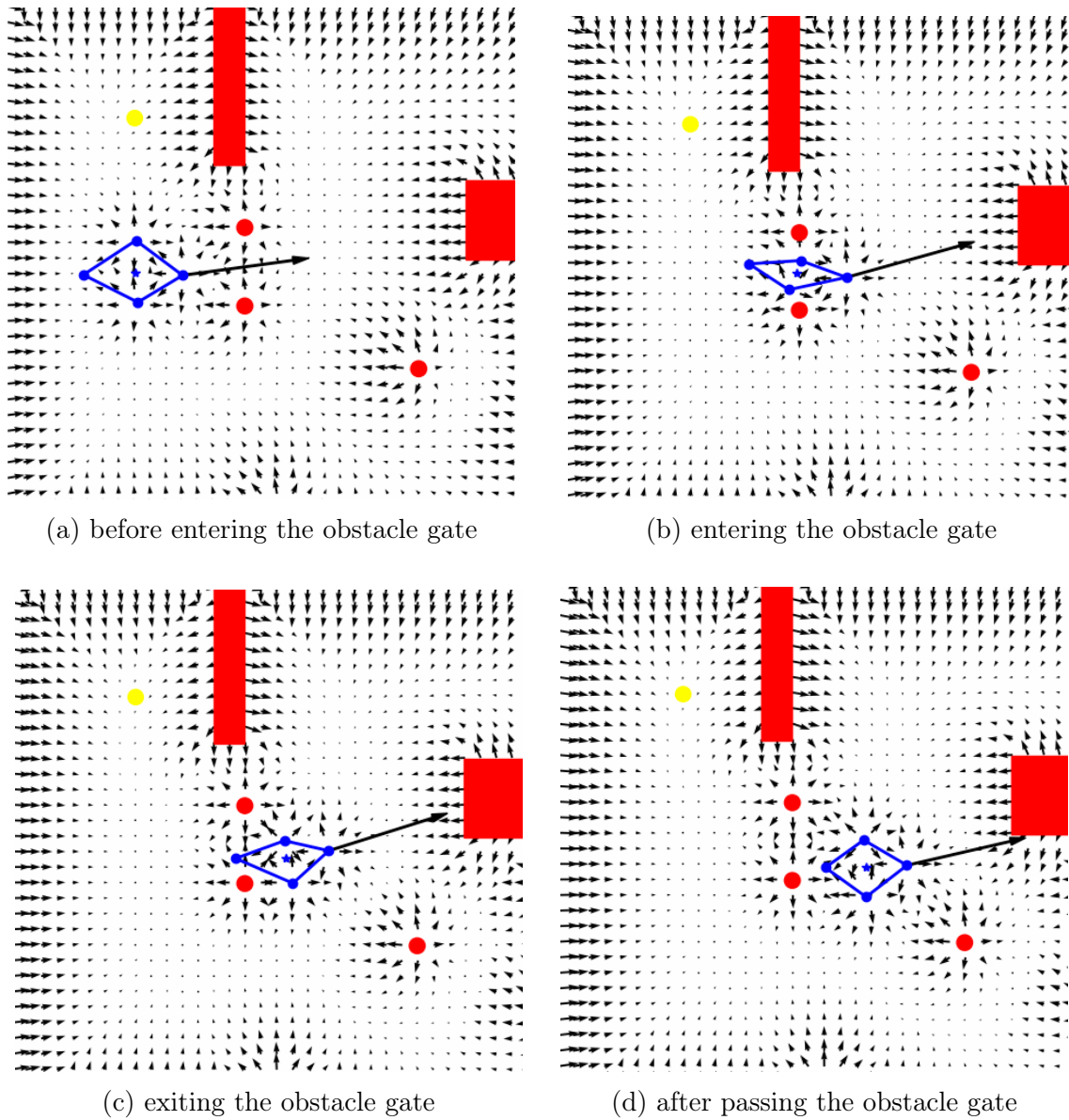
Figure 4-24: Formation of simulated drones adapts its geometrical shape in two dimensional case.
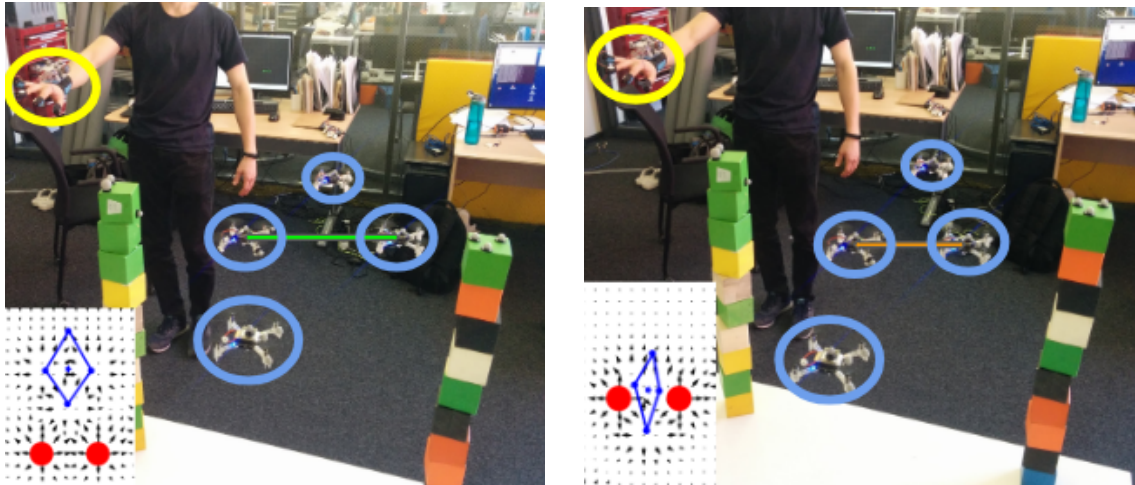
Figure 4-25: The formation of four drones is guided through the passage with artificial potential fields.

control, obstacle avoidance, and external disturbances. Despite the reason for the change of the swarm state, it is critically important to keep such a formation changes under control to ensure a safe flight mission. The next chapter considers the feedback design that helps the human be aware of the controlled system's changes.

Chapter 5

Tactile Feedback from the Swarm of Drones

HSI could significantly benefit if we couple the described control methods with tactile feedback, forming an interface (control and feedback) between a human and a formation. The initial hypothesis was that informing a human operator about the dynamic formation state (extension or contraction, for example) at the current time could potentially improve controllability. In this chapter, we overview the proposed wearable tactile display and its evaluation through the user study experiment.

5.1 SwarmGlove: Vibrotactile Wearable Glove

5.1.1 Technology

The wearable tactile displays, e.g., LinkTouch, represent multimodal information at the fingertips, i.e., a force vector, vibration, and contact state Tsetserukou et al. [2014]. However, vibration motors, which are easy to control, are widely applied in Virtual Reality Martinez et al. [2016], Maereg et al. [2017]. We used eccentric rotating mass (ERM) vibration motors that deliver the dynamic state of the swarm in the form of tactile patterns.

We have designed a tactile display prototype with five ERM vibrotactile actuators attached to the fingertips, as shown in Fig. 5-1(a). The vibration motors receive
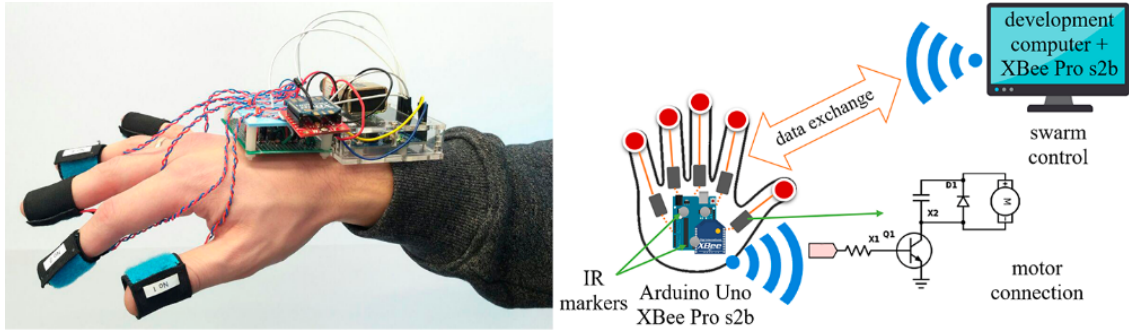
Figure 5-1: (a) - wearable tactile display, (b) - tactile device diagram.

control signals from an Arduino UNO controller. The unit with Arduino UNO and battery is worn on the wrist as a portable device. Infrared reflective markers are located on the top of the unit. The frequency of vibration motors is changed according to the applied voltage. The haptic device diagram is shown in Fig. 5-1(b). The glove microcontroller receives values of the formation state parameters from the PC. The Bluetooth and USB communications between the computer and haptic device were presented in the previous research Tsetserukou et al. [2014]. The approach in Tsetserukou et al. [2014] is limited in working distance and mobility. We implemented a radio frequency connection through XBee Pro s2b radio modules due to its robustness and high speed of data exchange. After the Arduino UNO gets the information about the current swarm state, it applies an appropriate vibration pattern.

5.1.2   Tactile Patterns Design

We designed eight tactile patterns for presenting the feeling of the swarm behavior at the operator's fingertips. My motivation for the selection of the particular tactile pattern was to bring valuable information that potentially can improve the quality (speed, safety, precision) of operation of the swarm in a complex outdoor environment.

During swarm manipulation by the operator, the formation can change its shape, becoming contracted or extended (Fig. 5-2(a, b, c). Therefore, the operator should consider this information since it contributes to better swarm operation in a cluttered environment. For instance, if the swarm gets too contracted, there is a risk of

a collision between the drones. On the other hand, while guiding the formation through the obstacles, the extended state of the swarm can also lead to the collision or a separation of the swarm to two groups. However, in many cases, the formation state is changing dynamically. In such a scenario, additional real-time information on state propagation direction could be provided to the human operator. In particular, it is important to know whether the drones are flying away from each other (distance between agents is increasing) or the drones are flying toward each other (distance is decreasing).
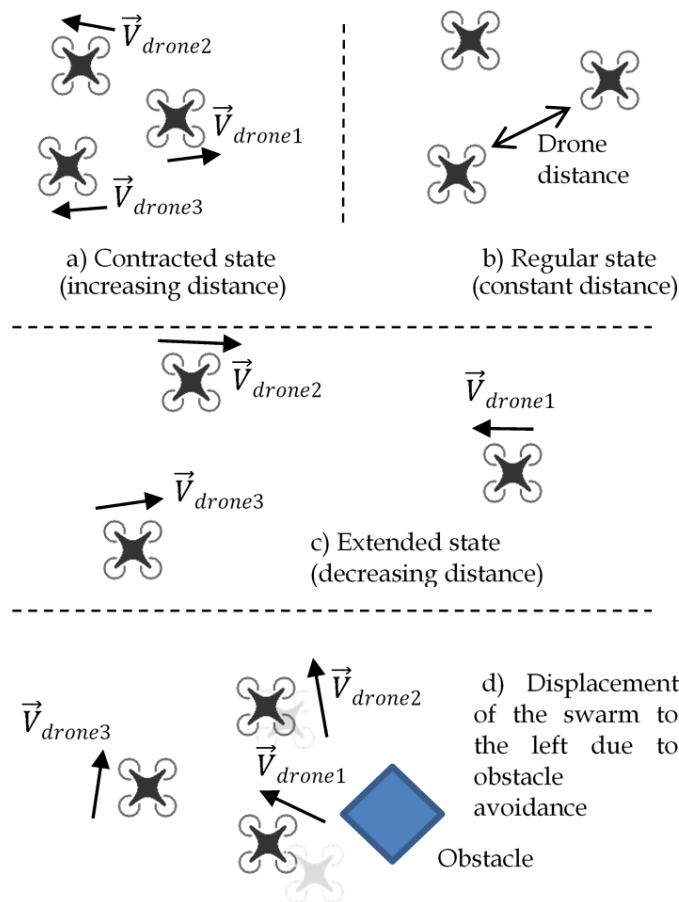
Figure 5-2: The information to be presented with the wearable tactile interface. Contracted (a), regular (b), extended (c) state of the formation, and displacement of the formation (d).

The tactile flow propagation presents the dynamic change of distance, e.g., if the distance is increasing, the flow goes from the middle finger to the outer fingers (Fig. 5-3(a, c, e)). Otherwise, the flow goes from the outer fingers to the middle one (Fig. 5-3(b, d, f)).
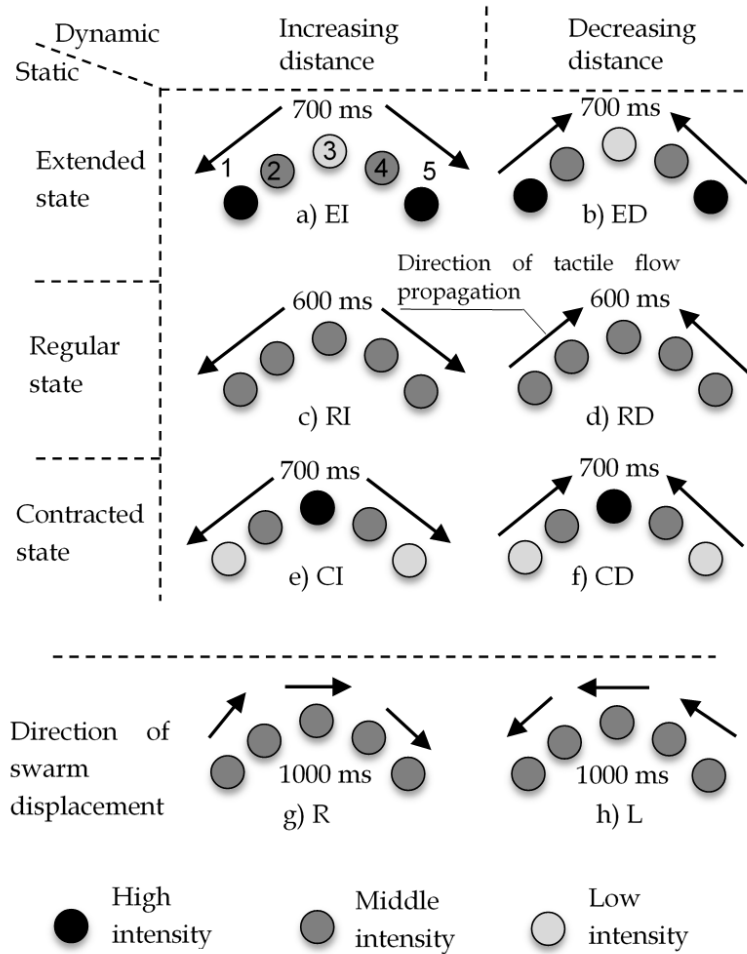
Figure 5-3: Tactile patterns for representing the state of the formation in terms of drone-to-drone distance and swarm displacement. Each circle represents finger of a right hand (view from the dorsal side of the hand). The gray scale color represents the intensity of tactor vibration.

The distance between drones is presented by the gradient of the tactor vibration intensity. If the formation is extended, then side vibration motors have a higher intensity than the middle one, see Fig. 5-3(a, b).

The other swarm state that we propose to present to the operator is the displacement of the center of mass of the swarm to the right or the left with respect to the direction of motion (Fig. 5-2(d)). Due to external factors as obstacles or wind, the swarm could move from the desired direction of motion. The swarm could separate into two groups while avoiding obstacles, which would also lead to the displacement of the center of mass. The direction of displacement is presented with the direction of tactile flow propagation, e.g., when the center of mass is moved to the right with

respect to the overall direction of motion, the tactile flow moves from the left finger to the right as shown in Fig. 5-3(g).

5.2   Experiment for Recognition of Tactile Patterns

Twenty-two right-handed volunteers (18 males and four females, aged 17-36) participated in the experiment. They were given a period for training (5-10 minutes) so that they could get used to the sensations and learn to recognize the signals. All participants positively responded to the device's convenience and level of perception.

5.2.1   Experimental Conditions

Optimal sensitivity of the skin is achieved at frequencies between 150 and 300 Hz Jones and Sarter [2008]. Therefore, for three vibration levels, we assigned average frequency values: 150 Hz, 200 Hz, 250 Hz (refer to three grayscale colors shown in Fig. 5-3). Tactile pulses lasted for 200 or 300 ms depending on the pattern since distinguishing tactile patterns is more comfortable with stimulus duration of 80 to 320 ms Jones and Sarter [2008].

5.2.2   Experimental Methodology for Recognition of Multimodal Patterns

The experiment was devoted to the detection of multi-modal patterns. The change of distance between drones was modulated by the vector of propagation of tactile stimuli (e.g., if the swarm is extending, firstly the third finger is activated, then, after shut down of the motor on the third finger, the second and fourth fingers are activated, and finally only the first and the fifth ones are vibrating, see Fig. 5-3(a) for reference). The gradient of the vibration intensity mapped the state of the formation (e.g., if the swarm is extended, side fingers have a higher intensity, see Fig. 5-3(a,b) for reference). To emphasize the direction of the gradient, we introduced a different duration of the tactile stimulus. The duration of the tactile pulse in the case of low (150 Hz) and middle (200 Hz) intensity was 200 ms; meanwhile, the

duration of the tactile pulses with high (250 Hz) intensity was 300 ms. There was no time interval between the tactile pulses within the same pattern. The total duration of tactile patterns is presented in Fig. 5-3 and ranged from 600 ms up to 1000 ms.

During the experiment, each pattern was repeated once, and the subject was asked to enter the number of experienced stimuli. Each of the subjects experienced 64 stimuli (8 patterns were repeated eight times in random order). The time of user response was also recorded. The results of the user study for the experiment are listed in Table 5.1. The name of the patterns goes as follows: Extended state, Increasing distance (EI) Fig. 5-3(a); Extended state, Decreasing distance (ED) Fig. 5-3(b); Regular state, Increasing distance (RI) Fig. 5-3(c); Regular state, Decreasing distance (RD) Fig. 5-3(d); Contracted state, Increasing distance (CI) Fig. 5-3(e); Contracted state, Decreasing distance (CD) Fig. 5-3(f); Right displacement (R) Fig. 5-3(g); Left displacement (L) Fig. 5-3(h). The diagonal term of the confusion matrix indicates the percentage of the correct responses of participants.

5.2.3 Experimental Results

The experiment results revealed that users detected all designed tactile patterns with an average recognition rate of 76.8%. Table 5.1 shows that the distinctive patterns EI, ED, RI, R, and L have higher percentages of recognition and therefore are recommended for the flight experiment's usage. On the other hand, patterns RD, CI, and CD have lower recognition rates. One common feature of CI and CD patterns is that they have low vibration intensity of the side fingers. Therefore, the intensity of the vibration of the fingers number 1 and number 5 (Fig. 5-1) (side fingers) plays a vital role in the higher recognition rate. It can be seen that participants mostly confused pattern CD with RD and pattern CI with RI, and pattern RD with ED, while other patterns are distinguished in majority cases. Therefore, it is required to design more distinctive tactile stimuli to improve the recognition rate in some cases. It is essential to notice that the direction of tactile flow propagating was distinguished in most cases both in cases middle-side/side-middle (EI, ED, RI, RD, CI, CD) or left-right/right-left (R, L) direction. Patterns R and L demonstrated the best recognition rates. One reason is that the direction of the tactile flow propagation

Table 5.1: Confusion Matrix

	EI	ED	RI	RD	CI	CD	R	L
EI	**89.8**	1.1	4.0	0.0	1.7	1.1	0.0	2.3
ED	1.1	**93.2**	0.0	1.7	0.0	2.3	0.6	1.1
RI	14.8	0.0	**76.1**	1.1	5.1	1.1	0.6	1.1
RD	0.0	21.6	1.1	**68.8**	1.1	4.5	0.6	2.3
CI	3.4	0.6	38.1	1.7	**53.4**	1.7	0.0	0.0
CD	1.7	1.7	2.8	48.3	0.6	**40.3**	1.1	0.0
R	0.6	0.0	2.8	0.6	0.0	0.0	**95.5**	0.6
L	0.0	0.6	0.6	0.6	0.0	0.0	0.6	**97.7**

Table 5.2: Average Time of Recognition Response

	EI	ED	RI	RD	CI	CD	R	L
Time, s	3.55	3.47	3.56	4.58	3.81	4.58	3.12	2.92

is easy to recognize. Another potential reason is that patterns R and L have the most prolonged duration. Finally, patterns R and L have a completely different structure - propagation from side to side, apart from all other patterns. Therefore, having six patterns, that have a similar structure (propagation in the middle-side/side-middle direction) could reduce the recognition rate.

In order to evaluate the statistical significance of the differences between patterns, we analyzed the results of the user study using single-factor repeated measures ANOVA, with a chosen significance level of $p < 0.05$. According to the ANOVA results, there is a statistically significant difference in the recognition rates for the different patterns, $F(7, 168) = 22.2$, $p = 4.3 \cdot 10^{-21} < 0.05$. The ANOVA showed that the type of patterns significantly influences the percentage of correct responses.

The paired t-tests showed statistically significant differences between most patterns. For example, there are significant differences between patterns EI and RI ($p = 0.023625 < 0.05$), EI and RD ($p = 0.000643 < 0.05$), EI and CI ($p = 7.53 \cdot 10^{-5} < 0.05$), EI and CD ($1.05 \cdot 10^{-6} < 0.05$), EI and R ($p = 0.029266 < 0.05$), EI and L ($p = 0.003584 < 0.05$), ED and RI ($p = 0.007042 < 0.05$) and others. However, the results of paired t-tests between patterns EI and ED, ED and R, ED and L, RI and RD, R and L did not reveal any significant differences, so these patterns have nearly the same recognition rate.

The average time of response, which is the time between the end of pattern exe-

cution and the moment when the key is pressed on the keyboard, is slightly different for each participant. From Table 5.2, we can conclude that participants have spent less time to guess pattern R and pattern L. Based on average recognition time, we could conclude that patterns R and L could contribute to more fast and intuitive immersion into the control process, which makes them good candidates for the verification during the flight experiment. The longest time was 8.92 seconds for Pattern EI. On the other hand, 1.72 seconds is the shortest time period for Pattern R. On average, 3.53 seconds have been spent to respond for pattern recognition. Important notice here is that time presented in Table 5.2 also include the time interval between the moment when the user understand the patter and the moment when the user pressed the button on the keyboard. Therefore, it is not clear recognition time.

5.3 Generalization to Other Types of Robotic Systems

Tactile feedback do not consider the plant dynamics directly. Instead, the developed tactile feedback delivers the information about the high-level swarm state dynamics: drone-to-drone distance and global displacement. Therefore can conclude that the generalization of the control method discussed in Section 4.3.7 is applicable to the tactile feedback as well. Although, the relaxation point is that the controlled system do not have to follow the same dynamics rule as discussed in Section 4.3.7 (e.f. being able to translate in any direction). The extended or contracted state and increasing or decreasing agent-to-agent distance can occur with most types of adaptive swarm systems. therefore, the developed SwarmGlove and tactile patterns can be applied for example to the swarm of fixed wing air crafts without any modification.

The important limitation here is the rate of the information we are able to deliver thought the tactile sensation. As can be seen in Table 5.2, it takes seconds to recognize the pattern. As a result, the change rate of the dynamics of the controlled system can not be faster than the information flow rate through the tactile channel.

5.4   Summary

We presented the developed wearable display SwarmGlove that is used to deliver the information about the swarm state to the human operator. SwarmGlove provides tactile sensation right to the human fingertips. We distinguish eight swarm states that the human operator has to be aware of. We designed a set of tactile patters representing a language that reports to the human about the dynamic and static swarm parameters during operation. To evaluate the device, we conducted a user study with 22 volunteers. We demonstrated statistically significant difference in the recognition rate for different patterns ($F(7, 168) = 22.2$, $p = 4.3 \cdot 10^{-21} < 0.05$). The user study revealed the average recognition rate of 76.8% for patterns. Some patterns were recognized in a better way, while the other has to be improved in order to be used in real flight experiments.

Chapter 6

Guidance of the Formation with Impedance Control and Tactile Feedback

In the previous Chapters 4 and 5, we developed the control methods and wearable tactile display for the swarm state feedback. Both control and feedback form the communication interface between the human operator and the swarm system. In the current chapter, we present the evaluation methodology and the experimental results of the guidance methods presented in the previous chapters.

We already presented a general overview of the interface in Fig. 1-3. In Fig. 6-1 we show a more detailed picture of the interface that we developed with all the components (impedance control, obstacle avoidance, tactile display, and tactile feedback). The information flow is the following. Formation of drones flies in the environment. State of the fleet can be changed due to control signals from the human or based on local control laws (drone-to-drone or drone-to-obstacle avoidance). The human is becoming aware about the state of the formation with the help of tactile feedback. Based on the information about the guided fleet of robots the operator generates the control signal with a glove, which is it turn changes the formation state. This is general overview of the interaction loop.

In the current chapter, we integrate the control and feedback part.

To estimate the performance of the proposed control methods and SwarmGlove
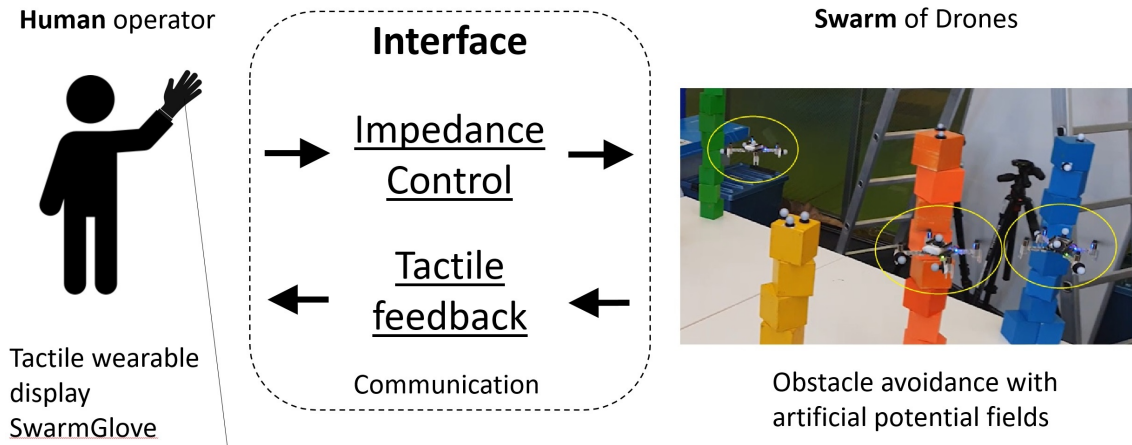
Figure 6-1: General diagram of the proposed guidance method.

during the guidance, we set up the real flight experiment in the indoor environment. During the experimental validation the user has to navigate the fleet of three Crazyflie 2.0 drones through the set of obstacles with different feedback conditions. The flying test bed represent a space (5 m × 5 m × 5 m) with a Vicon motion capture system and other infrastructure described in the previous chapters. We use the same facilities to validate the joint control and feedback.

6.1 Role of the Tactile Feedback

As discussed above, the proposed tactile interface could be helpful when the fleet operator's visual feedback has poor quality or overloaded with information. On the one hand, communication problems or limited field of view of onboard sensors could lead to the degradation of the visual channel. Additionally, the human operator's limited cognitive abilities prevent the user from fully understanding the state of the fleet, especially when the number of drones is high. In such cases, the tactile interface could supplement or even replace the visual feedback.

Considering small-sized drones, such as Crazyflie 2.0, which can move fast, and a limited flight space that we have in the laboratory (5 m × 5 m × 5 m), the state of the fleet could be changed in a fraction of a second during the experiment. To operate the formation in such an environment, the visual feedback is sufficient, because it is fast and can cover all flight space. Supplementing the visual feedback

with the tactile feedback is inefficient in the experimental conditions since it takes up to one second to execute a tactile pattern. We conducted several preliminary flights, providing both visual and tactile feedback to the subjects, but the users relied only on the visual channel. The other option is to replace the visual channel with a tactile sensation completely. It could be useful when the fleet flies through the areas where it is impossible to acquire or transfer high-quality visual information. For this reason, we conducted a flight experiment with only visual feedback and with only tactile feedback. Our hypothesis is based on the assumption that the developed tactile interface could help to navigate the fleet through the blind zones with no visual feedback.

Due to the reasons discussed above, current experimental conditions do not allow to supplement the visual channel with tactile. However, in real-life applications, the size of the operational area could be big enough to prevent direct visual observation of the whole space. The size of the robots and the size of the formation could lead to a relatively slow change in the fleet state. In such a case, developed tactile feedback could effectively contribute to the visual feedback, by not only replacing but also by supplementing it.

6.2   Information to be Presented to the Operator

The next decision we made was about the parameters of the fleet that have to be reported to the human operator through the tactile interface. As discussed before, for the flight experiment, we use small quadrotors and limited flight space. In such an operational condition, change of the formation shape (increasing or decreasing drone-to-drone distance) could happen quickly. Therefore, it is inefficient to provide slow tactile feedback (see Table 5.2) about it.

On the other hand, contracted (Fig. 6-2(a)) or extended (Fig. 6-2(b)) state of fleet could last for seconds, which makes them applicable candidates for the flight verification. For the experiment, we assume that the formation has a default configuration of the equilateral triangle. We decided that if the area of triangle or distance between any drone pair is more than 10% bigger or 10% less than the

default value, then the formation is considered to be in the extended or contracted state, respectively.

Along with the contracted or extended state, it is reasonable to provide the direction of the fleet center of mass (CoM) displacement. CoM displacement could happen in both extended or contracted state. For example, in the contracted state shown in Fig. 6-2(a), CoM moves to the left with respect to the direction of motion, as far as drone1 and drone2 move to the left from their default positions. Considering the extended state, as shown in Fig. 6-2(b), CoM moves to the right as far as drone2 avoiding the obstacle over the right side.

The displacement direction in the contracted state (Fig. 6-2(a)) is straightforward from the operator point of view, as all drones move collinear with CoM displacement (in Fig. 6-2(a) drone1 and drone2 move to the left and the CM displaces to the left as well). On the other hand, the displacement direction in the extended state is more complicated to understand, see Fig. 6-2(b), since the CoM moves on the right, but the majority of the drones go around the left side of the obstacle (the overall goal is to keep the default shape to be able to complete a successful flight mission, formation division is not allowed). To address this complication, we designed tactile feedback patterns to be more intuitive for the operator. To avoid misunderstanding from the user, for the experiment we designed the patterns to inform the user about the recommended direction of hand motion to minimize CoM displacement rather than the displacement of the CoM itself.

6.3   Simplified Patterns for the Flight Experiment

For the next step, we selected which patterns to use to represent contraction, extension, and displacement. Initially, we designed the system to be applied for outdoor operation in unstructured environments such as cities, where the fleet moves slowly, and the distances are much bigger than indoors. Considering the small flight facilities that were available for this research (5 m x 5 m x 5 m size room), the state of the fleet of three Crazyflies could change rapidly. Therefore, we decided to upgrade the high-quality patterns (EI, ED, R, and L from Chapter 5) and design faster and

a) Contracted state.
All of the drones move on the left side from obstacle

$\vec{V}_{drone3}$

$\vec{V}_{drone2}$

$\vec{V}_{drone1}$

Obstacle

Direction of motion

Obstacle

b) Extended state.
Most of the drones move on the left side from obstacle

$\vec{V}_{drone3}$

$\vec{V}_{drone2}$

$\vec{V}_{drone1}$
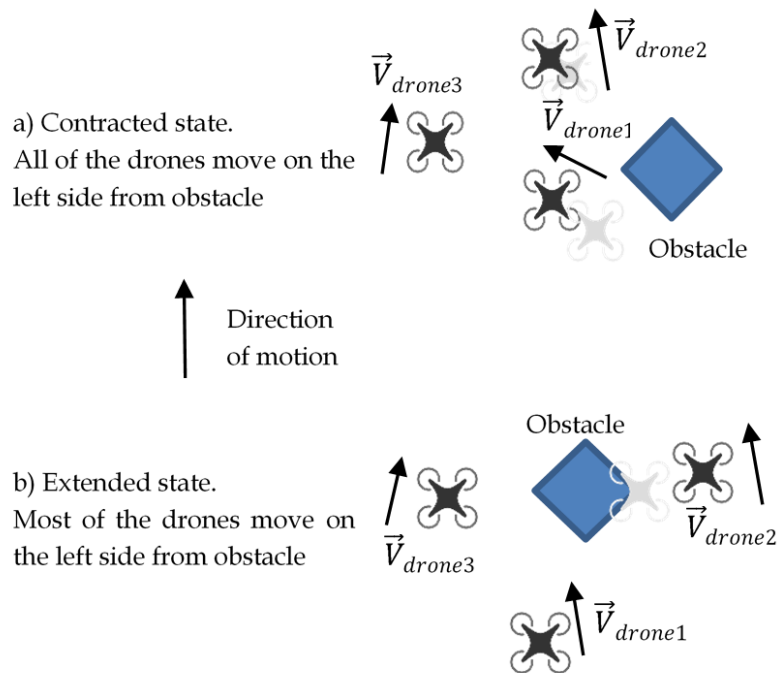
Figure 6-2: Information to be presented to the human operator. Drones avoid obstacles.

simpler versions of them for indoor flight test.

Our goal was to create patterns that will present two types of information: extension/contraction and the direction of motion to prevent the center of mass displacement. Developed multi-modal patterns are presented in Fig. 6-3 (CR – Contracted state, Right Direction; CL – Contracted state, Left Direction; ER – Extended state, Right Direction; EL – Extended state, Left Direction;). For the contracted state, we use three middle fingers (2, 3, 4), and for the extended state, we use side fingers (1 and 5). For the contraction, the direction of the displacement is shown with the tactile flow propagation. For the extension, the direction of the displacement is shown with the right or left finger. Presented patterns are easier to recognize and several times faster than the patterns shown in Fig. 5-3. The recognition rate is 100% (based on 160 trials among 8 participants).

In the case of CR or CL pattern, the best decision is to move the fleet towards the direction of the pattern. For the ER or EL patterns, the best strategy is to move a little bit back (to prevent separation of the fleet) and then move towards the vibrating finger. All of these strategies were presented to the subjects during
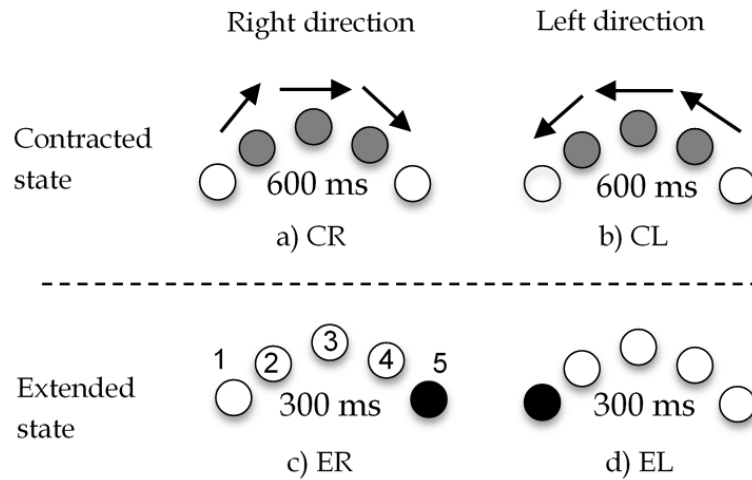
Figure 6-3: Simplified tactile patterns for representing the state of the formation in terms of drone-to-drone distance and fleet displacement. Designed for the flight experiment.

the training of the user study experiment. As discussed at the end of Section 6.2, the center of mass displacement correlates differently with the proper direction of the safety movement. That is why for the patterns CR or CL, the direction of displacement is collinear with the displacement of the center of mass, while for the ER or EL patterns, it is the opposite.

6.4 Experimental Methodology

Six right-handed male users (22 to 28 years old) took part in the flight experiment where they were asked to navigate the formation of three Crazyflie 2.0 drones through a labyrinth with obstacles (Fig. 6-4) using either only visual or only tactile feedback. The state of the formation could be changed due to obstacle avoidance or impedance interlinks, as described in the upper sections. The motion is constrained to be two-dimensional on the same height. In order to remove the sound of the drone motors, subjects wore noise-canceling headphones playing white noise. Each participant wore safety glasses. The protocol of the experiment was approved by a Skolkovo Institute of Science and Technology review board, and all participants gave informed consent.

In the beginning, the swarm takes off near the starting point of the labyrinth.

Figure 6-4: Human operator manipulates the formation of three quadrotors.

After takeoff, the recording of data about the position of all objects (drones, human, obstacles) starts. The obstacles that we used were vertical columns with unlimited height. Participants were not aware of the configuration of the labyrinth beforehand. The participants' main goal was to avoid the non-default states of the formation, such as contraction or extension. The default shape of the triangle has to be maintained. The default value for the area was 0.0693 m^2. The default drone-to-drone distance was 0.4 m. To make the visual trial more complicated, the physical obstacles (cubes on the table) were placed below the drones' flying altitude and were virtually extended to an unlimited height. Thus it is becoming more difficult to approximate the distance between a drone and an obstacle visually.

Before the flight experiments, we did not provide the users with certain values of the area or target drone-to-drone distance. We just asked them to keep the right triangle formed by three drones while going through the set of obstacles, receiving either visual or tactile feedback. The right triangle was demonstrated to users before the experiment when the drones were hovering with no obstacles nearby.

The trial of the experiment with pure tactile feedback is shown in Fig. 6-5. In Fig. 6-5 the user is receiving the 'Contracted Right' CR tactile pattern (shown in the down right corner). The obstacles are shown with the green columns on the simulation on the right.
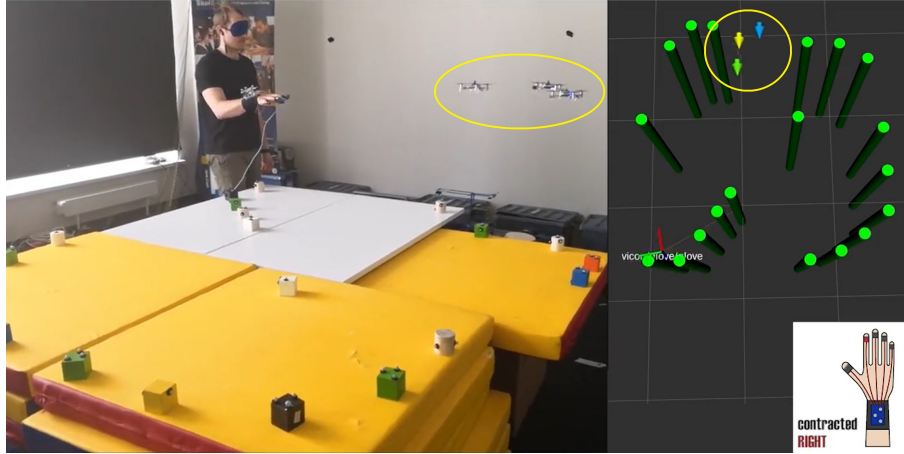
Figure 6-5: Human operator guides the group of robots using tactile feedback.

Training included learning patterns presented in Fig. 6-3. All possible decision strategies regarding different tactile patterns were presented to the users during the training period. Training also included guiding the formation through the maze with only tactile feedback first, and with only visual feedback after. SwarmGlove provided tactile patterns when the state parameters of the formation overcame the threshold values (e.g., becoming contracted). Regarding the tactile trial, in the default state, no tactile patterns were provided, which meant that it was possible to move forward.

After training, for the experiment, users overcame two different unknown configurations of obstacles, first with tactile and then with visual feedback (two trials with tactile and two with visual feedback in total). Configurations of obstacles were selected randomly for every user.

6.5   Flight Experiment Results

The initial hypothesis was confirmed. It is possible to navigate the fleet of drones in a cluttered environment using only tactile feedback about the state of the fleet. Users completed the labyrinth in 12 trials.

As discussed in Section 6.1, for the current experimental conditions ((when the controlled system right in front of the human and the operation space is small), performance with visual feedback is better than with tactile feedback. Which is

obvious result because the vast majority of information that the human receives from the environment comes with vision and as a result it is the most convenient feedback type, especially when the controlled drones are right in front of the operator. We compare some of the parameters to understand the behavior of participants better in both cases. The mean values of parameters for all participants are presented in Table 6.1.

Regarding the question of the acceptable parameter values - it can vary based on application. We actually did not couple the tactile or visual feedback with certain maximum thresholds of parameters. Therefore it is unfair to judge the swarm behavior from the experiment in terms of certain values. SwarmTouch technology was developed as a general approach to a guidance problem. The SwarmTouch technology can be fine tuned to meet specific target parameters of a certain application.

Moreover, the actual values of errors can vary for the different experimental setup. What is more important in our research, is the comparison of visual (which is considered as a state of the art or default solution to the feedback problem in the current experiment) and tactile feedback. You can see this comparison in the Table 6.1. The analysis is presented below.

The mean path length of the formation centroid is almost two times longer for the tactile feedback, which indicates that with tactile feedback subjects explore the space more actively. The mean velocity with tactile feedback is 65% slower. Considering the acceleration and jerk of the centroid, it could be concluded that with tactile feedback, the fleet is guided more smoothly by 47%.

One of the primary metrics is the area of the triangle (formed with actual drone positions) while going through the labyrinth. We picked the area as a high-level parameter because it is intuitive in some cases. For example, we want to collect the imagery data with a swarm over some agricultural field - we want to make sure that we cover the target area with images at every time step, therefore the swarm has to maintain the default area of its own.

But it is also true that it can be the case when the area is equal to the default one but the drone-to-drone distance is non-default. In addition, during image collection with a swarm of drones, it is critically important to maintain the distance

between neighbor drones to keep certain overlap between neighbor images. Based on these statements, we conclude that drone-to-drone distances also represent detailed information about the swarm behavior. Area error metrics are averaged over all participants. Drone-to-drone distance error metrics are averaged over all drone pairs and all participants.

Interestingly, tactile and visual performance does not differ much in case of area and distance metrics. Therefore, the developed tactile interface allows the possibility to navigate the fleet through cluttered environments and, in a precise manner, maintains the desired geometry of the formation. Although, there is no big difference in metrics for the area and drone-to-drone distances (if we compare visual and tactile case).

The mean drone-to-drone distance error was 5.7% and 8.5% from the default 0.4 m value, for Visual and Tactile feedback type respectively. The max drone-to-drone distance error was 50% and 63% from the default 0.4 m value, for Visual and Tactile feedback type respectively. The mean area error was 10% and 14% from the default 0.0693 m^2 value, for Visual and Tactile feedback type respectively. The max area error was 49% and 56% from the default 0.0693 m^2 value, for Visual and Tactile feedback type respectively.

Considering more closely the behavior of the users with respect to the executed patterns, we investigated the fleet behavior right after the patterns were performed (see Fig. 6-6). In the example of state change shown in Fig. 6-2(a) for example (contraction and displacement to the left), the user receives a CL pattern (Fig. 6-3). Then, as the formation is guided to the left, the fleet centroid should move to the left, and the area should increase back to the default value. We compared the area and centroid displacement at the current time (for the time interval 0-3300 ms after the start of each pattern execution) with the corresponding values at the time when the pattern started. Creating such comparisons for all patterns helped us to evaluate the correctness and duration of human operator response. The evaluation was performed for all participants. It is possible to see from Fig. 6-6 that, in general, the correctness of operator decisions reaches 75-80% after 2-3 seconds after pattern execution. CR/CL patterns work better for the displacement,

Table 6.1: Parameters of the Fleet Performance

Parameters	Feedback type		Difference of tactile with respect to visual feedback
	Visual	Tactile	
Centroid trajectory			
Mean centroid length of a path, m	3.76	6.00	↑**60%**
Mean centroid velocity, m/s	0.23	0.08	↓**65%**
Mean centroid acceleration, m/s^2	0.31	0.16	↓**48%**
Mean centroid jerk, m/s^3	1.92	1.03	↓**46%**
Drone-to-drone distance error (default distance is 0.4 m), averaged over all drone pairs and all participants			
Mean, m $mean(abs(Position_{drone_i} - Position_{drone_j}))$	0.023	0.034	↑**48%**
Standard deviation, m $std(Position_{drone_i} - Position_{drone_j})$	0.03	0.05	↑**67%**
Maximun, m $max(abs(Position_{drone_i} - Position_{drone_j}))$	0.20	0.25	↑**25%**
Swarm area error parameters (default area is 0.0693 m^2), averaged over all participants			
Mean, m^2 $mean(abs(Area - Area_{default}))$	0.007	0.01	↑**42%**
Standard deviation, m^2 $std(Area - Area_{default})$	0.008	0.012	↑**50%**
Maximum, m^2 $max(abs(Area - Area_{default}))$	0.028	0.039	↑**39%**
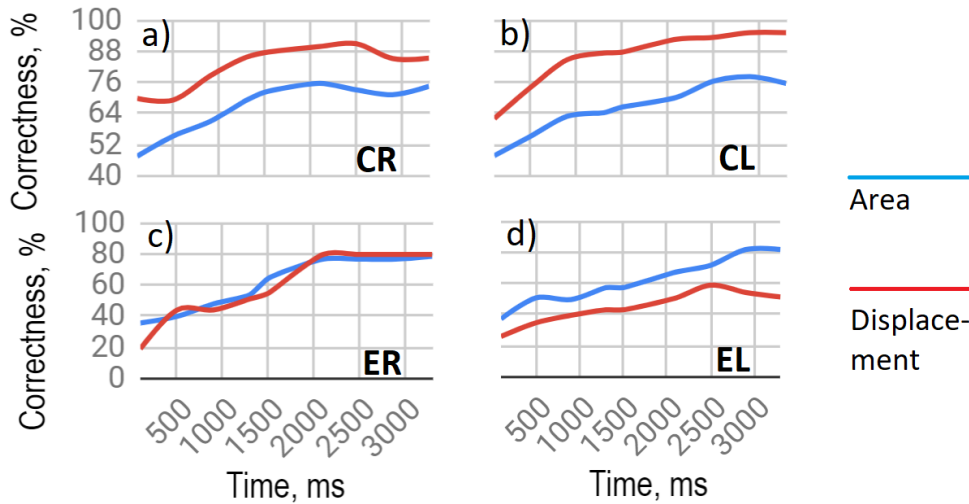
Figure 6-6: Percentage of proper correction (returning area to the default value and decrease of displacement) of fleet state after the start of pattern execution.

and the overall performance of CR/CL is higher than ER/EL. It might be because of a more simple behavior strategy for CR/Cl patterns (discussed in Section 6.3).

Examples of trajectories during the experiment are shown in Fig. 6-7. Drones trajectories (dashed lines) are represented in *XY*-plane (from the top view). The fleet flies among obstacles (small red squares). The yellow cylindrical safety zone surrounds each of the obstacles. The union of all these cylindrical obstacles vicinity defines the area where drones cannot fly. The solid blue line represents the fleet central point path.

It could be noticed in the left column of Fig. 6-7 (tactile trial) that the centroid trajectory has several turns near the obstacle vicinities. At these moments, a human operator receives tactile patterns that help him understand that the fleet is located near the obstacles and provides information on how to control drones to avoid collisions and reach the finish point. It can be seen that visual feedback allows a human operator to guide the fleet among obstacles (although with visual feedback, users do not pay much attention to the formation state, just going to the finish point).
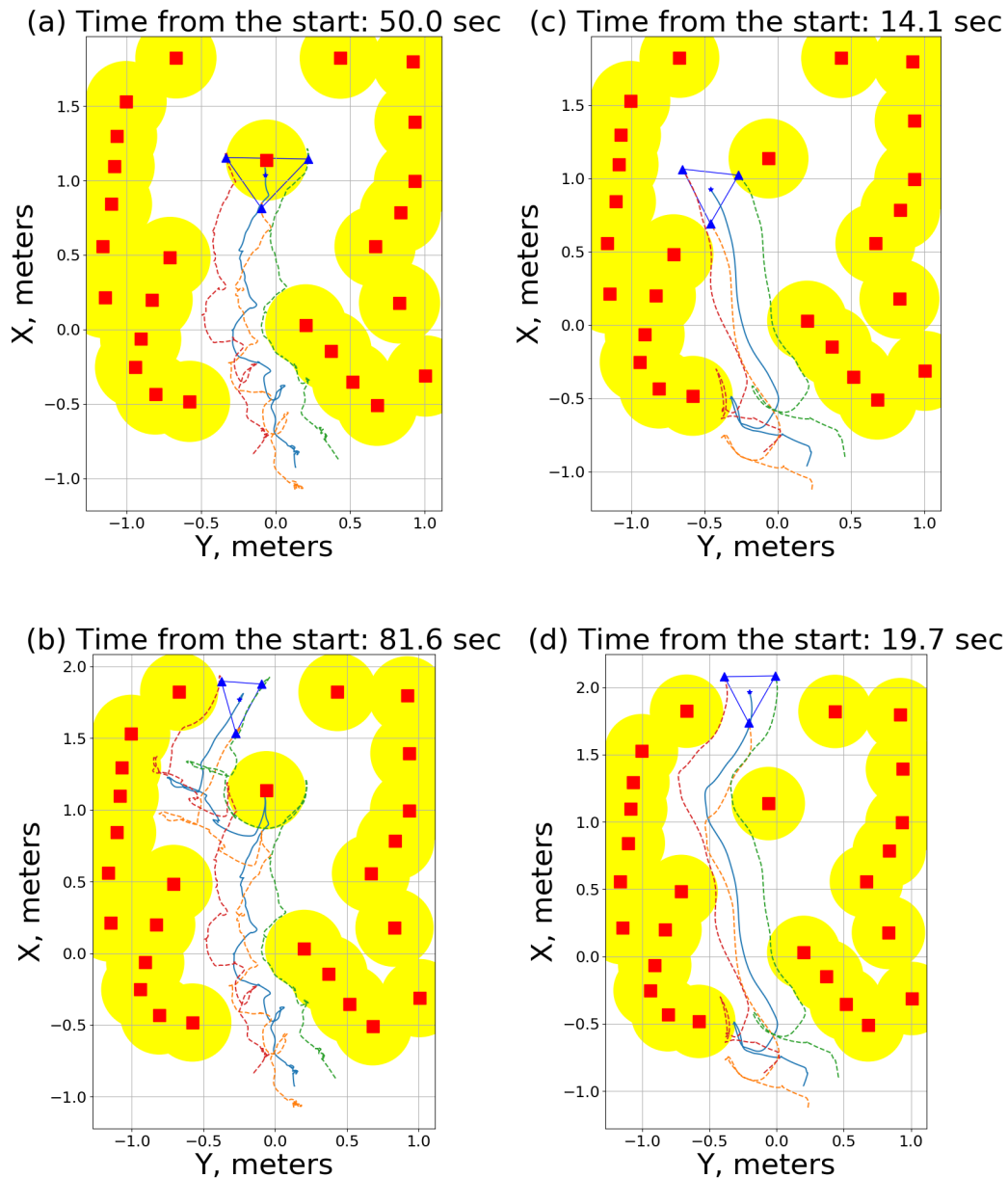
Figure 6-7: A top view of trajectories of drones and centroid while being manipulated thought the maze. Left column of two pictures (a-b) represents formation of three drones navigation with the help of pure *tactile feedback*. Two pictures on the right (c-d) - navigation with pure *visual feedback*. Solid line is the trajectory of the fleet centroid. Dashed lines are actual drones trajectories. Red squares represent real obstacles with yellow safety zones. Formation shape is depicted with blue triangle.

6.6 Limiting Factors

6.6.1 Control

The limitation that is rising from the proposed control approach is that each agent has to receive information regarding the human control input to be able to update the nearest impedance links. There are two way to accomplish it: establish direct communication with the ground control station or distribute the information via the swarm. As a result, the main constrain is that we are not able to implement the scenario when each agent relies purely on the local information.

6.6.2 Feedback

The swarm system is a complex structure which can have multiple state parameters, as shown in Fig. 5-2. Formation state changes dynamically during the operation. Therefore it is necessary to use multimodal patterns in order to represents the swarm behaviour to the operator. We proposed a set of intuitive tactile patterns in Section 5.1.2.

The performance of the multimodal tactile patterns is limited by the masking factor as reported in the literature by Evans [1987] and by Tan et al. [2003]. The problem of masking is revealed when the one tactile stimulus is immediately followed by the other without any time gap. It turns out that the human is not able to distinguish and recognize any of them. That is the reason why we introduced time delays between the tactile patterns and separate tactile stimulus.

As an outcome, the main limitation is that we are not able to increase the density or rate of the information provided with the tactile feedback. Information flow rate is asymptotically limited with the masking factor. Therefore, the awareness of the human operator about the swarm dynamics is also limited.

6.7 Summary

In this chapter, we coupled the control methods and the tactile feedback into a single interface. We considered the flight facilities and proposed the methods to

deliver feedback to the human during the experimental guidance. We extracted the most helpful information for the operator and proposed simplified tactile patters based on the user study experiment from the previous Chapter 5. We asked six right-handed users to participate in the research where they guided the group of three Crazyflie 2.0 drones troughs the maze with an unknown set of obstacles. We rearranged the obstacles for each separate trial. The volunteer received either tactile or visual feedback. The objective for the users was to maintain the default triangle shape of the robotic group during guidance.

It was demonstrated that it is possible to navigate robots in complex unknown environments with pure tactile feedback. It was an unfair comparison between visual and tactile in some sense because the visual channel provided extensive information in our limited flight space. Anyway, we compared some of the flight parameters and received noticeable results. With tactile feedback, users explore the environment more densely. Visual feedback led to three times faster guidance. Simultaneously, the tactile feedback's dynamical parameters are lower, which led to more smooth motion. The main objective (maintenance of the default geometry) was accomplished in a similar way for tactile and visual feedback.

We showed how the robotic team reacts to each tactile pattern. A human operator controls the formation behavior. Therefore we revealed the quality of user response to each tactile pattern. On average, the operator performed the correct action during 2-3 seconds after the start of tactile pattern execution.

Chapter 7

SwarmCloak: Deployment of Drones from the Human Hands

Guiding a swarm of quadrotors, which is discussed in the above Chapters, has a lot of challenges. Partially, these challenges are addressed in Chapter 4 and Chapter 5. Apart from that, takeoff and landing operations are the necessary sub-operations prior and after any flight.

In the current chapter, we propose a novel system SwarmCloak for multiple drones deployment in midair. Wearable tactile display with a light sensor makes it possible to land the fleet of nano-quadrotors on the human hands. The developed technology is based on a hypothesis that tactile feedback could improve the accuracy of landing, and human convenience, especially when several drones are landing on the human limbs simultaneously.

7.1   Design of Wearable Tactile Interface

The purpose of the designed tactile interface is to deliver the information about the drone's position relevant to the landing pads to the operator. The vibration, which is activated by light, is proportional to the light intensity. If the drone is far away, no vibration occurs. While the drone is approaching the human hand, the vibration intensity is gradually increasing. The tactile stimulus's location reveals the drone's position in a horizontal plane, and stimulus intensity shows the distance to the robot

Figure 7-1: Deployment of four drones with wearable tactile display SwarmCloak.

in the vertical direction. The higher the intensity, the closer drone to the user's skin.

The overall system consists of landing pads (with light sensors and vibration motors) and drones with LEDs on the bottom, as shown in Fig. 7-1. The single sensor-vibrator unit (SVU), shown in Fig. 7-2, is based on HALUX technology Uematsu et al. [2016] and comprises a linear resonant actuator (LRA) (LD14-002, Nidec Copal Corporation), a photo-transistor (PT19-21C, Everlight Electronics CO., Ltd.), and an oscillation circuit for LRA. LRA was selected for its fast response of less than 20 ms. Optimal sensitivity of the skin is achieved at frequencies between 150 and 300 Hz, according to research findings Jones and Sarter [2008]. Meanwhile, the resonance frequency of the oscillation circuit with LRA is 150Hz. Therefore, the vibration frequency is set to 150Hz.

The amplitude of vibrations is modulated by the photo-transistor. During the landing stage, the distance D between the drone and the landing pad is reducing. At the same time, the illuminance of the photo-transistor PT19-21C is increasing along with decreasing the illuminated area (LED viewing angle is fixed). Therefore, the illuminance is inversely proportional to the D2. As a result, when the drone is getting closer to the landing pad, the user experiences more intensive vibration. We keep the discussed vibration settings for all experiments which involve tactile
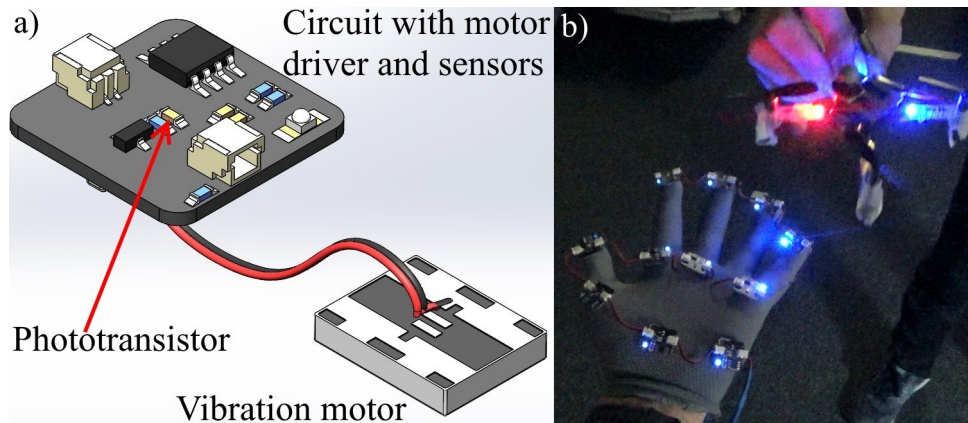
Figure 7-2: a) Sensor-vibrator unit (SVU), b) SVU operation.

feedback.

The models of the developed device with the main components are shown in Fig. 7-3. The electronic circuit of each sensor-vibrator unit is placed in the plastic cover, which has a hole above photo-transistor with a diameter of 3 mm for the light penetration (Fig. 7-3). The hole is of 10 mm deep, to protect the sensor from undesirable environmental lights and infrared emission of the motion capture system. The photo-transistors are pointed upwards to detect the light emitted from the array of LEDs at the drone's belly. The landing plates (Fig. 7-3) is made of transparent acrylic material (diameter and thickness of each plate are 160 mm and 3 mm, respectively).

Since human palm has a flat and wide contact area with high tactile resolution Weinstein and Weinstein [1964], for the hand-based landing pad, Fig. 7-3(b), eleven SVUs were integrated directly into the glove's palm and finger pad areas. Five of the SVU units were placed on the finger pads and the rest on the palm so that the user can easily distinguish single stimuli. For the hand based display, the vibromotor is directly attached to the circuit of the SVU unit. A cylinder with a height of 40 mm, a diameter of 75mm, and a thickness of 4.5 mm keeps the circular landing plate attached to the palm area of the glove. The landing pad, which has a diameter of 160 mm and a thickness of 3 mm, is made of transparent acrylic material so that IR light easily could pass through.

In the same manner, for the forearm-based landing pad shown in Fig. 7-3(c), seven LRAs were attached to a thin sponge rubber pad that is then placed directly
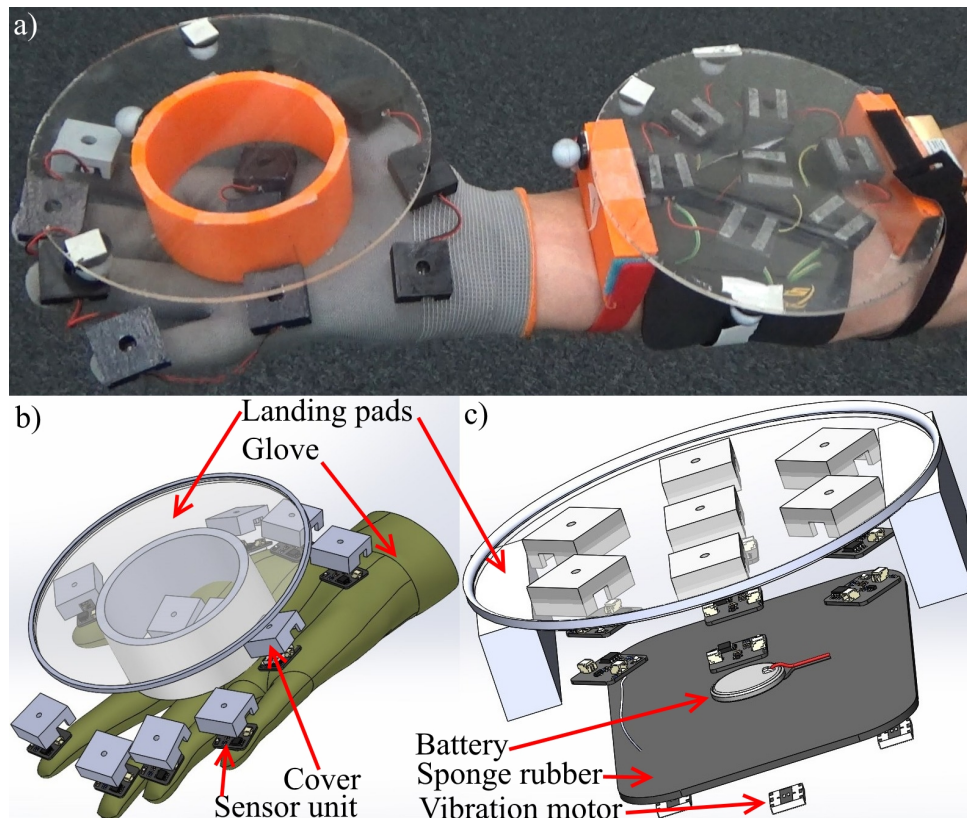
Figure 7-3: a) Landing pads, b) hand-based, c) forearm-based.

on the forearm, whereas the same number of sensor units were firmly attached to the ventral side of the landing pad. Such an arrangement helps to provide uniform sensing and tactile stimulation in case of a curved forearm surface. One unit is placed in the center, and the equal distribution of the rest units make a circle of radius 40 mm around the center in order to have a robust reaction on the IR light emitted by the nano-quadrotor. Moreover, the positional arrangement of the LRAs replicates the position of the sensors. It helps to have an explicit sensation of the drone position above the arm by avoiding position-sensation mapping. The circular landing plate has the same dimensions and material type as the hand-based one. It is noteworthy to mention that the operational mode of each unit is the same.

Airflow from the landing quadrotor could provide strong tactile cues, which may actually be used as a source of additional information about the position of drones. As far as in the experiments we aimed to investigate only vibrotactile feedback, the effect of tactile cues to the hand, which is caused by the airflow, was canceled by the increased size of landing plate with additional cardboard. The size of the cardboard

was 300 x 300 mm. It was employed only for the experiments, and in the case of real-life applications, the cardboard is not needed.

7.2 Aerial platform

For the experiments, we used Crazyflie 2.0 quadrotors, as shown in Fig. 7-4. Small size (9 cm2) and lightweight (27 grams) secure safety, which is crucial for applications involving human-robot physical interaction. Subjects have worn safety glasses during the experiment to protect the user's eyes from drones' sudden movement. Vicon motion capture system with 12 IR cameras covering 5 m $\times$ 5 m $\times$ 5 m space tracked the quadrotors, landing pads, and the human hands. We decreased the intensity of IR strobe of motion capture cameras to diminish the sensitivity of the photo-transistors of the landing pad to the infrared spectrum. We used the Robot Operating System (ROS) Kinetic framework to run the custom software and ROS stack for Crazyflie 2.0. Sensors of the landing pad are sensitive to the infrared spectrum; for that reason, we have decreased the intensity of IR strobe from the motion capture cameras.

The prototyping deck, which was modified with three IR LEDs and three 39 Ohm resistors, was directly attached to the micro-quadrotor's bottom side. Tactile display is sensitive to the visual and infra-red (IR) light spectrum. Therefore, to avoid any additional visual clues for the human operator, we used IR LEDs (IR333-A, Everlight Electronics Co Ltd) with peak wavelength 940nm and viewing angle of 20°. A small angle of view of LEDs allows for activating the part of tactile display, which is strictly below the drone, which helps to provide precise feedback. The IR LEDs and resistors were soldered onto the deck, as indicated by the schematic in Fig 7-5. As seen from the schematic, three IO pins were used to control each LED's state individually. The polarity to turn the LEDs on is reserved as they are connected between VCC and MCU pins. We modified the Crazyflie firmware to add a new parameter for controlling IO pins using the software code. The new firmware was flashed into each nano-quadrotor by the wireless bootloader. During the experiments, all the LEDs on the deck were switched on to create maximum
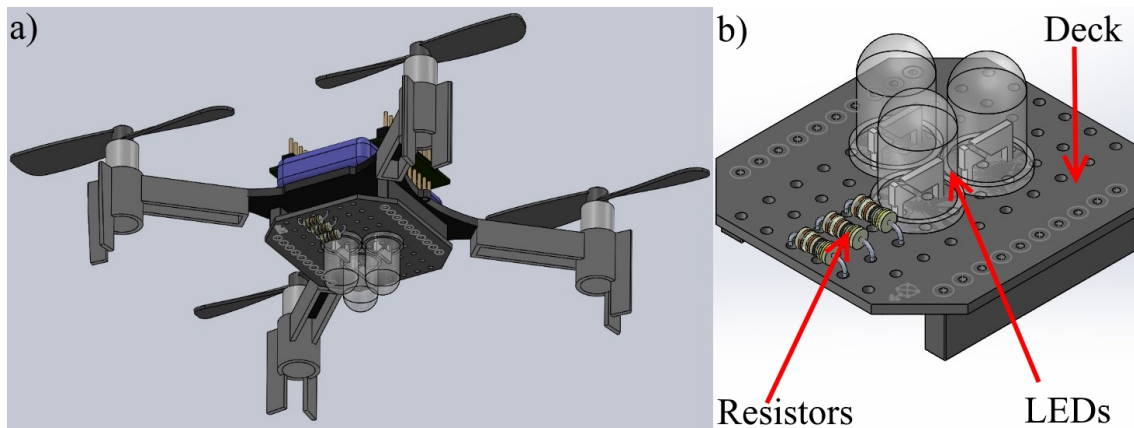
Figure 7-4: a) - Crazyflie 2.0, b) - prototyping deck with LEDs and resistors.
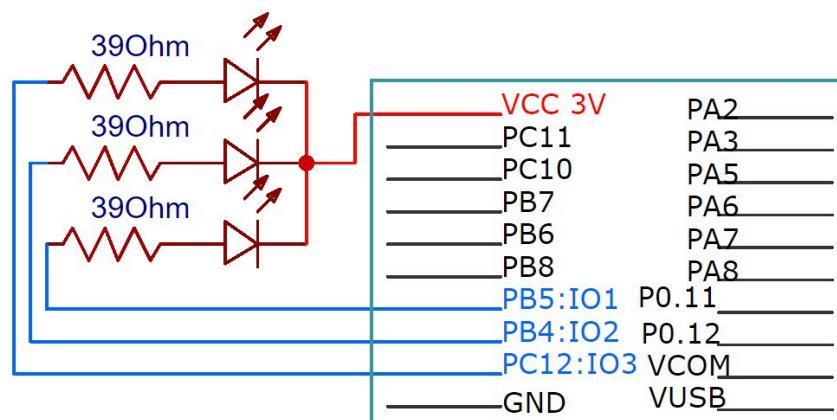
Figure 7-5: Electrical circuit of the Crazyflie 2.0 prototyping deck.

vibrotactile feedback.

7.3 Experiment with Landing of Two Drones

Seven right-handed users (six males and one female, 24 to 41 years old) took part in the experiments in which they landed one or two drones on the palms. The landing of two drones is shown in Fig. 7-6. In particular, the subjects were asked to adjust the landing pads' position so that each descending drone could land in the middle of the corresponding pad. There were three feedback conditions: only visual feedback, only tactile feedback, and tactile-visual feedback. The protocol of the experiment was approved by the Skolkovo Institute of Science and Technology review board, and all participants gave informed consent.

Figure 7-6: Landing of two drones using SwarmCloak (visual + tactile feedback condition).

7.3.1   Experimental methods

For the user study, we used two landing pads, placed on the human palms. Two types of experiments were conducted. Seven people participated in the study, and all seven subjects performed both experiments. During the experiment, the drones descended vertically, keeping the same position in the XY plane. The goal for the subject was to adjust the position of the landing pads, in a way that the drones land on the center of the landing pads. In Experiment 1, subjects were asked to land one drone on the right hand. Experiment 2 was more complicated, as two drones were descending on both palms at the same time (distance between drones was 1 meter; therefore, it was possible to observe visually only one of them at a time) This fact forced subjects to move the head from side to side.

The basic guidance policy was proposed to the users. In each experiment, users were asked to adjust the position of the palm to land one or two drones as close to the center of the landing plate as possible. If the user feels that the drone is above the right side of the palm (with the help of vision or vibromotor activation placed on the right side of the palm), then he/she was supposed to move the hand to the right. After the experiments, users were asked about the applied strategy for

a combination of different feedback types and the results are discussed below.

In both experiments, users were asked to land drones using one of three feedback conditions: only visual feedback (V), only tactile feedback (T) with closed eyes, or both visual and tactile feedback (VT). Users experienced the same tactile sensation for T and VT cases. Each feedback condition repeated ten times in a random order (10 times for each of three conditions: V, T, and VT). As a result, in each experiment, one subject had 30 trials of landing. For specific feedback condition, landing speed varied in a random order, so that five times landing speed was slow (0.1 m/s), and five times it was fast (0.15 m/s). As a result, all users experienced six conditions (set of 3 feedback types and two landing speeds) with five trials for each condition.

Before the experiments, users were asked to stand in the predefined spot and lower their hands. Users were not allowed to take steps while the drones were landing. Drones were placed in front of the users on the floor. They took off to the 2-meter height above the floor, then moved to the predefined position (approximately 0.5 meters in front of the human). Predefined positions were randomly selected within a range of 0.12 meters to prevent the learning of hand positioning. After that, the LED rings on the bottom of the quadrotors started to flash with constant light intensity in a visible spectrum, and the drones started to descend vertically. Subjects were told that they were allowed to start adjusting the landing pad position when the LED ring was on. When the difference between the height of the drone legs and the landing plate was less than 5 mm, the motors of the corresponding drone shut down. Turning off the motors also helped to prevent the drone drifting due to the aerodynamics of the ground effect. The ground effect was quite noticeable in tactile feedback when users were not able to visually maintain the horizontal position of the landing plate. Slightly tilted plate led to the drone drifting and jumping in the direction of tilt during the last 5 mm of landing. The subjects can select the height of the contact point (when the drone is landed) without any constraints. For Experiment 2, users were restricted to land both drones approximately at the same time, preventing sequential landing. After landing, drones were placed back on the floor, and the process was repeated.

For both experiments, the training involved one fast and one slow landing for each feedback condition. During learning, users were able to get feedback about the distance between the center of the drone and the center of the landing plate by closely observing after landing. Each participant was wearing safety glasses.

Drones and landing plates were tracked by a Vicon motion capture system, which recorded the position and orientation. For Experiment 2, we also asked participants to wear a cap which was tracked as well, for the analysis of the human head motion while catching both drones at the same time. Recording started after the drones initiated descending (after the LED ring started to flash) and stopped after the contact of a drone with a landing plate.

7.3.2   Results: Trajectory Analysis (of the landing pads and the user's head) During the Landing Stage

We analyzed the kinematic parameters and shape of the trajectories of human hands and human's head movement while landing drones. The landing stage begins when the drones start to descend and last until the drone actually touches the surface of the landing pad. For the analysis, we propose to consider the first four derivatives of the human position. Changes in the motion of parts of the human body could have a significant effect on the human experience. In general, humans are trying to minimize the changes in motion and the motion itself while doing different operations. Higher derivatives could have a strong effect on the human, although human tolerance to snap and jerk are not well investigated. However, many designers of elevators and roller coaster rides prefer to limit these parameters Eager et al. [2016]. The results are shown in Table 7.1 and Fig. 7-7.

Landing velocity affects the hand motion with V feedback for two drones (Experiment 2). When the drones descended faster, the human adjusted hand in a more aggressive way, as can be seen in Table 7.1, last column, Experiment 2, V rows (snap increased by multiple times for fast landing speed). Although this effect did not occur when we added tactile sensation to vision in the VT case (see Table 7.1, last column, Experiment 2, VT rows). This finding tells that tactile feedback helps

Table 7.1: Parameters of Hand Motion. During landing.

Feed-back type	Kinematic parameters, mean values, Slow / Fast landing			
	Velocity, m/s	Acceleration, m/s^2	Jerk, m/s^3	Snap, m/s^4
Experiment 1. One drone. Right hand				
V	0.026/0.025	0.20/0.22	12.9/12.7	1353/1306
T	0.029/0.043	0.21/0.30	11.8/15.0	1195/1570
VT	0.028/0.034	0.25/0.28	13.9/14.5	1488/1473
Experiment 2. Two drones. Left hand				
V	0.025/0.027	0.22/0.25	10.4/18.2	984/3816
T	0.031/0.038	0.27/0.30	13.9/12.3	1702/1182
VT	0.023/0.032	0.22/0.26	10.3/12.4	935/1167
Experiment 2. Two drones. Right hand				
V	0.028/0.027	0.23/0.27	11.8/21.5	1133/4712
T	0.033/0.044	0.28/0.37	12.4/14.9	1207/1415
VT	0.024/0.028	0.22/0.26	11.3/12.3	1061/1124

to make human motion more smooth when we try to land multiple drones.

For one drone case (Experiment 1), with T feedback, participants demonstrated more active landing plate adjustment for a fast landing. This shows that the proposed device design could inform the users about the rate of change of the distance between the drone and the landing plate.

Most users in Experiment 2 demonstrated slightly more dynamic work with the right hand than with left hand having V feedback (snap is 20% higher). All participants are right-handed and could control the right hand faster and more precisely. Again, this effect became negligible compared with the VT case for the right and the left hand.

Fig. 7-7 presents the landing pad trajectories of the right hand of all users in Experiment 2 (in XY plane) during the landing stage. The intersection of black lines is the position of the landing drone, which is moving vertically. It is easy to notice that in V case, the average position of the landing pad (showed with a blue circle) has an offset towards the location of human standing in the left upper corner. In contrast to that, in T case, the landing plate is moving below the drone without a noticeable offset. We averaged the distance in XY plane between the drone and the landing plate during the landing stage (measured before the drone
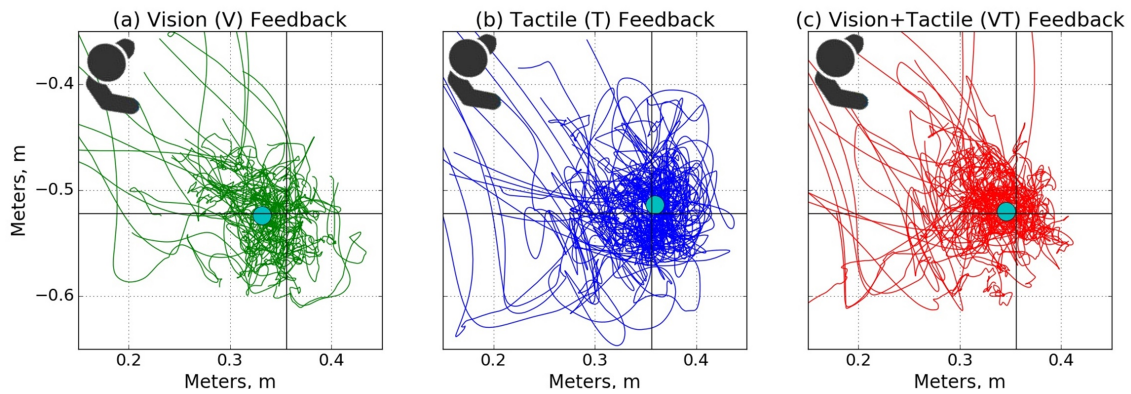
Figure 7-7: Trajectories of all participant's right hand in Experiment 2 for slow drone landing in XY plane (for the right hand). Drone is landing on the intersection of black lines. Average position of the landing pad is shown with blue circle.

touches the landing pad, for the slow landing on the right hand in Experiment 2): V: 24.2 mm, T: 8.6 mm, VT: 10.1 mm. Based on this evidence, we suggest that the tactile feedback helps align the position of the landing pad in such a way that the drone is located above the center of the pad during the landing.

One more finding is related to the motion pattern of the hand. Most subjects stated that it was easier to estimate the position of the drone based on the gradient of tactile sensation rather than when the vibration is always in the same palm spot. As a result, participants having T feedback always moved their palms from side to side (while landing). With V feedback, participants also adjusted the hand position all the time, trying to catch the drone with a smaller error. Trajectory analysis reveals that when visual feedback is presented (Fig. 7.1(a)), human mostly moves his/her hand along the line, which connects human and the drone. However, in trials with only tactile feedback (Fig. 7.1(b)), we see that hand motion is omnidirectional, which tells us that the users are exploring all space in a more uniform manner.

In Experiment 2, participants had to rotate its head fast to observe landing drones one by one (distance between drones is 1 meter). That is why we conducted the same trajectory analysis for the human head movement for the second experiment. The results are presented in Table 7.2 for V and VT conditions. Comparing V and VT cases in Table 7.2, it is easy to notice that VT feedback minimizes and smooths the human head motion. That means that VT requires to perform less

128

Table 7.2: Human Head Motion Parameters, During landing.

Feedback type	Average kinematic parameters, Slow/Fast landing			
	Vel., m/s	**Accel., m/s^2**	**Jerk, m/s^3**	**Snap, m/s^4**
Experiment 2. Two drones.				
V	0.085/0.11	0.72/1.24	27.4/121	2676/35947
VT	0.080/0.087	0.60/0.69	22.1/26.5	2129/2543

locomotion.

Users reported that they switched their attention from one drone to the other when landing both. That is true for V, T and VT case, therefore, tactile feedback also requires individual attention, the same as vision. The most popular strategy for VT and two drones was to set one landing pad position with vision and then use tactile sensation to update the position of it, while the second landing pad was positioned with vision mainly.

7.3.3 Results: Landing Position Analysis after the Landing is Completed

An important metric for the experiments was the distance between the center of the drone and the center of the landing plate after landing. In the current research, this distance is called displacement. The landing plate diameter was selected to be big enough so that in most experiment trials, participants were able to land a drone on its surface.

First of all, to compare the effects of each condition (the combination of feedback type and landing speed) on the displacement, we used a within-subject statistical comparison. We performed a two-way ANOVA with repeated measures, in which the dependent variable is displacement error, while drone number and feedback/speed conditions are two factors. The level of significance was set to α=0.05. The analysis revealed statistically significant difference in all conditions ($F(5, 170) = 9.459$, p = $5.653 \cdot 10^{-8}$). A number of drones do not affect the results significantly ($F(5, 170) = 1.027$, p = 0.404), thus, we can conclude that technology works similarly for landing one or two drones.

For the further displacement analysis, we used mean values of displacements and standard deviations, presented in Table 7.3 and paired t-test for different conditions. All displacement values of the drone after landing (with histogram), are plotted in Fig. 7-8.

The statistics of drone displacement changes drastically when the number of drones to land is changed from one to two (Table 7.3). V and VT cases revealed that the increase in the number of agents decreased the accuracy 2-3 times, although T condition performance remained the same. It can be concluded that the performance gap between visual (V) and tactile (T) feedback is becoming smaller while increasing the number of drones; meanwhile, the relation between the T and V performance is increasing with an increasing number of drones.

Comparing V and VT in Table 7.3, it is possible to conclude that VT, in general, showed slightly better average results than V. The best mean and absolute displacements for both experiments (best mean values: Experiment 1 – 9.5 mm, Experiment 2 – 18.3 mm) was also achieved with VT feedback and slow speed. Paired t-test showed no significant differences between V and VT in one drone landing, except V (slow landing case) and VT (fast landing case) case ($t = 2.654$, $p = 0.012$). Tactile feedback brings better performance to the right hand in the second experiment (comparing V and VT parameters in Table 7.3). For the right hand, visual plus tactile feedback is statistically better than only visual (V (fast landing case) and VT (slow landing case): $t = 2.825$, $p = 0.008$; V (fast landing case) and VT (fast landing case): $t = 2.46$, $p = 0.019$). As a conclusion, we could state that the combination of visual and tactile feedback showed a synergetic effect.

Based on Fig. 7-8, in T condition of Experiment 2, the right hand demonstrated higher accuracy but low precision. However, the left hand was more precise and less accurate. Surprisingly, in terms of mean displacement and standard deviation, the left hand worked out better for most participants. Left and right hands also performed in a different way with V feedback. Only in for VT, hands showed the same landing error parameters.

In general, performance with slow landing is better, which is obvious. Landing speed could strongly affect maximum error values, but on mean displacement and
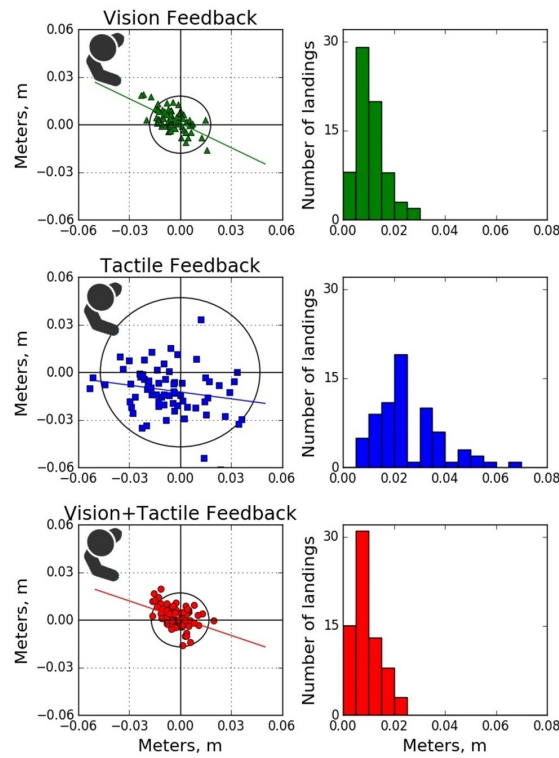
Experiment 1. Right hand.
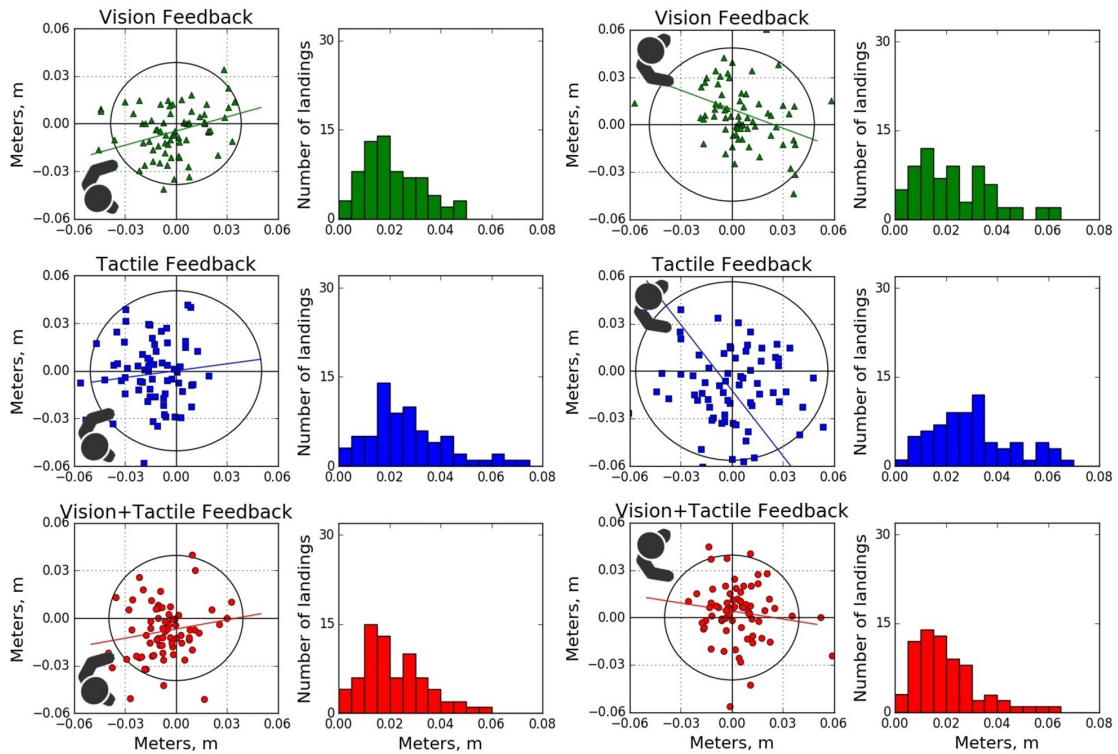
Experiment 2. Left hand.   Experiment 2. Right hand.

Figure 7-8: Drone positions on the landing pad after landing. XY axis are crossing in the center of the landing plate. Histograms represent the distribution of the displacements. Circles represents the area that fits 90% of landings. Lines represent predictions of drone landing spot, based on linear regression model.

131

Table 7.3: Drone Displacement, After Landing.

Feedback type	Displacement statistics in XY plane, mm		
	Mean, mm	Std. Deviation, mm	Maximum, mm
Experiment 1. One drone. Right hand (Slow / fast landing)			
V	11.1/9.9	6.9/4.3	29.7/20.1
T	29.2/25.2	12.8/21.4	65.8/133
VT	9.5/8.1	5.3/4.9	22.7/23.0
Experiment 2. Two drones. Left hand (Slow / fast landing)			
V	18.7/25.3	8.4/17.4	41.9/95.3
T	24.7/30.8	13.7/18.9	60.9/86.1
VT	20.7/22.2	11.5/13.4	45.5/57.3
Experiment 2. Two drones. Right hand (Slow / fast landing)			
V	31.4/19.2	23.1/14.5	116/58.8
T	28.7/51.1	14.6/113	63.5/143
VT	18.3/20.9	11.0/14.4	47.1/63.6

standard deviation it has a smaller effect in most cases.

Hand motion patterns have been discussed previously in the trajectories analysis section. Using Fig. 7-8 we could support previous findings. For each feedback condition and each hand (for both experiments) we build a linear regression model with the least-squares approach, that predicts the position of drone landing. The results are presented with color lines in Fig. 7-8. The lines are always tilted from the center of the landing plate toward the human.

One of the most practical outcomes from the analysis of the positions after landing is the selection of a landing plate diameter. Diameter is the most important decision variable in the landing pad design. For the experiments, we selected such a size, that almost all landings were successful. As a result, now we could choose the percentage of successful landing that we want, and select the appropriate diameter. For example, for 90% of successful landings, the diameters are shown in Table 7.4 (shown in Fig. 7-8 as circles). If the drone lands not on the central part but on its legs, then the value has to be increased by the length of the leg.

Table 7.4: Selection of the Landing Plate Diameter.

Feedback type	Diameter with 90% of successful landings, meters		
	Experiment 1, Right hand	Experiment 2, Left hand	Experiment 2, Right hand
V	0.018	0.038	0.048
T	0.047	0.051	0.056
VT	0.017	0.039	0.039

7.4 Experiment with Landing of Four Drones

Due to the small number of participants in the user study, the results do not have statistical significance. Therefore we consider this experiment as preliminary. we present this Section in order to frame the experimental methods to be accomplished in future work.

Four male right-handed users (21 to 29 years old) took part in the experiments in which they landed one or four drones on the palms and forearms. The landing of four drones is shown in Fig. 7-1. In particular, the subjects were asked to adjust the position of the landing pads so that each descending drone could land in the middle of the corresponding pad (the same as in the experiment with two drones). There were three experimental settings where subjects experienced: only visual feedback, only tactile feedback, and tactile-visual feedback. The protocol of the experiment was approved by a Skolkovo Institute of Science and Technology review board, and all participants gave informed consent.

7.4.1 Experimental methods

For the user study, we employed four landing pads, two hand-worn Fig. 7-3b and two forearm-worn 7-3c. Two types of experiments were conducted. Firstly, in Experiment 1, subjects were asked to land one drone on the random landing pad. Experiment 2 was more challenging to the users, as four drones were descending on four pads at the same time. The angle between arms was approximately 80°; therefore, subjects could observe visually only one arm at the same time. This fact forced users to turn the head from side to side if visual feedback was involved.

In both experiments, users were asked to land drones using one of three feedback conditions: only visual feedback (V), only tactile feedback (T) with closed eyes, or both visual and tactile feedback (VT). Users experienced the same tactile sensation for T and VT case (we kept the settings for the sensor-vibration motor units). In contrast to the experiment with two drones, we eliminated the condition on landing speed to make the experiment more simple (otherwise the experiment with four landing drones becomes too complicated). In experiment 1 each feedback condition repeated ten times in random order. In experiment 2 each feedback condition repeated three times in random order.

Before the experiments, users were asked to stand in the predefined spot. Drones were placed in front of the users on the floor. Drones took off to the 2-meter height above the floor, then moved towards the predefined positions, which was determined to take into account human anatomy (e.g., arm length, body width). Then, the LEDs at the bottom of the quadrotors started to flash, and the drones began to descend vertically. Subjects were told that they are allowed to begin adjusting the landing pads' position right after the drones start to descend. When the difference in height between the drone legs and the landing plate was less than 10 mm, the motors of the corresponding drone shut down. Turning off the motors also helped to prevent drone drifting due to the aerodynamics of the ground effect. The ground effect was quite noticeable in tactile feedback when users were not able to visually maintain the horizontal position of the landing plate. Slightly tilted plate led to the drone drifting and jumping in the direction of tilt during the last 5 mm of landing. In Experiment 2, users were restricted to land both drones approximately on the same height (to avoid sequential landing). After landing, drones were placed back on the floor, and the process was repeated.

For both experiments, the training involved only two landings for each feedback condition: V, T, and VT. In order to remove the sound of the drone motors, subjects wore noise-canceling headphones playing white noise. Each participant wore safety glasses. All objects, including drones and landing plates, were tracked by a Vicon motion capture system, with position and orientation recording. Recording started right after the drones began to descent and stopped when the drone's motors

Table 7.5: Displacement During Landing. Experiment 1

Feedback type	Displacement statistics, XY plane		
	Mean, mm	STD, mm	Max, mm
Visual	33	12	60
Tactile	36	13	61
Visual+Tactile	25	9	47

Table 7.6: Displacement During Landing. Experiment 2

Feedback type	Displacement statistics, XY plane		
	Mean, mm	STD, mm	Max, mm
Visual	38	16	78
Tactile	48	36	174
Visual+Tactile	32	10	56

switched off.

7.4.2 Experimental results

An important metric is a displacement between the drone and the landing pad *during* landing (in XY plane). Statistics for the displacement during landing is presented in Tables 7.5 and 7.6 for the Experiment 1 (one drone) and Experiment 2 (four drones) correspondingly (uniformed for all landing pads).

Another important metric for the experiments was the displacement between the center of the drone and the center of the landing plate *after* landing (in XY plane). Statistics for the displacement after landing is presented in Table 7.7 and 7.8 for the Experiment 1 (one drone) and Experiment 2 (four drones) correspondingly (uniformed for all landing pads).

The difference between T and V for all cases is noticeable with the advantage of V. While comparing V and VT, it is possible to say that VT, in general, showed slightly better average results than V. The best mean displacement after landing was achieved with VT feedback (Experiment 1 - 12 mm, Experiment 2 - 22 mm).

Table 7.7: Displacement After Landing. Experiment 1

Feedback type	Displacement statistics, XY plane		
	Mean, mm	STD, mm	Max, mm
Visual	16	10	46
Tactile	29	14	57
Visual+Tactile	12	7	33

Table 7.8: Displacement After Landing. Experiment 2

Feedback type	Displacement statistics, XY plane		
	Mean, mm	STD, mm	Max, mm
Visual	23	19	67
Tactile	37	24	11
Visual+Tactile	22	13	55

7.5 Voronoi Regions for Navigation during Deployment

Considering that P is a set of landing pads positions in $\mathbb{R}^2$, projected to the horizontal plane

$$P = \{p_1, p_2, p_3, p_4\} \tag{7.1}$$

we can calculate Voronoi cell $V_p(i)$ for each $p_i \in P$, for $i = 1, 2, 3, 4$

$$V_p(i) := \{q \in \mathbb{R}^2 \;\big|\; \|q - p_i\| \leqslant \|q - p\| \; for \; all \; p \in P\} \tag{7.2}$$

As a result, Voronoi diagram is created for two-dimensional case using the positions of landing pads and presented in Fig. 7-9. The distance is calculated using the Euclidean distance. The blue points represent the positions of the landing pads with drones. The green point represents the positions of the human operator.

When the position and orientation of human are known, the Voronoi diagram could be used to define the potential landing pad regions.

It could be seen from Fig. 7-9 that there is the point (orange) from which the distance is the same to all landing pads. This point is moving further from the human (green) when the angle between the arms is becoming more significant. That
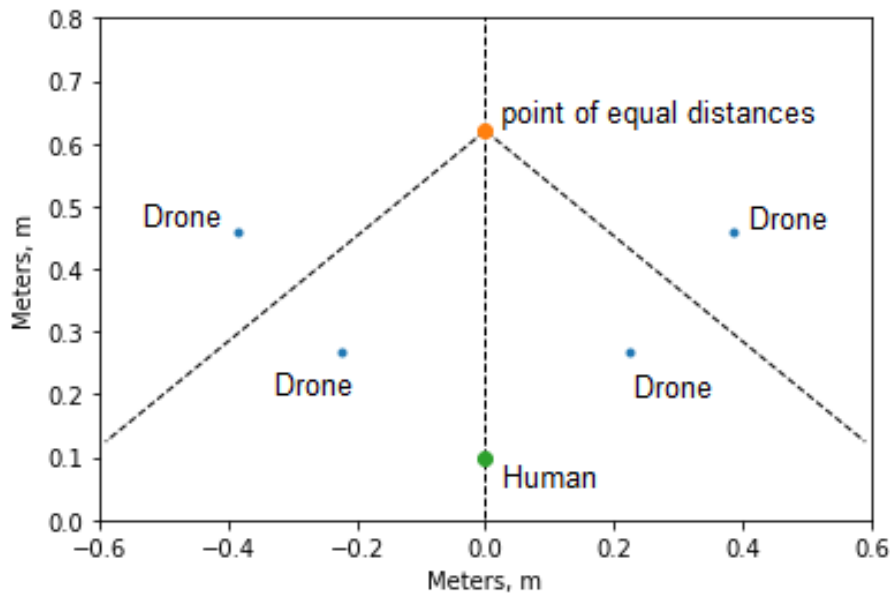
Figure 7-9: Example of Voronoi regions layout for the landing pads and the human operator. Orange point of equal distances can be used for navigation of the swarm before the takeoff.

property could be used, for example, for the navigation of the formation during deployment (before takeoff). The orange point could represent the global goal position for the swarm. Before takeoff, the human operator, having all the drones on landing pads, changes the angle between the arms, defining the orange point position. Right after the takeoff, the formation flies to the predefined set point. The properties of Voronoi regions guarantees that all drones will reach the formation set point approximately at the same time and without collisions.

7.6 Summary

In order to facilitate the guidance presented in Chapters 4 - 6 we designed and validated the SwarmCloak - a novel method for deployment multiple drones using the human body. Wearable tactile displays driven by light intensity help the user to localize the drones with respect to landing pads and therefore helps to precisely deploy the robots. We validated the SwarmCloak with the user study, where seven volunteers were asked to land multiple drones at the same time under different conditions. Two-way Anova revealed a statistically significant difference for all conditions. The

combination of visual and tactile feedback helped to reduce the positioning error. During the landing of drones, the combination of visual and tactile feedback reduced the motion dynamics of the human head (snap is decreased by 14 times). When we add the second drone, in case of visual feedback, the positioning error increases significantly. But for the tactile feedback, additional drones do not cause noticeable error increase.

Chapter 8

Conclusion

In this last chapter, we demonstrate the outcomes along with potential applications of the developed technologies. We also highlight the limitations of our work and discuss the perspectives of future work.

8.1   Discussion

With this work, we contributed to the Human-Swarm Interaction field. In particular, we developed a set of methods to facilitate the human-swarm interface for the formation guidance and deployment in cluttered environments using impedance control and tactile feedback.

All developed methods improve different parts of HSI, and, at the same time, all of them help achieve the same global objective. The developed technologies are connected with each other. Impedance control, integrated with wearable tactile display SwarmGlove, form an interface for effective guidance. SwarmCloak helps to deploy drones in any location, which is the essential sub-operation before any guided flight.

To be more explicit here, we recover the research questions mentioned at the beginning of this thesis in Chapter 3. This will help us to show how all research questions have been answered.

Research Question 1: How to achieve smooth, safe, and scalable control of a group of drones by a human operator using impedance control and artificial potential fields?

To reply to this question, we proposed a new position-based impedance control that helps to implement smooth and adaptive manipulation of a robotic group by a human operator, such as when the inter-robot distances and formation dynamics change following the operator state. The overall architecture is formed by mass-spring-damper inter-links located between pairs of agents, representing a connected directional graph. We established the relationship between the control input (human hand velocity) and the virtual external force applied to the mass of each impedance model. Therefore the human can affect the behavior of all drones globally while each agent relies on local information about the distances to neighbor vehicles. Impedance links change the formation geometry. To avoid drone-to-drone collisions and crashes with the environmental objects, we used an artificial potential field approach. That helps us not only to generate a safe trajectory but also to perform a smooth motion.

We started with the demonstration of how the proposed control method works on the simplified control problem, when we have to control a simulated point of mass (second order dynamical system) moving under the gravity force. We demonstrated the reduction of the dynamical parameters (snap standard deviation is decreased by 9% compared with the traditional PID control). As a result, we are able to obtain more smooth behaviour, following the control objectives. For the validation of the proposed method, we first selected all parameters of impedance models used for drones. Then we demonstrated the performance of the impedance model for the manipulation of a single quadrotor. Finally, we demonstrated the smooth and dynamically feasible behavior of the fleet of four drones while being guided by a human.

Research Question 2: How to provide a human operator with static and dynamic parameters of the swarm using wearable display and tactile feedback?

In response to this question we developed and evaluated a wearable tactile display SwarmGlove. We designed eight tactile patterns to represent different parameters of

the state of the swarm to the operator. The user study with 22 volunteers revealed the average recognition rate of 76.8 %. We were able to select the patterns with higher and lower recognition rate. According to the ANOVA statistical analysis, there is a statistically significant difference in the recognition rates for the different patterns, $F(7, 168) = 22.2$, $p = 4.3 \cdot 10^{-21} < 0.05$. The ANOVA showed that the type of patterns significantly influences the percentage of correct responses. The flight experiments demonstrated accurate guidance of the swarm using the proposed control methods and tactile sensation integrated together. Guidance with pure tactile feedback is close to visual feedback navigation in terms of geometry maintenance (mean of default area error decreased just by 30% when we uses visual feedback with respect to the tactile feedback). The experimental data are available at http://doi.org/10.5281/zenodo.3256614. We point out that the proposed methods for control and tactile feedback are applicable to different types and sizes of Vertical Takeoff and Landing (VTOL) vehicles.

> **Research Question 3**: How to use a human body to deploy a fleet of micro-quadrotors in any environment with the help of wearable display and tactile feedback?

To enhance the takeoff and landing operations, which are the essential parts of any flight mission, we proposed a novel method for deploying the swarm of micro-quadrotors and developed tactile interactive landing pads. During the experimental study, SwarmCloak demonstrated several significant advantages over pure visual feedback. It was shown that tactile feedback allows the increasing accuracy of the landing pad positioning. It was also demonstrated that during the landing of two drones, tactile-visual feedback helped to considerably reduce the motion dynamics of the human head (snap is decreased by 14 times). Therefore, we can conclude that potentially the tactile channel minimizes the stress of the operator. SwarmCloak is applicable when the vison feedback is not available, such as when users wear HMDs. Two-way ANOVA of drone positions showed a statistically significant difference for all feedback/speed conditions (F(5, 170) = 9.459, p = 5.653 $\cdot 10^{-8}$). In contrast to the visual feedback, the number of drones does not significantly affect the tactile

feedback's performance. The best landing positions were achieved with the combination of visual and tactile feedback. The paired t-test showed that for right-hand visual-tactile feedback is statistically better than only visual. During the landing of drones, the combination of visual and tactile feedback reduced the motion dynamics of the human head (snap is decreased by 14 times). SwarmCloak provides a strong relaxation on the micro-quadrotors complexity due to the fact that it is not required to perform high-precision localization during landing.

8.2 Applications

Due to its mobility and spatial distribution, the fleet of quadrotors could be the first responder for different emergencies, such as fire, earthquake, or flood. There are no requirements for the unique landing spots since the human operator supplements deployment using SwarmCloak. To gather information about a suffering area is a crucial task for first responders. Monitoring of the progress of disaster recovery is also necessary because an emergency can have a dynamically changing environment. Navigation of a swarm in a city environment, with multi-story buildings or even skyscrapers, could be a challenging task. Maintaining the default geometry of the formation is a reasonable requirement for real-life applications when data must be gathered evenly, or communication within the formation is necessary. As a result, the developed interaction methods could contribute to a quicker response to high risk and uncontrolled situations and a higher level of awareness of a swarm's surroundings for the operator.

8.3 Limitations and Future Work

Scalability of Guidance Methods

For future work, we want to consider the scalability of the proposed guidance methods to a bigger number of drones more closely. The impedance links represent the connected graph. Each node, or impedance link, is a self-sustained stricture with no parents or child. Therefore, all of the impedance models are on the same hierarchy

level and connected sequentially (see Fig. 4-9). Each impedance model requires only information about the human control input and nothing else, i.e., it is independent of neighbor impedance models or vehicles. The number of impedance links increases in a quadratic manner with the number of robots in a team (in the worst case, when each drone is connected to every other agent). If we have a formation of n agents, and each robot has a connection with k neighbors, we have nk impedance connections total. As a result, computational complexity increase with the quadratic rate in the worst case, which is manageable. In the case of a decentralized approach (discussed in Section 4.3.6), each impedance model can be calculated onboard of the corresponding drone, which will not require significant efforts due to distributed computation. Also, we did not experience any limiting factors when we scale the approach from single to four vehicles during the experiments.

The tactile feedback performance also does not affect by the number of agents in the team directly. With the SwarmGlove, we do not deliver the information about the certain agents or subgroups, but we provide the parameters of the state of the formation. The issue here is that in order to evaluate the swarm state parameters, the algorithms need information about the positions of the robots in space at every time frame. Therefore the possible limitation can be regarding the communication channels between the robots and the ground control station.

Human operator resources required to guide the swarm using the proposed control and feedback methods is limited for arbitrary number of robots. In other words, the single operator can control unlimited number of robots. The interactions between robots and their environment are implemented to be perform automatically. As a result, according to Fig. 2-2, the cognitive complexity of the human operator is $O(1)$ and do not grow with the number of agents in a team.

We can conclude that there are no theoretical bottlenecks for the scalability in the proposed guidance methods. If we want to scale to hundreds or thousands of units, we will face the limitation which will have a different nature, such as robustness of the radio communication channels between the agents and the ground control station, for example.

Impedance models integrated have many parameters to tune, which represent

an intensive problem to set them all before flight or even update them during the mission. In the case of hundreds of agents, it is impossible to tune all parameters, the number of which increases linearly with the number of graph connections, which can have a quadratic growth with the number of drones (depending on the connectivity level). For future work, we propose to train a Deep Reinforcement Learning (DRL) model to set all of the parameters on the fly. That is reasonable because the environmental conditions tend to change during missions, and the swarm needs to adapt accordingly. We believe that a deep architecture will be able to learn all possible behavior patterns for the flock. The training of the model will be performed in the simulator.

For the experimental verification of the guidance, we implemented a laboratory setup. Basically, we implemented a downsampled version of the real-life operation in the outdoor environment. But when we developed the laboratory experiment, we have been motivated the technical challenges from the real-life applications, discussed in the Introduction Chapter. The limited flight facilities even limited the performance of the tactile feedback with respect to visual feedback (we discussed it in Section 6.2). Based on that, we are sure that the proposed guidance methods will work outdoor. It can be easily shown by investigating the tool-set that we used during the experiments. The motion capture system can be replaced by the Global Navigation Satellite System (GNSS). Crazyflie radio modules actually can work outdoor with a range of up to 1 kilometer. But for the outdoor applications, there are a lot of well-designed radio communication systems working with a range of dozens of kilometers. Small Crazyflie drones, which can be affected outdoor by the wind, can be replaced with middle-size drones, based on the DJI F450 frame type, for example. Anyway, the application of the developed technology for the outdoor environment represents an interesting engineering challenge, which can be considered future work.

To track positions of quadrotors with Global Navigation Satellite System (GNSS) is accurate enough in most cases. However, it could be hard to track small hand motions with GPS. Therefore, the current work could be extended towards the development of the local positioning system for hand tracking. The other option is
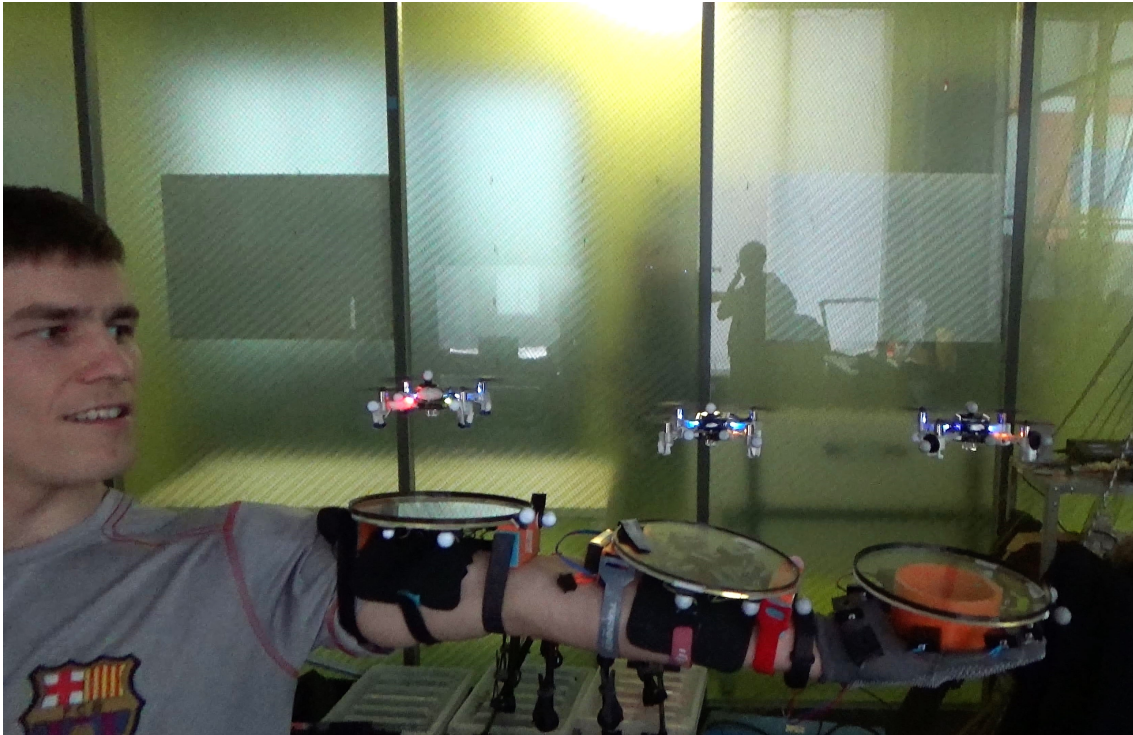
Figure 8-1: Landing of three quadrotors on one arm.

to replace the hand position and velocity as a control input with something else. The alternative method could be to use an inclination of hand (standard inertial-measurement unit (IMU) could measure all necessary information) instead of the hand position for the control input. It is also possible to use a joystick, rather than a glove, as a control input device.

Extension, Limitation and Application of SwarmCloak

Although SwarmCloak considers landing of up to four drones, a possible extension could be to arrange more landing pads on the upper arms to be able to land up to six drones on the operator body, which may require additional design development (the case of landing three drones on a hand is shown in Fig. 8-1). It is obviously impossible to use the SwarmCloak for the instantaneous deployment of hundred or even dozen of vehicles. The only solution is to imply the sequential deployment, e.g. when we land a small groups of six drones one by one. The queue or landing management algorithm has to be developed in order to facilitate such a big group deployment from the human body.

Figure 8-2: Interaction with flying objects in VR.

Regarding the other limitation of the SwarmCloak, it could be hard to use the technology outdoors during the day time due to the not proper lighting conditions. To address the lightning issue, it is possible to consider working in the optical spectrum, which is less sensitive to the environmental conditions. Drones also have to estimate the human position with an error no more than a meter, which could be hard to do in some cases.

Apart from standalone takeoff or landing of quadrotors, the SwarmCloak could be used in various applications. The proposed device can also significantly augment the perception of flying objects in VR applications, as shown in Fig. 8-2. Such tactile sensations as birds landing or taking off from the human hands can be simulated with SwarmCloak. Additionally, interaction with real or fictitious bioluminescence creatures, such as jellyfish or woodsprites of Tree of Souls from Avatar movie becomes possible. The gentle multi-contact touch by tentacles, and contact with hood can be simulated by activations of a set of vibration motors triggered by LED array and by landing the drone on the user's arm, respectively. The impact force can be adjusted through control of the drone acceleration or height of drop simulating dynamics of the virtual object.

A unique telecommunication system can be developed based on SwarmCloak technology. The partners can communicate through the distance by their avatars represented in VR and augmented by the swarm of drones. This swarm represents the skeleton structure of the human body flying in the air and capable of tactile interaction with VR user. This will bring a new level of immersion and interactivity of VR communication and teleconferencing.

Bibliography

[1] Aura glove controller. `http://aura-drone.com/us/`, 2019. [Online; accessed 03-March-2019].

[2] DroneDeploy: Drone UAV Mapping Platform. `https://www.dronedeploy.com/`, 2020. [Online; accessed 21-March-2020].

[3] Muhammad Abdullah, Minji Kim, Waseem Hassan, Yoshihiro Kuroda, and Seokhee Jeon. HapticDrone: An encountered-type kinesthetic haptic interface with controllable force feedback: Example of stiffness and weight rendering. In *2018 IEEE Haptics Symposium (HAPTICS)*. IEEE, mar 2018. doi:10.1109/haptics.2018.8357197.

[4] Parastoo Abtahi, Benoit Landry, Jackie (Junrui) Yang, Marco Pavone, Sean Follmer, and James A. Landay. Beyond the force: Using quadcopters to appropriate objects and the environment for haptics in virtual reality. In *Proceedings of the 2019 CHI Conference on Human Factors in Computing Systems - CHI '19*. ACM Press, 2019. doi:10.1145/3290605.3300589.

[5] Marco Aggravi, Florent Pause, Paolo Robuffo Giordano, and Claudio Pacchierotti. Design and evaluation of a wearable haptic device for skin stretch, pressure, and vibrotactile stimuli. *IEEE Robotics and Automation Letters*, 3 (3):2166–2173, jul 2018. doi:10.1109/lra.2018.2810887.

[6] Alin Albu-Schäffer, Christian Ott, and Gerd Hirzinger. A unified passivity based control framework for position, torque and impedance control of flexible joint robots. In *Springer Tracts in Advanced Robotics*, pages 5–21. Springer Berlin Heidelberg. doi:10.1007/978-3-540-48113-3_2.

[7] Javier Alonso-Mora, Tobias Naegeli, Roland Siegwart, and Paul Beardsley. Collision avoidance for aerial vehicles in multi-agent scenarios. *Autonomous Robots*, 39(1):101–121, jan 2015. doi:10.1007/s10514-015-9429-0.

[8] Brandon Araki, John Strang, Sarah Pohorecky, Celine Qiu, Tobias Naegeli, and Daniela Rus. Multi-robot path planning for a swarm of robots that can both fly and drive. In *2017 IEEE International Conference on Robotics and Automation (ICRA)*. IEEE, may 2017. doi:10.1109/icra.2017.7989657.

[9] Laura Attaccalite, Paola Di Mascio, Giuseppe Loprencipe, and Costantino Pandolfi. Risk assessment around airport. *Procedia - Social and Behavioral Sciences*, 53:851–860, oct 2012. doi:10.1016/j.sbspro.2012.09.934.

[10] F. Augugliaro, S. Lupashin, M. Hamer, C. Male, M. Hehn, M. W. Mueller, J. S. Willmann, F. Gramazio, M. Kohler, and R. D'Andrea. The flight assembled architecture installation: Cooperative construction with flying machines. *IEEE Control Systems Magazine*, 34(4):46–64, 2014.

[11] F. Aznar, M. Sempere, M. Pujol, R. Rizo, and M. J. Pujol. Modelling oil-spill detection with swarm drones. *Abstract and Applied Analysis*, 2014:1–14, 2014. doi:10.1155/2014/949407.

[12] Saptarshi Bandyopadhyay, Soon-Jo Chung, and Fred Y. Hadaegh. Probabilistic and distributed control of a large-scale swarm of autonomous agents. *IEEE Transactions on Robotics*, 33(5):1103–1123, oct 2017. doi:10.1109/tro.2017.2705044.

[13] Shishir Bashyal and Ganesh Kumar Venayagamoorthy. Human swarm interaction for radiation source search and localization. In *2008 IEEE Swarm Intelligence Symposium*. IEEE, sep 2008. doi:10.1109/sis.2008.4668287.

[14] Andreas Birk, Sören Schwertfeger, and Kaustubh Pathak. A networking framework for teleoperation in safety, security, and rescue robotics. *IEEE Wireless Communications*, 16(1):6–13, 2009.

[15] Sean Braley, Calvin Rubens, Timothy R. Merritt, and Roel Vertegaal. GridDrones. In *Extended Abstracts of the 2018 CHI Conference on Human Factors in Computing Systems - CHI '18*. ACM Press, 2018.

[16] J. Cacace, A. Finzi, V. Lippiello, M. Furci, N. Mimmo, and L. Marconi. A control architecture for multiple drones operated via multimodal interaction in search & rescue mission. In *2016 IEEE International Symposium on Safety, Security, and Rescue Robotics (SSRR)*. IEEE, oct 2016. doi:10.1109/ssrr.2016.7784304.

[17] Stuart K Card. *The psychology of human-computer interaction*. Crc Press, 2018.

[18] SP Chan and Hwee Choo Liaw. Generalized impedance control of robot for assembly tasks requiring compliant manipulation. *IEEE Transactions on Industrial Electronics*, 43(4):453–461, 1996.

[19] Jessie YC Chen, Ellen C Haas, and Michael J Barnes. Human performance issues and user interface design for teleoperated robots. *IEEE Transactions on Systems, Man, and Cybernetics, Part C (Applications and Reviews)*, 37(6):1231–1245, 2007.

[20] Seung Keun Cho, Hong Zhe Jin, Jang Myung Lee, and Bin Yao. Teleoperation of a mobile robot using a force-reflection joystick with sensing mechanism of rotating magnetic field. *IEEE/ASME Transactions On Mechatronics*, 15(1):17–26, 2009.

[21] Soon-Jo Chung, Aditya Avinash Paranjape, Philip Dames, Shaojie Shen, and Vijay Kumar. A survey on aerial swarm robotics. *IEEE Transactions on Robotics*, 34(4):837–855, aug 2018. doi:10.1109/tro.2018.2857475.

[22] Rafer Cooley, Shaya Wolf, and Mike Borowczak. Secure and decentralized swarm behavior with autonomous agents for smart cities. In *2018 IEEE International Smart Cities Conference (ISC2)*. IEEE, sep 2018. doi:10.1109/isc2.2018.8656939.

[23] Juan Manuel Cruz-Hernandez. Systems and methods for increasing haptic bandwidth in an electronic device, May 19 2011. US Patent App. 12/947,321.

[24] Neel Dhanaraj, Nathan Hewitt, Casey Edmonds-Estes, Rachel Jarman, Jeong-woo Seo, Henry Gunner, Alexandra Hatfield, Tucker Johnson, Lunet Yifru, Julietta Maffeo, et al. Adaptable platform for interactive swarm robotics (apis): a human-swarm interaction research testbed. In *2019 19th International Conference on Advanced Robotics (ICAR)*, pages 720–726. IEEE, 2019.

[25] John C Doyle, Bruce A Francis, and Allen R Tannenbaum. *Feedback control theory*. Courier Corporation, 2013.

[26] David Eager, Ann-Marie Pendrill, and Nina Reistad. Beyond velocity and acceleration: jerk, snap and higher derivatives. *European Journal of Physics*, 37(6):065008, oct 2016. doi:10.1088/0143-0807/37/6/065008.

[27] Paul M. Evans. Vibrotactile masking: Temporal integration, persistence, and strengths of representations. *Perception & Psychophysics*, 42(6):515–525, nov 1987. doi:10.3758/bf03207983.

[28] T Flash and N Hogan. The coordination of arm movements: an experimentally confirmed mathematical model. *The Journal of Neuroscience*, 5(7):1688–1703, jul 1985. doi:10.1523/jneurosci.05-07-01688.1985.

[29] Markus Funk. Human-drone interaction: let's get ready for flying user interfaces! *Interactions*, 25(3):78–81, 2018.

[30] J.A. García-Pulido, G. Pajares, S. Dormido, and J.M. de la Cruz. Recognition of a landing platform for unmanned aerial vehicles by using computer vision-based techniques. *Expert Systems with Applications*, 76:152–165, jun 2017. doi:10.1016/j.eswa.2017.01.017.

[31] Veysel Gazi and Barış Fidan. Coordination and control of multi-agent dynamic systems: Models and approaches. In *Swarm Robotics*, pages 71–102. Springer Berlin Heidelberg. doi:10.1007/978-3-540-71541-2_6.

[32] F. A. Geldard. Some neglected possibilities of communication. *Science*, 131 (3413):1583–1588, may 1960. doi:10.1126/science.131.3413.1583.

[33] Frank A. Geldard. Adventures in tactile literacy. *American Psychologist*, 12 (3):115–124, 1957. doi:10.1037/h0040416.

[34] N. K. Gentry. Adjustable landing gear assembly for unmanned aerial vehicles, 2017.

[35] Guido Gioioso, Antonio Franchi, Gionata Salvietti, Stefano Scheggi, and Domenico Prattichizzo. The flying hand: A formation of UAVs for cooperative aerial tele-manipulation. In *2014 IEEE International Conference on Robotics and Automation (ICRA)*. IEEE, may 2014. doi:10.1109/icra.2014.6907490.

[36] Alessandro Giusti, Jawad Nagi, Luca M. Gambardella, Stéphane Bonardi, and Gianni A. Di Caro. Human-swarm interaction through distributed cooperative gesture recognition. In *Proceedings of the seventh annual ACM/IEEE international conference on Human-Robot Interaction - HRI '12*. ACM Press, 2012. doi:10.1145/2157689.2157818.

[37] Keng Goh, Daniel Melia Boix, James McWhinnie, and Gareth Smith. Control of rotorcraft landing gear on different ground conditions. In *2016 IEEE International Conference on Mechatronics and Automation*. IEEE, aug 2016. doi:10.1109/icma.2016.7558557.

[38] Javier V. Gomez, Alejandro Lumbier, Santiago Garrido, and Luis Moreno. Planning robot formations with fast marching square including uncertainty conditions. *Robotics and Autonomous Systems*, 61(2):137–152, February 2013. doi:10.1016/j.robot.2012.10.009.

[39] Michael A. Goodrich and Alan C. Schultz. *Human-Robot Interaction: A Survey.* now Publishers Inc, 2007. doi:10.1561/9781601980939.

[40] Michael A Goodrich, Sean Kerman, and Shin-Young Jun. On leadership and influence in human-swarm interaction. In *2012 AAAI Fall Symposium Series*, 2012.

[41] Neville Hogan. Impedance control: An approach to manipulation. In *1984 American Control Conference*. IEEE, jul 1984. doi:10.23919/acc.1984.4788393.

[42] Wolfgang Honig, Christina Milanes, Lisa Scaria, Thai Phan, Mark Bolas, and Nora Ayanian. Mixed reality for robotics. In *2015 IEEE/RSJ International Conference on Intelligent Robots and Systems (IROS)*. IEEE, sep 2015. doi:10.1109/iros.2015.7354138.

[43] Matthias Hoppe, Pascal Knierim, Thomas Kosch, Markus Funk, Lauren Futami, Stefan Schneegass, Niels Henze, Albrecht Schmidt, and Tonja Machulla. VRHapticDrones. In *Proceedings of the 17th International Conference on Mobile and Ubiquitous Multimedia - MUM 2018*. ACM Press, 2018. doi:10.1145/3282894.3282898.

[44] Wolfgang Hönig, T. K. Satish Kumar, Liron Cohen, Hang Ma, Hong Xu, Nora Ayanian, and Sven Koenig. Summary: Multi-agent path finding with kinematic constraints. In *Proceedings of the Twenty-Sixth International Joint Conference on Artificial Intelligence*. International Joint Conferences on Artificial Intelligence Organization, aug 2017. doi:10.24963/ijcai.2017/684.

[45] Roman Ibrahimov, **Evgeny Tsykunov**, Vladimir Shirokun, Andrey Somov, and Dzmitry Tsetserukou. DronePick: Object picking and delivery teleoperation with the drone controlled by a wearable tactile display. In *2019 28th IEEE International Conference on Robot and Human Interactive Communication (RO-MAN)*, pages 280–285. IEEE, oct 2019. doi:10.1109/roman46459.2019.8956344.

[46] H. Il Son, J. Kim, L. Chuang, A. Franchi, P. Robuffo Giordano, D. Lee, and H. H. Bülthoff. An evaluation of haptic cues on the tele-operator's perceptual awareness of multiple uavs' environments. In *2011 IEEE World Haptics Conference*, pages 149–154, June 2011. doi:10.1109/WHC.2011.5945477.

[47] Lynette A. Jones and Nadine B. Sarter. Tactile displays: Guidance for their design and application. *Human Factors: The Journal of the Human Factors and Ergonomics Society*, 50(1):90–111, feb 2008. doi:10.1518/001872008x250638.

[48] Lynette A. Jones and Nadine B. Sarter. Tactile displays: Guidance for their design and application. *Human Factors*, 50(1):90–111, 2008. doi:10.1518/001872008X250638. PMID: 18354974.

[49] Yuichiro Katsumoto. Bottomless joystick. In *SIGGRAPH ASIA 2016 Emerging Technologies on - SA '16*. ACM Press, 2016. doi:10.1145/2988240.2988245.

[50] Oussama Khatib. Real-time obstacle avoidance for manipulators and mobile robots. *The International Journal of Robotics Research*, 5(1), April 1986.

[51] J. Kiefer, M. Ward, and M. Costello. Rotorcraft hard landing mitigation using robotic landing gear. *Journal of Dynamic Systems, Measurement, and Control*, 138(3), jan 2016. doi:10.1115/1.4032286.

[52] Pascal Knierim, Thomas Kosch, Valentin Schwind, Markus Funk, Francisco Kiss, Stefan Schneegass, and Niels Henze. Tactile drones - providing immersive tactile feedback in virtual reality through quadcopters. In *Proceedings of the 2017 CHI Conference Extended Abstracts on Human Factors in Computing Systems - CHI EA '17*. ACM Press, 2017. doi:10.1145/3027063.3050426.

[53] Haruna Kokubo, Taro Shibanoki, Takaaki Chin, and Toshio Tsuji. Obstacle avoidance method for electric wheelchairs based on a multi-layered non-contact impedance model. In *International Conference on Artificial Life and Robotics (ICAROB 2017)*, Miyazaki, Japan, 2017.

[54] Andreas Kolling, Phillip Walker, Nilanjan Chakraborty, Katia Sycara, and Michael Lewis. Human interaction with robot swarms: A survey. *IEEE Transactions on Human-Machine Systems*, 46(1):9–26, feb 2016. doi:10.1109/thms.2015.2480801.

[55] Thomas Kosch, Markus Funk, Daniel Vietz, Marc Weise, Tamara Müller, and Albrecht Schmidt. Dronectrl: A tangible remote input control for quadcopters. In *The 31st Annual ACM Symposium on User Interface Software and Technology Adjunct Proceedings*, pages 120–122. ACM, 2018.

[56] Aleksandr Kushleyev, Vijay Kumar, and Daniel Mellinger. Towards a swarm of agile micro quadrotors. In *Robotics: Science and Systems VIII*. Robotics: Science and Systems Foundation, jul 2012. doi:10.15607/rss.2012.viii.028.

[57] Luiza Labazanova, Akerke Tleugazy, **Evgeny Tsykunov**, and Dzmitry Tsetserukou. SwarmGlove: A wearable tactile device for navigation of swarm of drones in VR environment. In *Lecture Notes in Electrical Engineering*, pages 304–309. Springer Singapore, 2019. doi:10.1007/978-981-13-3194-7_67.

[58] A. Ledergerber, M. Hamer, and R. D'Andrea. A robot self-localization system using one-way ultra-wideband communication. In *2015 IEEE/RSJ International Conference on Intelligent Robots and Systems (IROS)*, pages 3131–3137, 2015.

[59] Séverin Lemaignan, Mathieu Warnier, E Akin Sisbot, Aurélie Clodic, and Rachid Alami. Artificial cognition for social human–robot interaction: An implementation. *Artificial Intelligence*, 247:45–69, 2017.

[60] N.E. Leonard and E. Fiorelli. Virtual leaders, artificial potentials and coordinated control of groups. In *Proceedings of the 40th IEEE Conference on Decision and Control)*, Orlando, FL, USA, USA, 2001. doi:10.1109/CDC.2001.980728.

[61] Michael Lewis. Human interaction with multiple remote robots. *Reviews of Human Factors and Ergonomics*, 9(1):131–174, nov 2013. doi:10.1177/1557234x13506688.

[62] Michael Lewis, Jijun Wang, and Paul Scerri. Teamwork coordination for realistically complex multi robot systems. 2006.

[63] Quentin Lindsey, Daniel Mellinger, and Vijay Kumar. Construction of cubic structures with quadrotor teams. In *Robotics: Science and Systems VII*. Robotics: Science and Systems Foundation, jun 2011. doi:10.15607/rss.2011.vii.025.

[64] Vincenzo Lippiello and Fabio Ruggiero. Cartesian impedance control of a UAV with a robotic arm. *IFAC Proceedings Volumes*, 45(22):704–709, 2012. doi:10.3182/20120905-3-hr-2030.00158.

[65] Giuseppe Loianno and Vijay Kumar. Cooperative transportation using small quadrotors using monocular vision and inertial sensing. *IEEE Robotics and Automation Letters*, 3(2):680–687, apr 2018. doi:10.1109/lra.2017.2778018.

[66] Sergei Lupashin, Markus Hehn, Mark W. Mueller, Angela P. Schoellig, Michael Sherback, and Raffaello D'Andrea. A platform for aerial robotics research and demonstration: The flying machine arena. *Mechatronics*, 24(1):41–54, feb 2014. doi:10.1016/j.mechatronics.2013.11.006.

[67] Andualem Tadesse Maereg, Atulya Nagar, David Reid, and Emanuele L. Secco. Wearable vibrotactile haptic device for stiffness discrimination

during virtual interactions. *Frontiers in Robotics and AI*, 4, sep 2017. doi:10.3389/frobt.2017.00042.

[68] Alain Anthony Mangiat, Unnikrishna Sreedharan Pillai, and Jonathan Sheldon Kupferstein. Method for controlling and communicating with a swarm of autonomous vehicles using one-touch or one-click gestures from a mobile platform, 2013. US Patent App. 13/455,594.

[69] Jonatan Martinez, Arturo Garcia, Miguel Oliver, Jose Pascual Molina, and Pascual Gonzalez. Identifying virtual 3d geometric shapes with a vibrotactile glove. *IEEE Computer Graphics and Applications*, jan 2016. doi:10.1109/mcg.2014.81.

[70] Henrique Martins and Rodrigo Ventura. Immersive 3-d teleoperation of a search and rescue robot using a head-mounted display. In *2009 IEEE Conference on Emerging Technologies & Factory Automation*, pages 1–8. IEEE, 2009.

[71] S. H. Mason. Helicopter self-leveling landing gear, 1974.

[72] Silvia Mastellone, Dušan M. Stipanović, Christopher R. Graunke, Koji A. Intlekofer, and Mark W. Spong. Formation control and collision avoidance for multi-agent non-holonomic systems: Theory and experiments. *The International Journal of Robotics Research*, 27(1):107–126, jan 2008. doi:10.1177/0278364907084441.

[73] Tomoo Matsuda. Robot system and robot control device, October 20 1998. US Patent 5,825,981.

[74] James Mclurkin, Jennifer Smith, James Frankel, David Sotkowitz, David Blau, and Brian Schmidt. Speaking swarmish: Human-robot interface design for large swarms of autonomous mobile robots. pages 72–75, 01 2006.

[75] Daniel Mellinger and Vijay Kumar. Minimum snap trajectory generation and control for quadrotors. In *2011 IEEE International Conference on Robotics and Automation*. IEEE, may 2011. doi:10.1109/icra.2011.5980409.

[76] A. Menshchikov, D. Lopatkin, E. Tsykunov, D. Tsetserukou, and A. Somov. Realizing body-machine interface for quadrotor control through kalman filters and recurrent neural network. In *2020 25th IEEE International Conference on Emerging Technologies and Factory Automation (ETFA)*, volume 1, pages 595–602, 2020.

[77] Nathan Michael, Daniel Mellinger, Quentin Lindsey, and Vijay Kumar. The GRASP multiple micro-UAV testbed. *IEEE Robotics & Automation Magazine*, 17(3):56–65, sep 2010. doi:10.1109/mra.2010.937855.

[78] Ashwin S. Thirunahari Michael Jassowski. Drone swarm for increased cargo capacity, 2016.

[79] Mark Micire, Jill L Drury, Brenden Keyes, and Holly A Yanco. Multi-touch interaction for robot control. In *Proceedings of the 14th international conference on Intelligent user interfaces*, pages 425–428, 2009.

[80] UM Rao Mogili and B B V L Deepak. Review on application of drone systems in precision agriculture. *Procedia Computer Science*, 133:502–509, 2018. doi:10.1016/j.procs.2018.07.063.

[81] E. Montijano, E. Cristofalo, D. Zhou, M. Schwager, and C. Sagüés. Vision-based distributed formation control without an external positioning system. *IEEE Transactions on Robotics*, 32(2):339–351, 2016.

[82] Daniel Morgan, Giri P Subramanian, Soon-Jo Chung, and Fred Y Hadaegh. Swarm assignment and trajectory optimization using variable-swarm, distributed auction assignment and sequential convex programming. *The International Journal of Robotics Research*, 35(10):1261–1285, feb 2016. doi:10.1177/0278364916632065.

[83] Yash Mulgaonkar, Gareth Cross, and Vijay Kumar. Design of small, safe and robust quadrotor swarms. In *2015 IEEE International Conference on Robotics and Automation (ICRA)*. IEEE, may 2015. doi:10.1109/icra.2015.7139491.

[84] Anand Nayyar. Flying adhoc network (FANETs): Simulation based performance comparison of routing protocols: AODV, DSDV, DSR, OLSR, AOMDV and HWMP. In *2018 International Conference on Advances in Big Data, Computing and Data Communication Systems (icABCD)*. IEEE, aug 2018. doi:10.1109/icabcd.2018.8465130.

[85] Wyatt S Newman and Mark E Dohring. Augmented impedance control: An approach to compliant control of kinematically redundant manipulators. In *Proceedings. 1991 IEEE International Conference on Robotics and Automation*, pages 30–31. IEEE Computer Society, 1991.

[86] N.S. Nise. *Control Systems Engineering*. Bejamin/Cummings Publishing Company, 1995. ISBN 9780805354249. URL https://books.google.com/books?id=OSkfAQAAIAAJ.

[87] M. Nithya and M.R. Rashmi. Gazebo - ROS - simulink framework for hover control and trajectory tracking of crazyflie 2.0. In *TENCON 2019 - 2019 IEEE Region 10 Conference (TENCON)*. IEEE, oct 2019. doi:10.1109/tencon.2019.8929730.

[88] Miguel A. Olivares-Mendez, Iván F. Mondragón, and Pascual Campoy. Autonomous landing of an unmanned aerial vehicle using image-based fuzzy control. *IFAC Proceedings Volumes*, 46(30):79–86, 2013. doi:10.3182/20131120-3-fr-4045.00011.

[89] Claudio Pacchierotti, Stephen Sinclair, Massimiliano Solazzi, Antonio Frisoli, Vincent Hayward, and Domenico Prattichizzo. Wearable haptic systems for

the fingertip and the hand: taxonomy, review, and perspectives. *IEEE transactions on haptics*, 10(4):580–600, 2017.

[90] Aditya A. Paranjape, Kevin C. Meier, Xichen Shi, Soon-Jo Chung, and Seth Hutchinson. Motion primitives and 3-d path planning for fast flight through a forest. In *2013 IEEE/RSJ International Conference on Intelligent Robots and Systems*. IEEE, nov 2013. doi:10.1109/iros.2013.6696773.

[91] Z-X Peng and Norihiko Adachi. Compliant motion control of kinematically redundant manipulators. *IEEE Transactions on Robotics and Automation*, 9 (6):831–836, 1993.

[92] Pavel Petráček and Martin Saska. Decentralized aerial swarms using vision-based mutual localization. In *2018 IEEE/RSJ International Conference on Intelligent Robots and Systems (IROS)*, 11 2018.

[93] Gaëtan Podevijn, Rehan O'Grady, Youssef SG Nashed, and Marco Dorigo. Gesturing at subswarms: Towards direct human control of robot swarms. In *Conference Towards Autonomous Robotic Systems*, pages 390–403. Springer, 2013.

[94] Gaëtan Podevijn, Rehan O'Grady, Youssef S. G. Nashed, and Marco Dorigo. Gesturing at subswarms: Towards direct human control of robot swarms. In *Towards Autonomous Robotic Systems*, pages 390–403. Springer Berlin Heidelberg, 2014.

[95] V. Potdar, A. Sharif, and E. Chang. Wireless sensor networks: A survey. In *2009 International Conference on Advanced Information Networking and Applications Workshops*, pages 636–641, 2009.

[96] Shokoofeh Pourmehr, Valiallah Mani Monajjemi, Richard Vaughan, and Greg Mori. &#x201cyou two! take off!&#x201d: Creating, modifying and commanding groups of robots using face engagement and indirect speech in voice commands. In *2013 IEEE/RSJ International Conference on Intelligent Robots and Systems*. IEEE, nov 2013. doi:10.1109/iros.2013.6696344.

[97] James A. Preiss, Wolfgang Honig, Gaurav S. Sukhatme, and Nora Ayanian. Crazyswarm: A large nano-quadcopter swarm. In *IEEE International Conference on Robotics and Automation (ICRA)*. IEEE, 2017. doi:10.1109/icra.2017.7989376.

[98] Carine Rognon, Stefano Mintchev, Fabio DellAgnola, Alexandre Cherpillod, David Atienza, and Dario Floreano. FlyJacket: An upper body soft exoskeleton for immersive drone control. *IEEE Robotics and Automation Letters*, 3 (3):2362–2369, jul 2018. doi:10.1109/lra.2018.2810955.

[99] Juan Jesus Roldan, Pablo Garcia-Aunon, Elena Pena-Tapia, and Antonio Barrientos. SwarmCity project: Can an aerial swarm monitor traffic in a

smart city? In *2019 IEEE International Conference on Pervasive Computing and Communications Workshops (PerCom Workshops)*. IEEE, mar 2019. doi:10.1109/percomw.2019.8730677.

[100] Sajad Saeedi, Michael Trentini, Mae Seto, and Howard Li. Multiple-robot simultaneous localization and mapping: A review. *Journal of Field Robotics*, 33(1):3–46, jul 2015. doi:10.1002/rob.21620.

[101] Andrea Sanna, Fabrizio Lamberti, Gianluca Paravati, and Federico Manuri. A kinect-based natural interface for quadrotor control. *Entertainment Computing*, 4(3):179–186, 2013.

[102] Yuri S. Sarkisov, Grigoriy A. Yashin, **Evgeny V. Tsykunov**, and Dzmitry Tsetserukou. DroneGear: A novel robotic landing gear with embedded optical torque sensors for safe multicopter landing on an uneven surface. *IEEE Robotics and Automation Letters*, 3(3):1912–1917, jul 2018. doi:10.1109/lra.2018.2806080.

[103] Martin Saska, Jan Chudoba, Libor Precil, Justin Thomas, Giuseppe Loianno, Adam Tresnak, Vojtech Vonasek, and Vijay Kumar. Autonomous deployment of swarms of micro-aerial vehicles in cooperative surveillance. In *2014 International Conference on Unmanned Aircraft Systems (ICUAS)*. IEEE, may 2014. doi:10.1109/icuas.2014.6842301.

[104] Stefano Scheggi, Fabio Morbidi, and Domenico Prattichizzo. Human-robot formation control via visual and vibrotactile haptic feedback. *IEEE Transactions on Haptics*, 7(4):499–511, oct 2014. doi:10.1109/toh.2014.2332173.

[105] Weisen Shi, Haibo Zhou, Junling Li, Wenchao Xu, Ning Zhang, and Xuemin Shen. Drone assisted vehicular networks: Architecture, challenges and opportunities. *IEEE Network*, 32(3):130–137, may 2018. doi:10.1109/mnet.2017.1700206.

[106] Lilly Spirkovska. Summary of tactile user interfaces techniques and systems. Technical report, NASA Ames Research Center, Moffett Field, California CA, 2005.

[107] Stefan Spiss, Yeongmi Kim, Simon Haller, and Matthias Harders. Comparison of tactile signals for collision avoidance on unmanned aerial vehicles. In *Lecture Notes in Electrical Engineering*. Springer Singapore, jul 2017. doi:10.1007/978-981-10-4157-0_66.

[108] James Stephan, Jonathan Fink, Vijay Kumar, and Alejandro Ribeiro. Concurrent control of mobility and communication in multirobot systems. *IEEE Transactions on Robotics*, 33(5):1248–1254, oct 2017. doi:10.1109/tro.2017.2705119.

[109] Stefano Stramigioli, Robert Mahony, and Peter Corke. A novel approach to haptic tele-operation of aerial robot vehicles. In *IEEE International Conference on Robotics and Automation*. IEEE, may 2010. doi:10.1109/robot.2010.5509591.

[110] Jurgen Sturm and Daniel Cremers. Autonomous navigation for flying robots. https://vision.in.tum.de/teaching/ss2015/autonavx, 2015. Accessed 06/07/20.

[111] Housheng Su, Xiaofan Wang, and Zongli Lin. Flocking of multi-agents with a virtual leader. *IEEE Transactions on Automatic Control*, 54(2):293–307, feb 2009. doi:10.1109/tac.2008.2010897.

[112] David Sumpter. The principles of collective animal behaviour. *Philosophical transactions of the Royal Society of London. Series B, Biological sciences*, 361 (1465):5–22, 2006. doi:10.1098/rstb.2005.1733.

[113] Hong Z. Tan, Charlotte M. Reed, Lorraine A. Delhorne, Nathaniel I. Durlach, and Natasha Wan. Temporal masking of multidimensional tactual stimuli. *The Journal of the Acoustical Society of America*, 114(6):3295–3308, dec 2003. doi:10.1121/1.1623788.

[114] Sarah Tang and Vijay Kumar. Autonomous flight. *Annual Review of Control, Robotics, and Autonomous Systems*, 1(1):29–52, may 2018. doi:10.1146/annurev-control-060117-105149.

[115] Sarah Tang, Justin Thomas, and Vijay Kumar. Hold or take optimal plan (HOOP): A quadratic programming approach to multi-robot trajectory generation. *The International Journal of Robotics Research*, 37(9):1062–1084, dec 2017. doi:10.1177/0278364917741532.

[116] Lucas Teixeira, Fabiola Maffra, Marco Moos, and Margarita Chli. VI-RPE: Visual-inertial relative pose estimation for aerial vehicles. *IEEE Robotics and Automation Letters*, 3(4):2770–2777, oct 2018. doi:10.1109/lra.2018.2837687.

[117] **E. Tsykunov**, L. Labazanova, A. Tleugazy, and D. Tsetserukou. Swarm-Touch: Tactile interaction of human with impedance controlled swarm of nano-quadrotors. In *2018 IEEE/RSJ International Conference on Intelligent Robots and Systems (IROS)*, pages 4204–4209. IEEE, oct 2018. doi:10.1109/iros.2018.8594424.

[118] **Evgeny Tsykunov** and Dzmitry Tsetserukou. WiredSwarm: High resolution haptic feedback provided by a swarm of drones to the user's fingers for VR interaction. In *25th ACM Symposium on Virtual Reality Software and Technology*. ACM, nov 2019. doi:10.1145/3359996.3364789.

[119] **Evgeny Tsykunov**, Ruslan Agishev, Roman Ibrahimov, Luiza Labazanova, Taha Moriyama, Hiroyuki Kajimoto, and Dzmitry Tsetserukou. SwarmCloak: on human arms. In *SIGGRAPH Asia 2019 Emerging Technologies*, pages 46–47. ACM, nov 2019. doi:10.1145/3355049.3360542.

[120] **Evgeny Tsykunov**, Ruslan Agishev, Roman Ibrahimov, Luiza Labazanova, Akerke Tleugazy, and Dzmitry Tsetserukou. SwarmTouch: Guiding a

swarm of micro-quadrotors with impedance control using a wearable tactile interface. *IEEE Transactions on Haptics*, 12(3):363–374, jul 2019. doi:10.1109/toh.2019.2927338.

[121] **Evgeny Tsykunov**, Roman Ibrahimov, Derek Vasquez, and Dzmitry Tsetserukou. SlingDrone: Mixed reality system for pointing and interaction using a single drone. In *25th ACM Symposium on Virtual Reality Software and Technology*. ACM, nov 2019. doi:10.1145/3359996.3364271.

[122] **Evgeny Tsykunov**, Ruslan Agishev, Roman Ibrahimov, Taha Moriyama, Luiza Labazanova, Hiroyuki Kajimoto, and Dzmitry Tsetserukou. SwarmCloak: Landing of two micro-quadrotors on human hands using wearable tactile interface driven by light intensity. In *2020 IEEE Haptics Symposium (HAPTICS)*, pages 987–992. IEEE, mar 2020. doi:10.1109/haptics45997.2020.ras.hap20.89.9286fc30.

[123] Sandesh Thapa, He Bai, and J. Á. Acosta. Cooperative aerial manipulation with decentralized adaptive force-consensus control. *Journal of Intelligent & Robotic Systems*, 97(1):171–183, jul 2019. doi:10.1007/s10846-019-01048-4.

[124] D. Tsetserukou, R. Tadakuma, H. Kajimoto, and S. Tachi. Optical torque sensors for implementation of local impedance control of the arm of humanoid robot. In *Proceedings 2006 IEEE International Conference on Robotics and Automation*. IEEE, 2006. doi:10.1109/robot.2006.1641947.

[125] D. Tsetserukou, J. Sugiyama, and J. Miura. Belt tactile interface for communication with mobile robot allowing intelligent obstacle detection. In *2011 IEEE World Haptics Conference*. IEEE, jun 2011. doi:10.1109/whc.2011.5945471.

[126] Dzmitry Tsetserukou, Shotaro Hosokawa, and Kazuhiko Terashima. LinkTouch: A wearable haptic device with five-bar linkage mechanism for presentation of two-DOF force feedback at the fingerpad. In *2014 IEEE Haptics Symposium (HAPTICS)*. IEEE, feb 2014. doi:10.1109/haptics.2014.6775473.

[127] Matthew Turpin, Nathan Michael, and Vijay Kumar. Capt: Concurrent assignment and planning of trajectories for multiple robots. *The International Journal of Robotics Research*, 33(1):98–112, jan 2014. doi:10.1177/0278364913515307.

[128] Matthew Turpin, Nathan Michael, and Vijay Kumar. An approximation algorithm for time optimal multi-robot routing. In *Springer Tracts in Advanced Robotics*, pages 627–640. Springer International Publishing, 2015. doi:10.1007/978-3-319-16595-0_36.

[129] Haruya Uematsu, Daichi Ogawa, Ryuta Okazaki, Taku Hachisu, and Hiroyuki Kajimoto. Halux: projection-based interactive skin for digital sports. In *ACM SIGGRAPH 2016 Emerging Technologies on - SIGGRAPH '16*. ACM Press, 2016. doi:10.1145/2929464.2929479.

[130] Gábor Vásárhelyi, Csaba Virágh, Gergő Somorjai, Tamás Nepusz, Agoston E Eiben, and Tamás Vicsek. Optimized flocking of autonomous drones in confined environments. *Science Robotics*, 3(20):eaat3536, 2018.

[131] Sonia Waharte, Niki Trigoni, and Simon Julier. Coordinated search with a swarm of UAVs. In *2009 6th IEEE Annual Communications Society Conference on Sensor, Mesh and Ad Hoc Communications and Networks Workshops*. IEEE, jun 2009. doi:10.1109/sahcnw.2009.5172925.

[132] Dangxiao Wang, Meng Song, Afzal Naqash, Yukai Zheng, Weiliang Xu, and Yuru Zhang. Toward whole-hand kinesthetic feedback: A survey of force feedback gloves. *IEEE transactions on haptics*, 12(2):189–204, 2018.

[133] Jijun Wang and Michael Lewis. Assessing coordination overhead in control of robot teams. In *2007 IEEE International Conference on Systems, Man and Cybernetics*. IEEE, 2007. doi:10.1109/icsmc.2007.4414055.

[134] Barbara Webb. Swarm intelligence: From natural to artificial systems. *Connection Science*, 14(2):163–164, jun 2002. doi:10.1080/09540090210144948.

[135] Deanna Weinstein and Sidney Weinstein. Intensity and spatial measures of somatic sensation as a function of body-part, laterality, and sex, 1964.

[136] Guilin Yang, Hui Leong Ho, Weihai Chen, Wei Lin, Song Huat Yeo, and Mustafa Shabbir Kurbanhusen. A haptic device wearable on a human arm. In *IEEE Conference on Robotics, Automation and Mechatronics, 2004.*, volume 1, pages 243–247. IEEE, 2004.

[137] Liangzhe Yuan, Christopher Reardon, Garrett Warnell, and Giuseppe Loianno. Human gaze-driven spatial tasking of an autonomous mav. *IEEE Robotics and Automation Letters*, 4(2):1343–1350, 2019.

[138] Dingjiang Zhou, Zijian Wang, Saptarshi Bandyopadhyay, and Mac Schwager. Fast, on-line collision avoidance for dynamic vehicles using buffered voronoi cells. *IEEE Robotics and Automation Letters*, 2(2):1047–1054, apr 2017. doi:10.1109/lra.2017.2656241.

[139] Y. Zhou, X. Dong, G. Lu, and Y. Zhong. Time-varying formation control for unmanned aerial vehicles with switching interaction topologies. In *2014 International Conference on Unmanned Aircraft Systems (ICUAS)*, pages 1203–1209, 2014.